
Process Design Based on CO₂-Expanded Liquids as Solvents

Dissertation

zur Erlangung des akademischen Grades

Doktoringenieur

(Dr.-Ing.)

von: M.Sc. Kongmeng Ye

geb.am: 16.April 1982

in: Zhejiang, China

genehmigt durch die Fakultät für Verfahrens- und Systemtechnik der
Otto-von-Guericke-Universität Magdeburg

Gutacher Prof. Dr.-Ing. habil. Kai Sundmacher
Prof. Dr.-Ing. Hannsjörg Freund
Prof. Dr.-Ing. habil. Jens-Uwe Repke

eingereicht am: 04. Februar 2014

Promotionskolloquium am: 20. Juli 2014

Abstract

Chemical engineering evolves in order to achieve higher efficiency in terms of materials and energy and as a consequence of the desire to design cleaner processes. Currently, most chemical processes in chemical industry still employ conventional organic solvents, which lead to volatile organic compound (VOCs) emissions and consequently damage the environment as well as human health. To avoid this, rather a sophisticated and expensive exhaust treatment has to be performed. In the past decade, a number of benign solvents have been proposed as potential alternatives. However, due to the costs of these benign solvents, the complex phase behavior caused by these benign solvents, and the lack of case studies in industrial applications, the implementation of these solvents remains a great challenge for chemical engineers. In order to solve this problem, the scope of this thesis is to provide a method that allows for the implementation of a novel process based on such a benign solvent, namely CO₂-expanded liquids (CXLs).

The first part of this work is a fundamental study of phase equilibrium, including the systematic understanding of the phase behavior of CXLs with thermodynamics and the dynamic determination of the complex phase equilibrium. First, thermodynamic models are discussed and selected to predict quite a few systems, and appropriate thermodynamic models are designated for further process design and analysis. Then, once the phase equilibrium determination has been taken into account, a dynamic method is formulated with clear physical understanding and validated by several different scenarios.

In the second part, the applications of CXLs in separation and reaction processes are demonstrated respectively. Based on an experimental discovery of miscibility change, a new separation concept that changes the miscibility by phase behavior tuning using pressurized CO₂, is proposed, developed, and applied for azeotropic

mixture separation. This concept is validated using two classes of azeotropic systems and more detailed analysis of this new concept is performed. Further generalization of this new concept's feasibility is also proposed. The long-chain alkene hydroformylation in CXLs is investigated as an example for a multiphase reaction system which is strongly influenced by the gas solubility. Several preliminary predictions of analyzing CXLs in terms of several key factors are achieved through simulation for systematic understanding of CXLs. Thus, the accurate prediction results suggest that this model can be employed to guide the rational selection of CXLs in specific systems.

In summary, this thesis provides a fundamental understanding of the phase behavior of CXLs and enables the implementation of CXLs in chemical processes. The benign solvent provides a novel pathway for improving and possibly leading to new chemical processes that in the future would play an important role in the field of green chemistry.

Zusammenfassung

Die Verfahrenstechnik entwickelt sich kontinuierlich weiter um Effizienzsteigerungen in Bezug auf Materialeinsatz und Energieverbrauch zu erreichen und in der Folge umweltverträglichere Prozesse zu entwickeln. Heutzutage werden in den meisten Prozessen der chemischen Industrie nach wie vor konventionelle organische Lösungsmittel eingesetzt, die zu Emissionen flüchtiger organischer Bestandteile (volatile organic compounds, VOCs) führen und deshalb eine Gefahr für Umwelt und Gesundheit darstellen. Um dies zu vermeiden, muss das Abgas oft aufwändig und kostspielig aufbereitet werden. In der letzten Dekade wurde eine Reihe von milderen Lösungsmitteln als Alternativen vorgeschlagen. Nichtsdestotrotz ist die Verwendung derartiger Lösungsmittel aufgrund ihrer Kosten, dem von ihnen verursachten komplexen Phasenverhalten und dem Mangel an Studien in der industriellen Praxis nach wie vor eine große Herausforderung. Um zur Lösung dieser Probleme beizutragen, widmet sich diese Dissertation der Entwicklung einer Methode, die die Auslegung von Prozessen, welche auf milden Lösungsmitteln (hier: CO₂-expanded liquids (CXLs)) basieren, zu ermöglichen.

Der erste Teil dieser Arbeit beschäftigt sich mit der grundlegenden Untersuchung des Phasengleichgewichts, sowohl in Hinblick auf ein systematisches Verständnis des Phasenverhaltens von CXLs mit Hilfe der Thermodynamik, als auch der dynamischen Bestimmung komplexer Phasengleichgewichte. Zunächst werden thermodynamische Modelle diskutiert und ausgewählt um ausgesuchte Stoffsysteme zu beschreiben und geeignete thermodynamische Modelle für das weitere Prozessdesign und die Prozessanalyse vorzuschlagen. Anschließend, nachdem die Bestimmung des Phasengleichgewichts berücksichtigt wurde, wird ein dynamisches Modell basierend auf physikalischen Zusammenhängen formuliert und mit Hilfe verschiedener Beispielszenarios validiert.

Im zweiten Teil wird die Anwendung von CXLs in Reaktions- und Trennprozessen demonstriert. Basierend auf der experimentellen Beobachtung von Mischbarkeitsveränderungen wird ein neues Trennverfahren, bei dem das Phasenverhalten durch verdichtetes CO₂ verändert wird, vorgeschlagen, entwickelt und für die Trennung azeotroper Gemische angewendet. Dieses Konzept wird anhand von zwei Klassen azeotroper Systeme validiert und weitergehend analysiert. Auch eine Verallgemeinerung dieses Konzeptes wird vorgeschlagen. Als Beispiel für ein Mehrphasenreaktionssystem, welches stark durch die Gaslöslichkeit der beteiligten Stoffe beeinflusst wird, wird die Hydroformylierung langkettiger Alkene in CXLs untersucht. Eine Vielzahl von Simulationen zur Vorhersage des Verhaltens verschiedener CXLs in Bezug auf relevante Schlüsselfaktoren ermöglicht ein systematisches Verständnis der CXLs. Aufgrund der genauen Vorhersagen lässt sich dieses Modell für die rationale Auswahl von CXLs für spezifische Systeme nutzen.

Zusammenfassend kann festgehalten werden, dass diese Dissertation einen fundamentalen Beitrag zum Verständnis des Phasenverhaltens von CXLs und ihrer Verwendung in verfahrenstechnischen Prozessen bietet. Milde Lösungsmittel bieten dabei neue Wege chemische Prozesse zu entwerfen und zu verbessern, und werden so auch zukünftig eine wichtige Rolle im Bereich der nachhaltigen Chemie spielen.

To my parents

Contents

Abstract.....	iii
Zusammenfassung.....	v
Notation.....	xii
Chapter 1 Introduction.....	1
1.1 Aim of this work	5
1.2 This Thesis in a Nutshell.....	6
Part I Fundamentals	9
Chapter 2 Thermodynamic Modeling of CO ₂ -Expanded Liquids	10
2.1 Introduction	10
2.2 Modeling VLE	13
2.3 Modeling VLLE	16
2.4 Chapter Summary.....	19
Chapter 3 Dynamic Determination of Phase Equilibria	20
3.1 Introduction	21
3.2 Dynamic Equations.....	24
3.3 Validation and Evaluation	27
3.4 Towards Engineering Problems.....	30
3.5 Chapter Summary.....	32

Part II Applications	34
Chapter 4 Azeotropic Mixture Separation Using CO ₂	35
4.1 Introduction	35
4.2 Process Concept.....	37
4.3 Case: Acetonitrile/H ₂ O.....	45
4.4 Case: 1,4-Dioxane/H ₂ O.....	50
4.5 Discussion.....	53
4.6 Chapter Summary.....	55
Chapter 5 Reaction Intensification Using CO ₂	58
5.1 Introduction	58
5.2 Features of CXLs	61
5.3 CO ₂ -Expanded TMS.....	68
5.4 Chapter Summary.....	70
Chapter 6 Summary, Conclusion, and Outlook.....	71
6.1 Summary	71
6.2 Conclusion.....	72
6.3 Outlook.....	73
Appendix	74
Appendix 1: CEoS/GE model.....	74
Appendix 2: Parameters of investigated systems.....	77
Appendix 3: Extra Diagrams of Chapter 2	84
Appendix 4: Extra Tables and Diagrams of Chapter 3	87
Appendix 5: Extra Diagrams of Chapter 4	94
Appendix 6: Extra Diagrams of Chapter 5	102
Bibliography	103

List of Figures.....	115
List of Tables.....	120
Declarations	122
Curriculum Vitae.....	124

Notation

Latin Symbols

Name	Description	Unit
T	Temperature	K
p	Pressure	Pa
v	Molar volume	$m^3 \cdot mol^{-1}$
R	Gas constant	$J \cdot mol^{-1} \cdot K^{-1}$
V	Volume	m^3
B	Virial coefficient	Unit is universal
a	Parameter of CEoS	$J \cdot m^{-3} \cdot mol^2$
b	Parameter of CEoS	$m^{-3} \cdot mol^1$
u	Coefficient of CEoS	--
w	Coefficient of CEoS	--
U	Inner energy	J
H	Enthalpy	J
A	Helmholtz energy	J
G	Gibbs energy	J
S	Entropy	$J \cdot K^{-1}$
t	Time	s
n	Mole	mol
J	Fluxes	<i>Depends on flux type</i>
X	Forces	<i>Depends on force type</i>
k	Mass transfer coefficient	$mol \cdot m^{-2} \cdot s^{-1}$
A	Sectional area	m^2
f	Fugacity	Pa
z	Feed composition (mole fraction)	--
y	Composition of vapor (mole fraction)	--
x	Composition of liquid (mole fraction)	--

Latin Symbols (continuous)

Name	Description	Unit
NC	Number of components	--
NP	Number of total phases	--
ic	Component ID	--
ip	Phase ID	--
φ	Fugacity coefficient	--
Z	A parameter of CEoS, $Z=pV/RT$	mol
A	A parameter of CEoS, $ap/(RT)^2$	--
B	A parameter of CEoS, $bp/(RT)$	--
C	A function of CEoS	--
ε	A parameter of CEoS, A/B	--
C	A constant of mixing rule, C^*	--
$q1$	Parameter of mixing rule	--
$q2$	Parameter of mixing rule	--
q	Variable of Exact mixing rule	
U	Variable of LPVP mixing rule	mol^1

Greek Symbols

Name	Description	Unit
δ	<i>Parameter of mixing rule</i>	--
θ	<i>Phase partitioning coefficient</i>	--
μ	<i>Chemical potential</i>	J
ν	<i>Stoichiometric coefficient</i>	--
σ	<i>Rate of entropy production</i>	$J \cdot K^{-1} \cdot s^{-1}$
σ	<i>Component sink or source rate</i>	$mol \cdot s^{-1}$

Superscripts

Name	Description	Example
E	<i>Excess</i>	V^E
$()$	<i>ID of phases</i>	$(\alpha), (k), (k \rightarrow \alpha)$
tot	<i>total</i>	n^{tot}
V	<i>Vapor phase</i>	f^V
$L1$	<i>1st liquid</i>	f^{L1}
$L2$	<i>2nd liquid</i>	f^{L2}
$L3$	<i>3rd liquid</i>	f^{L3}
$*$	<i>A specific state</i>	C^*

Subscripts

Name	Description	Example
i, j	<i>Components</i>	k_{ij}
2	<i>Second Virial coefficient</i>	B_2
3	<i>Third Virial coefficient</i>	B_3
s	<i>Entropy</i>	σ_s
ic	<i>Component ID</i>	σ_{ic}
r	<i>Reaction</i>	σ_r
0	<i>Initial state, $t=0$</i>	n_0
m	<i>Mixture property</i>	$B_{2,m}, \varphi_m$

Abbreviations

Name	Description
1PVDW	One parameter VDW mixing rule
2PVDW	Two parameter VDW mixing rule
BLCVM	Modified LCVM mixing rule with second Virial coefficient
CEoS	Cubic equation of state
CEoS/GE	Mixing rule combining the CEoS and GE model

Abbreviations (continuous)

Name	Description
CHV2	Modified HV by adjusting the constant, 2 nd version
CHV1	Modified HV by adjusting the constant, 1 st version
COSMO	Conductor-like screening model
CXLs	CO ₂ -expanded liquids
DFG	German Research Foundation
EAL	Mixing rule developed by Esmailzadeh, As'adi and Lashkarbolooki
EoS	Equation of state
EPF	Elementary Process Functions
Exact	Mixing rule named by Kalospiros et al.
GE	Excess Gibbs free energy model
HK	Mixing rule developed by Heidemann and Kokal
HP	High pressure
HV	Huran-Vidal mixing rule
HVOS	Modified HV by Orbey and Sandler mixing rule
HVLP	Modified HV mixing rule with low pressure reference
HVT	Modified HV mixing rule developed by Tochigi, et al.
IG	Ideal gas model
ILs	Ionic liquids
KTK	Mixing rule developed by Kurihara, Tochigi and Kojima
LCSP	Lower critical solution pressure
LCVM	Linear combination of HV and MHV1 mixing rule
LLE	Liquid-liquid equilibria
LLLE	Liquid-liquid-liquid equilibria
LP	Low pressure
LPVP	Low pressure mixing rule employed vapor pressure standard state
MHV1	Modified HV with 1st order simplification mixing rule
MHV2	Modified HV with 2nd order simplification mixing rule

Abbreviations (continuous)

Name	Description
MPR	PR with modified α function
MSRK	SRK with modified α function
MTC	Modified Twu-Coon mixing rule
NRTL	Non-Random Two Liquids model
ODE	Ordinary differential equation
PC-SAFT	Perturbed chain- statistical associating fluid theory
PR	Peng-Robinson EoS
PRWS	Peng-Robinson EoS with Wong-Sandler mixing rule
PSD	Pressure-swing distillation
PSRK	Predictive SRK mixing rule or model
Ref.	Reference
RRE	Rachford-Rice equation
scCO ₂	Supercritical CO ₂
SCF	Supercritical fluids
Soave	Mixing rule developed by Soave
SRK	Soave-Redlich-Kwong EoS
TCO	The original version of mixing rule developed by Twu and Coon
TCB(0)	Modified TCO with pressure reference=0
TCB(r)	Modified TCO with varied r
TPDF	tangent plane distance function
TMS	thermomorphic (or temperature-dependent) multi-component solvent
UCSP	Upper critical solution pressure
UNIFAC-PSRK	Modified UNIFAC, version used in PSRK
UNIFAC-Lby	Modified UNIFAC, Lyngby version
UNIFAC-Do	Modified UNIFAC, Dortmund version
UNIQUAC	Universal quasi chemical model

Abbreviations (continuous)

Name	Description
USD	U.S. dollar
Uniwaals	An EoS developed by Gupte et al. 1986
VDW	van der Waals mixing rule
VLE	Vapor-liquid equilibria
VLLE	Vapor-liquid-liquid equilibria
VOC	Volatile Organic Compounds
Wilson	Wilson activity coefficient model
WS	Wong-Sandler mixing rule

Chemicals

Name	Description
H ₂ O	Water
MeOH	Methanol
EtOH	Ethanol
1PrOH	1-propanol
2PrOH	Isopropyl alcohol
1BuOH	1-butanol
MePOH	2-methyl-2-propanol
tBuOH	Tert-butyl alcohol
DME	Dimethyl ether
ACE	Acetone
BUE	2-butanone
HAC	Acetic acid
HPA	Propionic acid
HBA	Butyric acid
MeCN	Acetonitrile
OCT	1-octene

Chemicals (continuous)

Name	Description
NAL	1-nonanal
PhMe	Toluene
DIOX	1,4-dioxane
THF	Tetrahydrofuran
DMSO	dimethyl sulfoxide
MeCE	Methyl cyclohexane
PNE	n-pentane
Ph	Benzene
C6	Cyclohexane
EA	Ethyl acetate
NBA	n-butyl acetate
CO ₂	Carbon dioxide
CO	Carbon monoxide
H ₂	Hydrogen
CH ₄	Methane
C ₂ H ₄	Ethylene
C ₂ H ₆	Ethane
C ₃ H ₈	Propane
C ₄ H ₁₀	Isobutane
CClF ₃	Trifluorochloromethane
CHF ₃	Trifluoromethane
1Do	n-dodecene
C10	decane
NC13	1-dodecanal
OCT	1-octene
NAL	1-nonanal

Solvents are widely used in commercial manufacturing and service industries. Despite abundant precaution, they are difficult to contain and recycle. Researchers have therefore focused on reducing solvent use through the development of solvent-free processes and more efficient recycling protocols. However, these approaches have their limitations, necessitating a pollution prevention approach and the search for environmentally benign solvent alternatives.

Joseph M. DeSimone, Nature, 2002

Chapter 1

Introduction

Nowadays, the organic solvents have been widely used in almost every manufacturing and processing industry, e.g., textile, dry cleaning, fabrication process, and food processing, etc. The wide use of these traditional solvents leads to the majority of the Volatile Organic Compounds (VOC) emissions. Although the total amount of the VOC emissions all over the world have been decreased by 3-folds since 1970s (as shown in **Fig. 1.1**) [1], the current annual emission of over 10 million tons is still unacceptable.

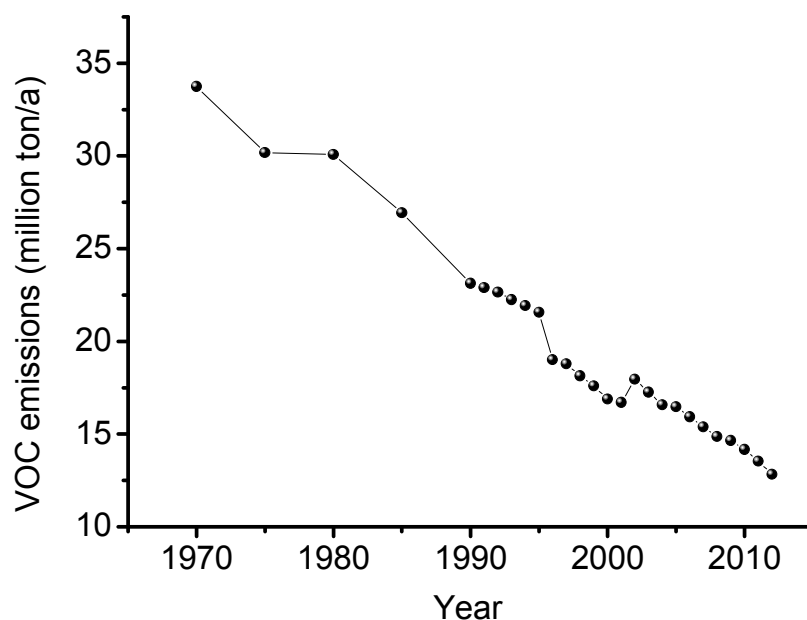


Figure 1.1: VOC annual emissions (without wildfire)

The solvent-caused emissions affect the human health and environment [2-4] through waste generation [5, 6]. To limit these negative effects, governments place policies to regulate the emissions, such as the U.S. Pollution Prevention Act in 1990 [7], while chemical engineers

search for new strategies to reduce the use of solvents, recycle the solvents, or design a solvent-free process [8-12]. However, currently these strategies have their limitations, and quite a number of instances of such processes have been shown to require process 'liquid' of some kind [6]. Therefore, a new strategy using benign solvent alternatives would be more attractive. The benign solvent alternatives are sorted in the following categories in accordance with previous works [5, 6, 13, 14], i.e., supercritical fluids (SCF) [15-18], ionic liquids (ILs) [19-22], fluoruous phases [23-27], carbon dioxide (including supercritical CO₂ (scCO₂) and CO₂-expanded liquids (CXLs) [28-31]), and selected combinations of former benign solvent alternatives [32, 33] (Fig. 1.2).

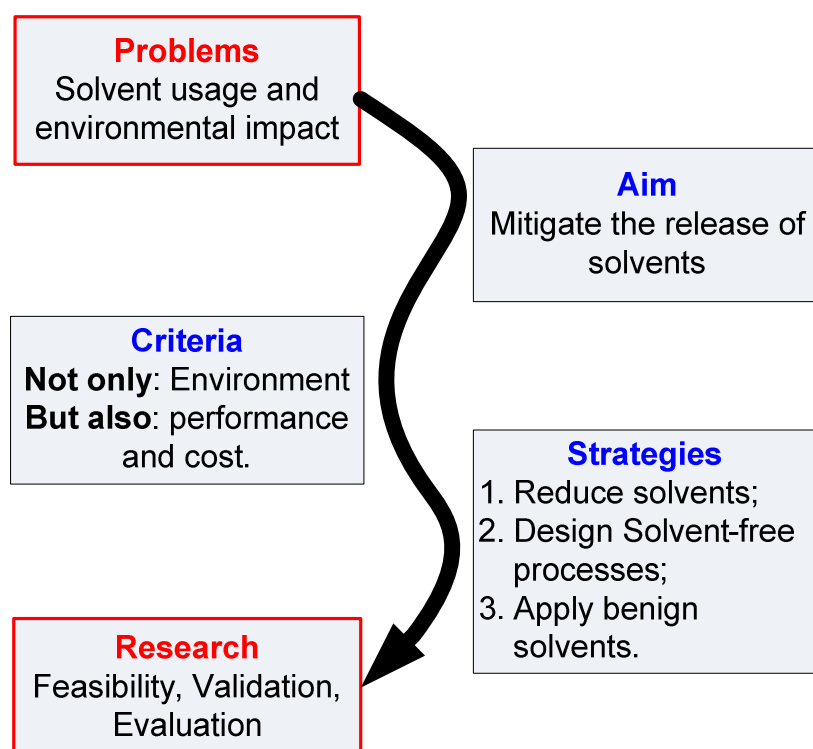


Figure 1.2: Motivation of research on benign solvents

Fluids near their critical points possess dissolving features comparable to those of conventional liquids, but are much more compressible than dilute gases, and exhibit transport properties intermediate between gas- and liquid-like phases. These exceptional physicochemical properties can be advantageously exploited in environmentally benign separation and reaction processes, as well as for new material processing [13]. Carbon dioxide (CO₂), a special chemical with low critical temperature (31.06°C) and modest critical pressure (73.83bar), has received intensive attentions since 1950 [31], evidenced by the continuously increasing number of relevant scientific publications, especially since the year of 2000 (Fig. 1.3).

There are two general categories of CO₂ as solvent, i.e., scCO₂ and CXLs. The former one, scCO₂, which is a fluid state of CO₂ at or above its critical temperature and pressure, is widely applied as indicated by **Fig. 1.3**. But the latter one, CXLs, a specific mixture of a compressed CO₂ dissolved in an organic solvent, stays in the range of subcritical state of CO₂. The CO₂ applications (including scCO₂ and CXLs) in chemical engineering have been reviewed systematically [5, 13] as shown in **Fig. 1.4**.

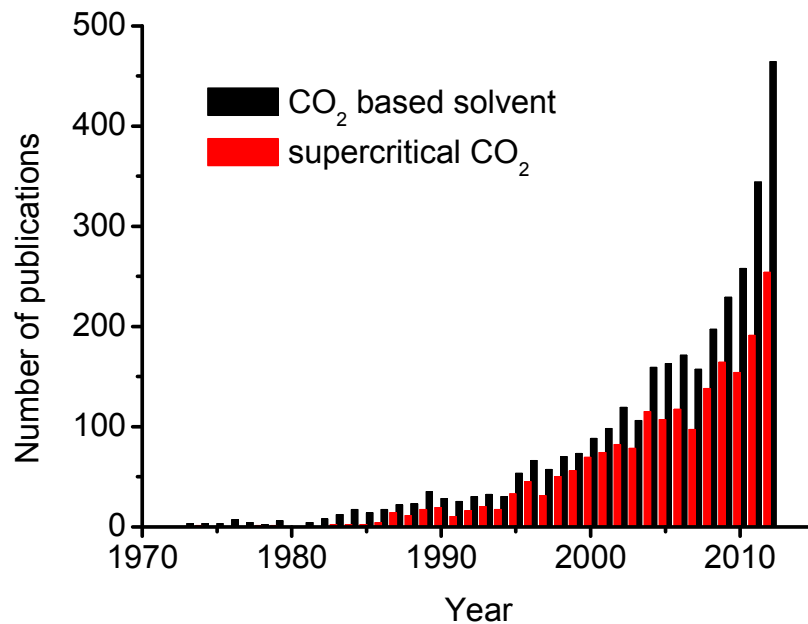


Figure 1.3: The publication review involved CO₂ based solvents (inquired by SCOPUS with carbon dioxide, solvent in title or abstract or keyword in the field of chemical engineering)

CXLs, a continuum of liquid media ranging from the neat organic solvent to scCO₂, can be adjusted by tuning the operating pressure according to its specific properties, and they have been shown to be optimal solvents in a variety of roles [5]. The main advantages are as follows:

- Eco-friendly feature;
- Easy removal of the CO₂;
- Capacity to enhance solubility of gases;
- Fire suppression capability of the CO₂;
- Milder process pressures in comparison with scCO₂;
- Enhanced transport rates due to density of the CO₂;
- Sustainable alternative compared to organic solvents.

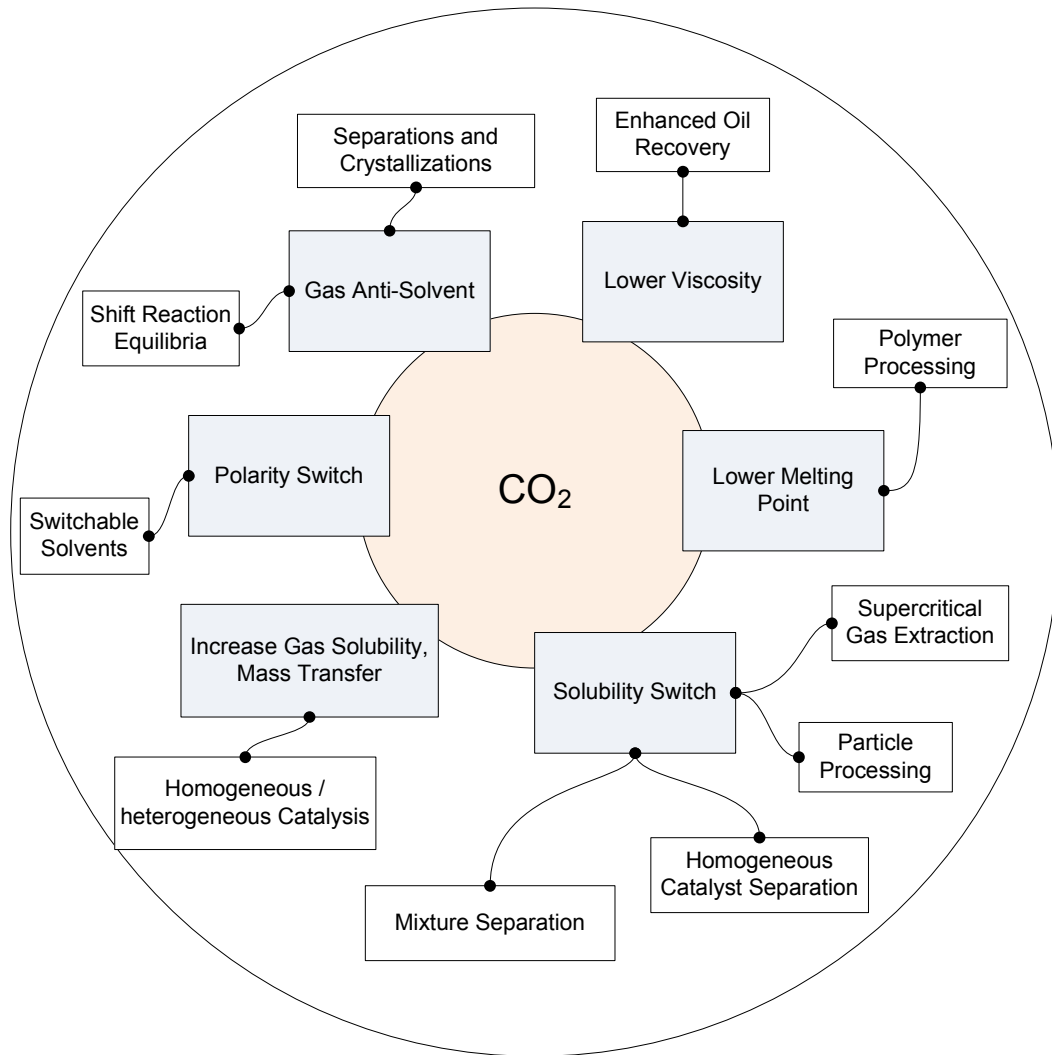


Figure 1.4: A schematic diagram of CO₂ application in chemical engineering

Although quite a few research efforts have been directed to CXLs and their applications, most of them lie on the basic understanding of CXLs in accordance with the experimental exploration and the thermodynamic modeling. Moreover, there are still few indication at the 'know-how' of whole chemical process, due to the complexity of CXLs which require abundant experimental investigations, such as the phase behavior (e.g., solubility, miscibility change), transfer properties, and reactions, etc.

Clearly, the balance between the environmental concerns and the performance, cost and sustainability of a novel benign solvent must be taken into account [3, 6]. The **Fig. 1.5** displays the pyramid of production processes in chemical engineering. The most efficient 'dream processes' might be designable if engineers are able to manipulate all hierarchical levels involved in a process system simultaneously [34]. There is a strong connection between the suggested benign alternatives in **Fig. 1.2** and the pyramid in **Fig. 1.5**: Usually, the benign alternatives benefit the reaction and/or separation process due to their particular

phase properties, e.g., by homogenizing the system to intensify the reaction and/or by heterogenizing the system after reaction to separate the products. The difficulty lies on the changes that happen in the phase level which will bring significant influence on the process design and process efficiency.

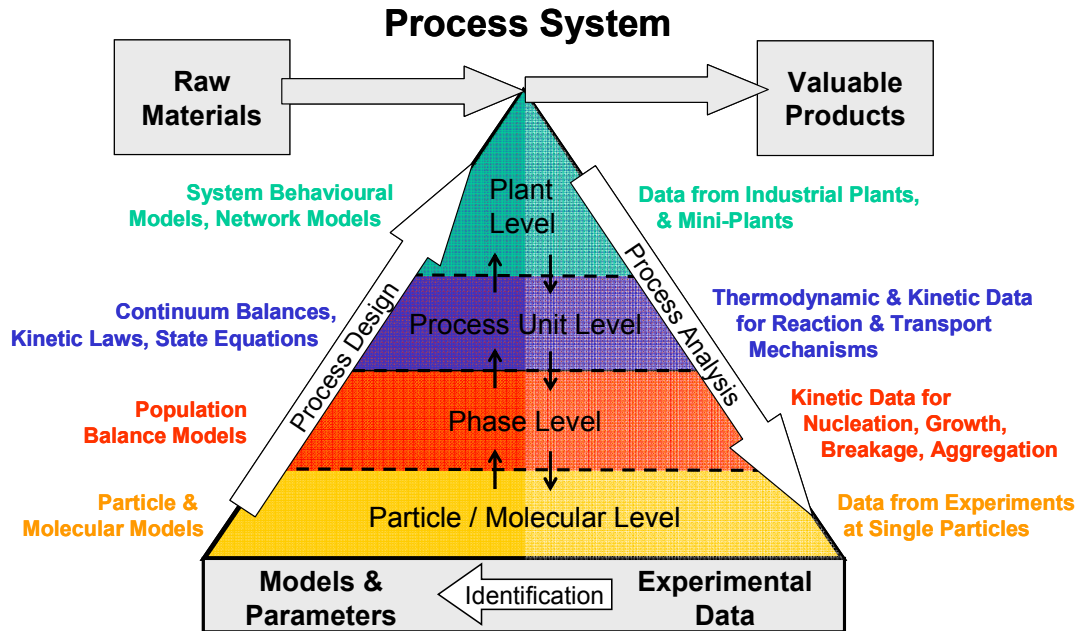


Figure 1.5: Pyramid of production processes in chemical engineering [34]

The questions of particular interests would be: how can the switchable properties of the benign alternatives be used to intensify the process due to phase behavior tuning; what is the subsequent influence on the above process?

Realizing the diversified branches of benign alternatives (e.g., the diversity of ionic liquids) and the manifold research directions (e.g., the thermodynamics, transport, reaction, process development, etc.), as well as the open questions mentioned above, current research activities focus mainly on CXLs. The process design based on CXLs by exploiting phase behavior tuning is currently still in a very explorative phase. However, the thesis is driven not only by such engineering and economic aspects, but also the academic curiosity to validate the fundamental idea of process intensification by changing the phase of the benign alternatives in use.

1.1 Aim of this work

Thermodynamic understanding of the phase behavior is the prerequisite for process design. A valid yet suitable thermodynamic model as well as an efficient method to determine the phase equilibria is essential. To validate the applications of CXLs in chemical engineering, the

thermodynamic phase behavior needs to be studied with priority. With clear understanding of the phase behavior and efficient calculation, the goal of this work is thus to provide a share of contribution to the designing of special processes based on CXLs, which are dependent on and/or dominated by pressure variation. Hence, the following questions need to be answered:

- How to describe the phase behavior of CXLs? Would there be any model to predict the phase behavior? If so, which one is the most suitable (i.e., simplest with satisfactory accuracy)?
- How to determine the phase equilibria efficiently? Do we have any innovative method in contrast to the conventional methods? If yes, what is it? Does it have physical sense? How to validate it? What is the advantage from an engineering standpoint?
- What is the idea or concept of designing separation processes based on CXLs? What is the difference from conventional solvent systems? How to realize it? Is it potentially applicable? If yes, under which circumstances?
- Is the solubility of gas in gas liquid reactions so important? Can CXLs be used to enhance reaction rate and selectivity? What kinds of exemplifications are interpreted? What important information can be found to conduct further research?

There are other questions in the subject of CXLs which are not addressed in the scope of this work. To clarify, these aspects are:

- scCO_2 and other benign alternatives;
- Detailed experimental work to achieve phase equilibrium information. In this work, most of phase behavior data are obtained from literature and project collaborators;
- The following methods to predict phase behavior, i.e., molecular simulation, multi-parameter EoS (e.g., PC-SAFT) and COSMO, are not a topic of this thesis. The reason is that the achievement of the parameters between/among the manifold components involved in this thesis is extremely difficult;
- Process optimization and further process designing, such as process control and apparatus, are not the main focus of this thesis.

1.2 This Thesis in a Nutshell

In this thesis, the general separation and reaction strategy by phase behavior tuning using CXLs, detached from a particular system, stands in the foreground. To this end, phase equilibria determination, including thermodynamic modeling and calculation method, is demonstrated at the beginning; the further process design and analysis can then be possible with such basis. In a sense, thermodynamics and the strategy by phase behavior tuning are

two threads in parallel in this thesis. With the final goal of process design and analysis, thermodynamics provide an appropriate analytical method for particular systems.

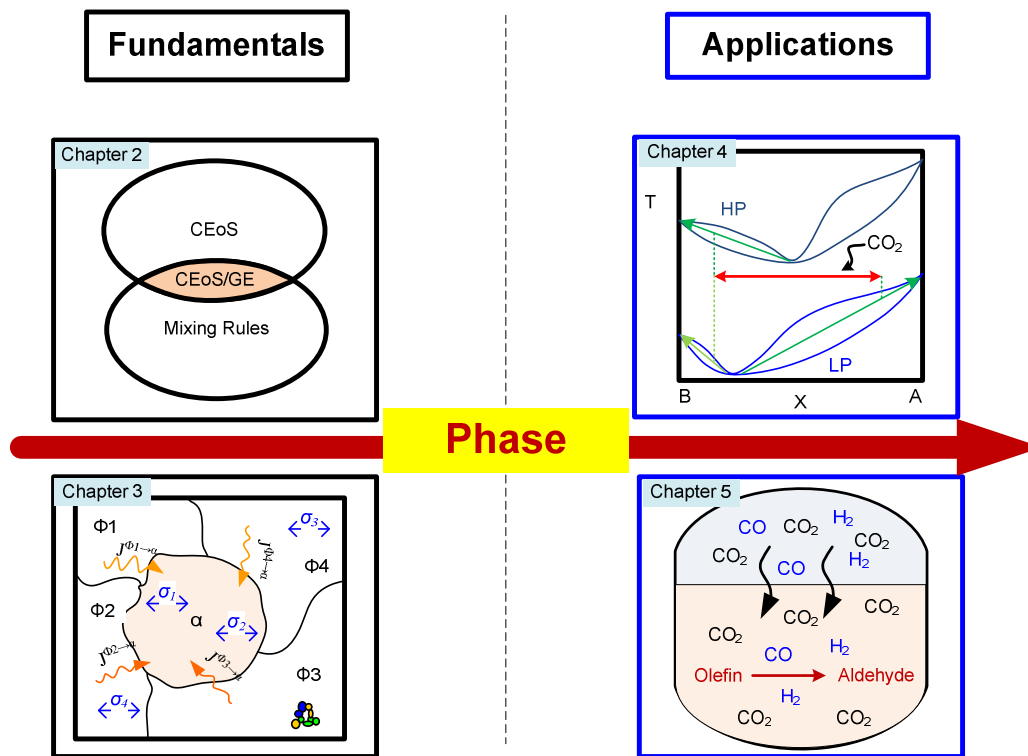


Figure 1.6: Structure of this thesis

The structure of the main body of this thesis is displayed in **Fig. 1.6**.

In **Chapter 2**, the reasons to apply the CEoS/GE model are explained through a basic introduction, and then a detailed description of CEoS/GE model is illustrated briefly in terms of CEoS, mixing rule and activity model. Following the theoretical thermodynamic equations, the CEoS/GE model structure is highlighted. In addition, mixing rules are summarized and classified intuitively. Thus, a terse model scheme is provided. This model is used continuously in **Chapters 3-5**.

Chapter 3 covers thermodynamic modeling work of CXLs. At the beginning, a review of phase equilibria is summarized; followed by a general dynamic method being proposed to determine complex phase equilibria, which is independent of the particular system, the phase behavior type, phase number, component scale, and thermodynamic method. The detailed formulation is derived step by step and validated in terms of the thermodynamic theory. The simplified formulation particularly for flash problem is then derived and attested in a multitude of cases.

In **Chapter 4**, an experimental discovery is introduced in the first place. Based on the experimental phenomenon, a novel separation concept is proposed and developed for azeotropic mixture separation by tuning phase behavior using pressurized CO₂. Based on the

concept, two process variants are put forward and validated using two classes of azeotropic system, i.e., a pressure sensitive and asymmetric azeotropic system MeCN/H₂O and a pressure sensitive and symmetric azeotropic system DIOX/H₂O. Finally, the performance of the concept is evaluated in comparison with conventional separation technology, and the feasibility of the new concept is categorized for different azeotropic systems.

In **Chapter 5**, the application of CXLs in reactions is reviewed briefly with the research of CXLs for hydroformylation being emphasized in particular. The thermodynamic analysis is highlighted to the level of understanding of components distribution for such reaction systems, including the factors which can affect CXLs. Besides, a new ideal, CXTMS, is put forward and the LLE phase behavior of 1-dodecene hydroformylation in TMS is modeled using UNIFAC-Do.

Chapter 6 is the summary and conclusion section. The outlook on major topics, including the experimental work, the predictive thermodynamic modeling, the hydroformylation and the dynamic equations to determine phase equilibrium for open system, which may play a role in future development, are also given.

The former two chapters (chapter 2 and chapter 3) are focusing on the fundamentals of the phase thermodynamically and numerically. Based on the well-understanding the phase identification, the latter two chapters (chapter 4 and chapter 5) are applying this knowledge to the process concept. Therefore, they are tightly connected by the phase, and it is the golden thread of this work.

Part I
Fundamentals

It is of special interest in chemistry and chemical engineering because so many operations in the manufacture of chemical products consist of phase contacting: ...; an understanding of any one of them is based, at least in part, on the science of phase equilibrium.

John M. Prausnitz, et al.
Molecular Thermodynamics of Fluid-Phase Equilibria, 3rd ed.,
1999

Chapter 2

Thermodynamic Modeling of CO₂-Expanded Liquids

Most industrial processes are designed for and operate near equilibrium conditions; even when this is not the case, the knowledge of what would happen at equilibrium is often still important [36]. Thermodynamics determines the principal feasibility of a process and often allows an estimate of its operational costs, while kinetics give evidence about its technical feasibility and its capital costs (e.g., reactor size). Therefore, before going to the unit level or plant level, as shown in the pyramid of production processes in chemical engineering in **Chapter 1**, the understanding of phase behavior of CXLs is very important, and it is the core of this chapter. Furthermore, the design and development of the chemical process in this thesis is based on the thermodynamic modeling work. Two types of phase behavior, i.e., vapor-liquid equilibria (VLE) and vapor-liquid-liquid equilibria (VLLE), are of particular interest. **Section 2.1** reviews phase behavior modeling using a fugacity coefficient approach within elevated pressure; **Section 2.2** highlights the performance of CEoS/GE modeling in terms of several VLE systems; **Section 2.3** displays prediction for several VLLE systems using Peng-Robinson EoS with a Wong-Sandler mixing rule (PRWS).

2.1 Introduction

CXLs, especially CO₂-expanded organic solvents, can dissolve large amount of CO₂, whereby every physical property of the mixture can be significantly changed [5]. The understanding of such non-ideal behavior of CXLs is significantly important for chemical process design, analysis, and optimization.

The most common approach to modeling the phase behavior of such non-ideal pressure dependent systems is to use a fugacity-fugacity (ϕ - ϕ) approach [35-39]. Other methods, as

reported by Mühlbauer and Ralal [38], are rarely applied for modeling CXLs, e.g., molecular simulation can be used to model systems with only a few constituents [40-42]. The calculation of the fugacity of each constituent in a mixture must include the equation-of-state (EoS) and the mixing rule.

The EoS can be classified either as cubic equation-of-state (CEoS) or multi-parameter equation-of-state (EoS). The CEoS, notably those by Soave-Redlich-Kwong (SRK) [43] and Peng-Robinson (PR) [44] are real successful cases of applied thermodynamics in chemical engineering. A multi-parameter EoS, which can probably offer higher accuracy, needs more parameters that are sometimes not available. So its application is often not convenient. With CEoS, the equation type is often less important than the mixing rules [35, 38], so special attention must often be paid to the selection of appropriate mixing rules.

Mixing rules are quite diverse [38]. For simplicity, two types may be classified as reported by Ghosh [39] and Adrian, et al. [35], namely mixing rules not incorporating excess Gibbs free energy (GE) models and mixing rules incorporating GE models.

The first type of mixing rule includes the van der Waals mixing rule (VDW) and its extensions [38]. A combination of CEoS and this first type have been employed to predict several CXLs [45-51] but there are several drawbacks to using this combination. First, in asymmetric systems prediction, VDW often fails to use constant k_{ij} (the adjustable interaction parameters between component i and component j). For example, Ghosh, concluded that the combination of VDW and CEoS cannot yield promising results for prediction of hydrocarbon solubility in water [39]. Hence, for asymmetric, highly polar, and associating systems, temperature and/or composition dependency must be implemented [35, 38, 39] in mixing rules. However, most mixing rules of this type are empirical in integrating the temperature and composition factors, and this may produce difficulties in modeling complex systems. Another well-known drawback is that k_{ij} must be regressed from experimental data [37, 39, 52], which requires reliable parameter estimation and time-consuming experimental work. Additionally, the extrapolation of k_{ij} to a state beyond the experimental range is connected with uncertainty.

The second type of mixing rule incorporates GE into CEoS models to produce the CEoS/GE mixing rule (see **Fig. 2.1**) firstly attributed to Huron and Vidal [53, 54]. Since that time, quite a number of modified mixing rules have been developed (see **Table 2.1**), e.g., the Predictive SRK mixing rule (PSRK), the Modified HV mixing rule with 1st order simplification (MHV1), the Modified HV mixing rule with 2nd order simplification (MHV2), and the Wong-Sandler mixing rule (WS). A detailed description of the CEoS/GE models is provided in **Appendix 1**.

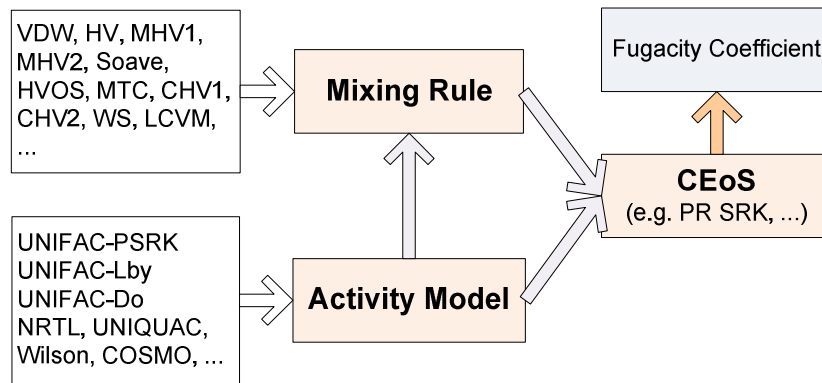


Figure 2.1: Structure of the CEoS/GE model

Table 2.1: A review of mixing rules incorporating GE

Name	ρ ref.	Fluid ref.	B ₂ constraint	B ₃ constraint	Function	Year	Ref.
1 HVO	∞	ideal	No	No	explicit	1978	[53, 54]
2 KTK	∞	ideal	No	No	explicit	1987	[55]
3 WS	∞	ideal	Yes	No	explicit	1992	[56]
4 HVOS	∞	ideal	No	No	explicit	1995	[57]
5 TCO	∞	VDW	Yes	No	explicit	1996	[58]
6 CHV1	∞	ideal	No	No	explicit	1997	[59]
7 MTC	∞	VDW	No	No	explicit	1998	[60]
8 EAL	∞	ideal	Yes	Yes	explicit	2009	[61]
9 HVLP	0	ideal	No	No	implicit	1986	[62]
10 MHV1	0	ideal	No	No	explicit	1990	[63, 64]
11 MHV2	0	ideal	No	No	explicit	1990	[65, 66]
12 HK	0	ideal	No	No	implicit	1990	[67]
13 PSRK	0	ideal	No	No	explicit	1991	[68, 69]
14 Soave	0	ideal	No	No	explicit	1992	[70]
15 HVT	0	ideal	Yes	No	implicit	1994	[71]
16 LPVP	0	ideal	No	No	implicit	1995	[72]
17 Exact	0	ideal	No	No	implicit	1995	[73]
18 TCB0	0	VDW	Yes	No	implicit	1997	[74]
19 CHV2	0	ideal	No	No	explicit	2009	[75]
20 Uniwaals	none	ideal	No	No	implicit	1986	[76]
21 LCVM	none	ideal	No	No	explicit	1994	[77, 78]
22 TCB(r)	none	VDW	Yes	No	implicit	1998	[60]
23 BLCVM	none	ideal	Yes	No	implicit	2004	[79]

Note:

- ‘*p* ref.’ denotes the reference pressure of mixing rules, an important quantity in their simplification. Quite a few mixing rules (**No. 1-8**) use infinite pressure as a reference pressure, while several mixing rules (**No. 9-19**) use zero pressure as a reference pressure. Others (**No. 20-23**) use a reference pressure somewhere between zero and infinity;
- ‘Fluid ref.’ denotes the fluid reference. Most mixing rules use an ideal fluid as a reference, but the mixing rules developed by Twu [58, 60, 74] use van der Waals fluid as a reference;
- B_2 and B_3 are the second and third Virial equation coefficients of CEoS defined as: $B_2 = b - a/RT$, $B_3 = b^2 + (u + w)ab/RT$. B_2 and B_3 constraints are also used in several mixing rules. For that, B_2 constraint is: $B_{2,m} = \sum_i^{NC} \sum_j^{NC} x_i x_j B_{2,ij}$ and B_3 constraint is: $B_{3,m} = \sum_i^{NC} \sum_j^{NC} x_i x_j B_{3,ij}$;
- There are two types of mixing rules concerning the calculation procedure. One approach calculates b_m first, and then calculate a_m , an explicit function. Another approach combines a_m , b_m together as an algebraic equation with two unknowns and finally, an implicit function is formed.

The CEoS/GE mixing rule is likely to achieve better performance than VDW and its extensions, particularly in predicting complex systems such as asymmetric, highly polar, or associating systems. Extrapolation to modest-scale temperature and/or pressure using parameters of activity models, used for lower temperature and lower pressure, can also be performed using the CEoS/GE mixing rule [39, 80]. This model provides a pathway to employing abundant UNIFAC parameters to study the system at a high-temperature and/or high-pressure state, for which little or no experimental data may be available. This is exactly the rationale for developing the PSRK [68, 69], a popular CEoS/GE model. Additionally, researchers have recently implemented a conductor-like screening model (COSMO) into CEoS [81, 82] that shows even greater potential with respect to the versatility of COSMO.

As shown in **Table 2.1**, there are more than 20 mixing rules. It is not our aim to evaluate all mixing rules and some of the more complex mixing rules, such as TCO with VDW fluid as a reference, or EAL bounded with the second and third Virial coefficients, have not been investigated in detail in this work. In this chapter we will, however, evaluate the performance of several mixing rules in reproducing the VLE and VLLE phases.

2.2 Modeling VLE

22 VLE systems are modeled using several CEoS/GE models [52, 83] (**Table 2.2**), i.e., four binary systems, 13 ternary systems, four quaternary systems, and one quinary system. The modeling work covers four CEoS (PR, SRK, MPR, MSRK), 11 mixing rules (HVO, HVOS, MTC, MHV1, MHV2, Soave, CHV2, LCVM, CHV1, WS, PSRK), and two versions of UNIFAC (UNIFAC-Lby and UNIFAC-PSRK). The performance of the combination of CEoS and mixing rule for the 1-octene hydroformylation reaction system is discussed in one of our publications [52]. The detailed modeling work is given in **Appendix 2**. Several multicomponent VLE systems studied in **Chapter 3** (See **Figs. A5.1-A5.4**) are modeled by NRTL-IG model, a necessary distinction.

Table 2.2: Investigated VLE systems [52, 83]

No.	System	CEoS	Mixing rule	Activity model
1	H ₂ O/MeOH	PR	WS	UNIFAC-Lby/-PSRK
2	H ₂ O/CO ₂	PR	WS	UNIFAC-Lby/-PSRK
3	MeOH/DME	PR	WS	UNIFAC-Lby/-PSRK
4	MeOH/CO ₂	PR	WS	UNIFAC-Lby/-PSRK
5	MeOH/DME/CO ₂	PR	WS	UNIFAC-Lby/-PSRK
6	H ₂ O/MeOH/CO ₂	PR	WS	UNIFAC-Lby/-PSRK
7	H ₂ O/MeOH/DME	PR	WS	UNIFAC-Lby/-PSRK
8	H ₂ O/MeOH/DME/CO ₂	PR	WS	UNIFAC-Lby/-PSRK
9	CO ₂ /CO/OCT	4 CEoS	9 mixing rules	UNIFAC-PSRK
10	CO ₂ /CO/NAL	4 CEoS	9 mixing rules	UNIFAC-PSRK
11	CO ₂ /H ₂ /OCT	4 CEoS	9 mixing rules	UNIFAC-PSRK
12	CO ₂ /H ₂ /NAL	4 CEoS	9 mixing rules	UNIFAC-PSRK
13	CO/CO ₂ /ACE	4 CEoS	9 mixing rules	UNIFAC-PSRK
14	H ₂ /CO ₂ /ACE	4 CEoS	9 mixing rules	UNIFAC-PSRK
15	H ₂ /CO/OCT	4 CEoS	9 mixing rules	UNIFAC-PSRK
16	H ₂ /CO/NAL	4 CEoS	9 mixing rules	UNIFAC-PSRK
17	H ₂ /CO/CO ₂ /OCT	4 CEoS	9 mixing rules	UNIFAC-PSRK
18	H ₂ /CO/CO ₂ /NAL	4 CEoS	9 mixing rules	UNIFAC-PSRK
19	H ₂ /CO/OCT/NAL	4 CEoS	9 mixing rules	UNIFAC-PSRK
20	H ₂ /CO/CO ₂ /OCT/NAL	4 CEoS	9 mixing rules	UNIFAC-PSRK
21	O ₂ /CO ₂ /MeCN	4 CEoS	9 mixing rules	UNIFAC-PSRK
22	H ₂ /CO ₂ /PhMe	4 CEoS	9 mixing rules	UNIFAC-PSRK

Note:

- 4CEoS include PR, SRK, and their modifications with Mathias-Copeman α function;

- 9 mixing rules include HV, HVOS, MTC, MHV1, MHV2, Soave, CHV2, LCVM, and CHV1 (See **Appendix 1**).

This chapter gives results for six selected systems, i.e., the VLE of two binary systems (**Figs. 2.2-2.3**), two ternary systems (**Figs. 2.4-2.5**) and two quaternary systems (**Figs. 2.6-2.7**). The results for some other systems are given in **Appendix 3**. The predictive features of the CEoS/GE model for the VLE phase behavior of CXLs is discussed in details [52]. Three main conclusions may be summarized as:

- The CEoS/GE model is considered to be a versatile tool for reproduction of multicomponent VLE phase behavior of CXLs with little data or even no experimental data;
- A priori prediction is essential to the rational selection of CXLs for specific systems to receive a high accuracy;

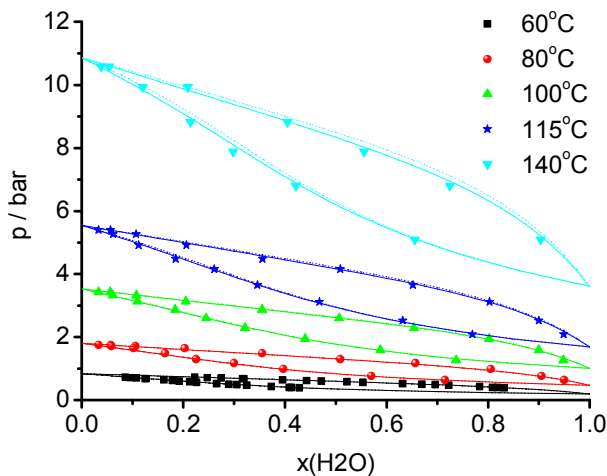


Figure 2.2: Isothermal VLE diagram of H₂O/MeOH system, predicted by PRWS with UNIFAC-PSRK (solid line) and UNIFAC-Lby (dot line)

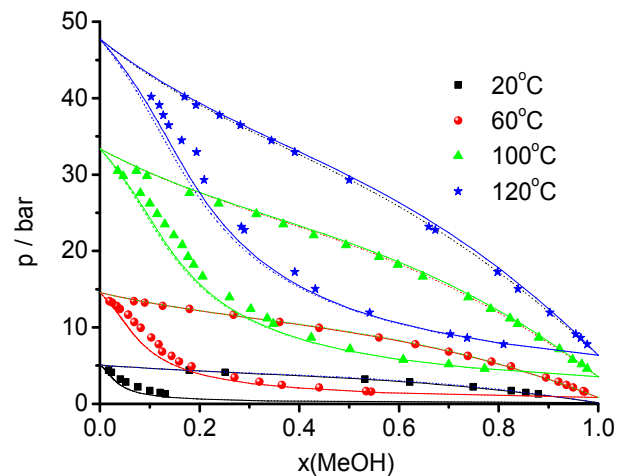


Figure 2.3: Isothermal VLE diagram of MeOH/DME system, predicted by PRWS with UNIFAC-PSRK (solid line) and UNIFAC-Lby (dot line)

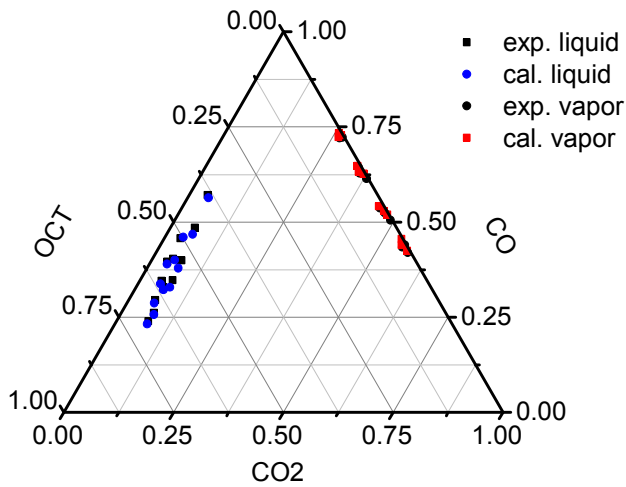


Figure 2.4: VLE diagram of CO₂/CO/OCT at 80bar, 40°C-80°C, predicted by PSRK

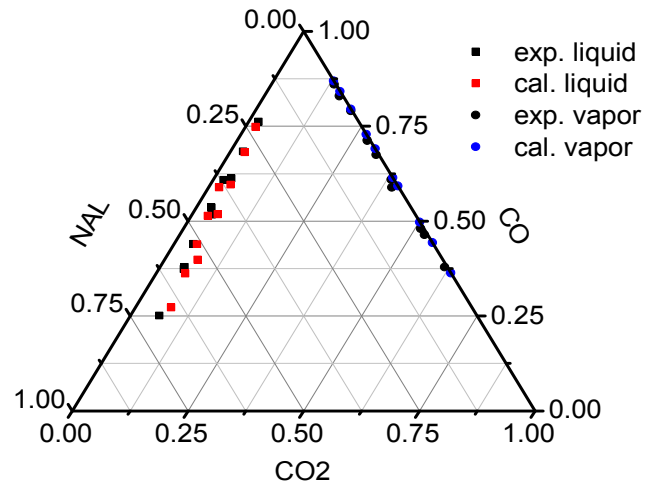


Figure 2.5: VLE diagram of CO₂/CO/NAL at 80bar, 40°C-80°C, predicted by MSRK-LCVM

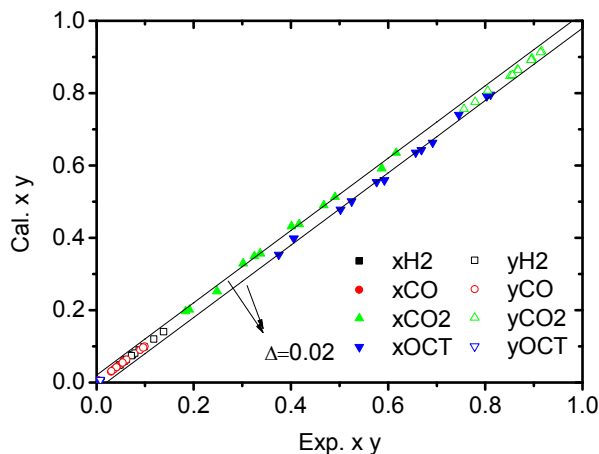


Figure 2.6: VLE parity plot of H₂/CO/CO₂/OCT system between the experimental results and the calculation at 40°C-60°C, 23.0bar-65.6bar, predicted by PSRK

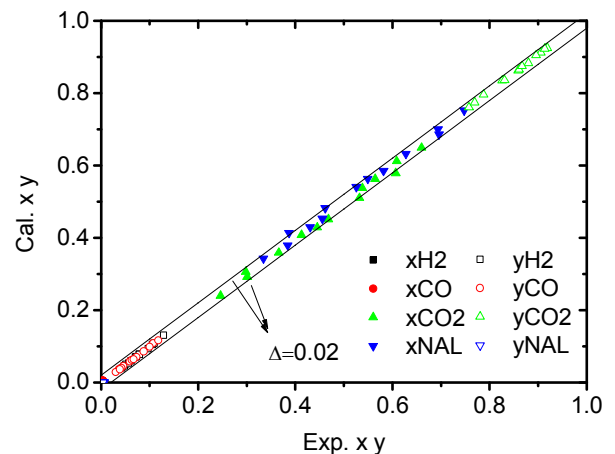


Figure 2.7: VLE parity plot of H₂/CO/CO₂/NAL system between the experimental results and the calculation at 40°C-60°C, 26.9bar-67.1bar, predicted by MSRK-LCVM

2.3 Modeling VLLE

This section describes a more complex phase behavior, VLLE, that has received particular attention. Its application can be found in **Chapter 4**. The WS mixing rule developed by Wong and Sandler [56] has several specific advantages [80], i.e., the ability to predict nonideal and

polar mixtures due to the B_2 constraint and the adjustable interaction parameter k_{ij} and the convenience of applying the UNIFAC activity model due to zero-pressure reference (See **Table 2.1**). On these grounds, five VLE systems (**Table 2.3**) are represented by the PRWS model with three activity models, including UNIFAC-Lby, UNIFAC-PSRK, and NRTL. Moreover, this PRWS is integrated into Aspen Plus, so that process simulation can be conveniently carried out based on the thermodynamic modeling.

The most complex system discussed in this thesis is a quaternary system. Systems with more than four components are not addressed because of a lack of experimental data. The detailed modeling parameters are given in **Appendix 2**, and selected results are shown in **Figs. 2.8-2.11**. More results of investigated systems are given in **Appendix 3**.

Table 2.3: Investigated VLE systems predicted by the CEoS/GE in this thesis [52, 83]

No.	System	CEoS	Mixing rule	Activity model
1	H ₂ O/DME	PR	WS	UNIFAC-Lby/-PSRK
2	H ₂ O/DME/CO ₂	PR	WS	UNIFAC-Lby/-PSRK
3	H ₂ O/MeOH/DME/CO ₂	PR	WS	UNIFAC-Lby/-PSRK
4	H ₂ O/MeCN/CO ₂	PR	WS	UNIFAC-PSRK
5	H ₂ O/DIOX/CO ₂	PR	WS	NRTL

Figs. 2.8-2.9 show a binary system predicted by two different CEoS/GE models, i.e. PRWS and PSRK. However, the two models perform differently both quantitatively and qualitatively. Obviously, the PSRK yields a VLE system, while the H₂O/DME system is in fact a VLE system (**Fig. 2.8**). However, the PRWS succeeds in accurately predicting the VLE system (**Fig. 2.9**). This different behavior arises from the strong non-ideality of the H₂O/DME system (**Fig. A4**) [83]. Similarly, the VLE diagrams of two ternary systems at 39.85°C are accurately reproduced by PRWS (**Figs. 2.10-2.11**).

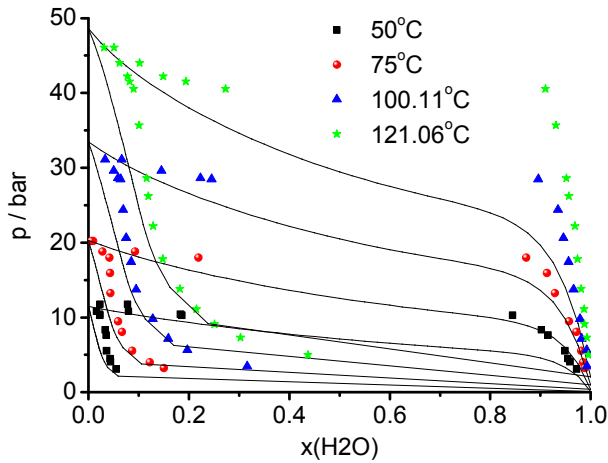


Figure 2.8: Isothermal VLE diagram of H₂O/DME system, predicted by PSRK

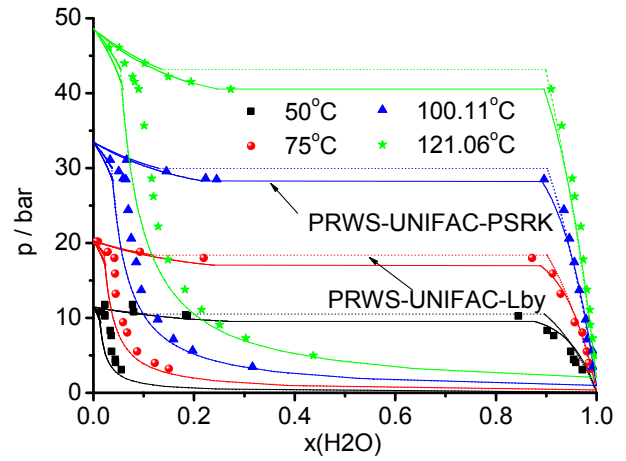


Figure 2.9: Isothermal VLLE diagram of H₂O/DME system, predicted by PRWS

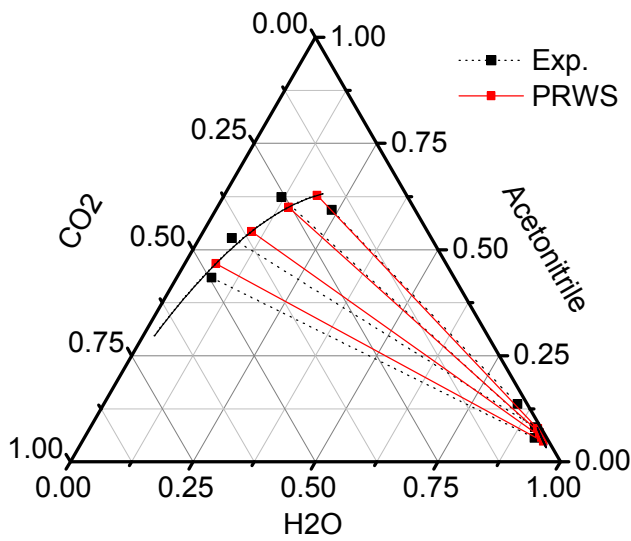


Figure 2.10: Isothermal VLLE diagram of H₂O/CO₂/MeCN system at 39.85°C, 24bar-52bar, predicted by PRWS. Experimental data reference [84].

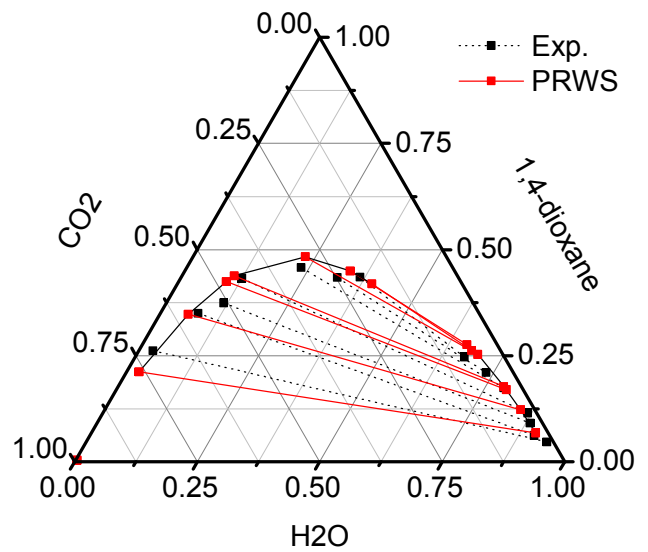


Figure 2.11: Isothermal VLLE diagram of H₂O/CO₂/DIOX system at 39.85°C, 28bar-57bar, predicted by PRWS. Experimental data reference [84].

In short, PRWS is an appropriate model for describing the VLLE phase behavior of CXLs because of the adjustable parameter integrated in the WS mixing rule that allows the model a more flexible fit for strongly non-ideal systems. Moreover, the WS is essentially bounded by

the second Virial coefficient (B_2), producing better performance than mixing rules without such constraints [56].

2.4 Chapter Summary

The CEoS/GE model succeeds in predicting the VLE phase behavior of CXLs, consistent with results of earlier researches with respect to the performance of this model (see **Section 2.1**), but also through our own validation for quite a number of multi-component systems. We find that most of the CEoS/GE models accurately reproduce the VLE phase behavior of CXLs.

However, while not all CEoS/GE models can predict the VLLE phase behavior accurately, in this work, PRWS succeeds in predicting the VLLE phase behavior of several systems. In contrast, PSRK, sometimes recommended as a popular model for predicting the VLE phase behavior of CXLs [52], fails to model the VLLE phase behavior of some systems, such as the VLLE of systems involving DME and H₂O.

The results presented in this chapter demonstrate the advantage of using UNIFAC. The convenience of implementing UNIFAC into the CEoS/GE model provides a means for predicting phase behavior in systems with little or no experimental data.

Science has no final formulation. And it is moving away from a static geometrical picture towards a description in which evolution and history play essential roles.

Dilip Kondepudi
Modern Thermodynamics-From Heat Engines to
Dissipative Structures, 2004.

Chapter 3

Dynamic Determination of Phase Equilibria

In the previous chapter, the importance of phase equilibria to industrial processes is emphasized and the thermodynamic models are used to predict the VLE and VLLE phase behavior of CXLs systems. Another point regarding the field of the phase equilibria is the question on how to determine the phase equilibria numerically in an efficient manner. This knowledge is indispensable, especially for process simulation. Considering the complex nature multiphase and multicomponent systems involved in this thesis (e.g., VLLE), an efficient method to determine the phase equilibria is of particular importance. Therefore, the main work of this chapter is on developing such an efficient approach to determine phase equilibria. It has to be mentioned that this approach developed here is not only suitable for calculating phase equilibria involved in this thesis, but also for other types of complex phase equilibria.

With this purpose, a novel idea is proposed in the first place. The mass balance equations are formulated based on the mass transfers among phases with respect to each constituent in a closed system. The mass balance equations are derived according to the chemical potential theory. As a result, a set of ODEs is formulated (dynamic equations) (**Section 3.2**). After that, the new approach is evaluated by the universal criteria of phase equilibrium, which have been developed in accordance with the second law of thermodynamics and dissipative thermodynamics, and then this approach is exemplified by 17 systems with different phase behaviors and thermodynamic methods (**Section 3.3**). Finally, the new approach towards two engineering problems of phase behavior determination is discussed (**Section 3.4**). All results show that the new approach is an efficient and powerful alternative for phase behavior determination to conventional approaches.

3.1 Introduction

The scientific literature on fluid phase equilibria goes back well over 150 years [85], and the fundamental extremum thermodynamic principle of phase equilibria criteria has been established: all isolated systems evolve to the state of equilibrium in which the entropy (S) reaches its maximum value. However, physical or chemical systems are subject to constant pressure and/or temperature more often in practical situations. Thus, the evolution of a system to the state of equilibrium corresponds to the extremization of a thermodynamic potential, including the Gibbs free energy (G), Helmholtz free energy (A), enthalpy (H), and internal energy (U) [86] (**Table 3.1**).

Table 3.1: A brief review of phase equilibrium criteria

Constraints	Equilibrium criteria	Stability criteria	Systems	Reference
Constant U, V	Max. $S, dS=0$	$d^2S < 0$	Isolated system	[36, 86, 87]
Constant S, V	Min. $U, dU=0$	$d^2U > 0$	Closed system	[86]
Constant S, p	Min. $H, dH=0$	$d^2H > 0$	Closed system	[86]
Constant T, V	Min. $A, dA=0$	$d^2A > 0$	Closed system	[36, 86, 87]
Constant T, p	Min. $G, dG=0$	$d^2G > 0$	Closed system	[36, 86, 87]

In accordance with the extension of the second law of thermodynamics [86, 87], the entropy changes in a system are due to internal changes as well as external interactions:

$$dS = d_e S + d_i S, \text{ where}$$

$d_i S$ represents entropy change in the interior of the system;

$d_e S$ represents entropy change due to energy and matter exchange with the external surroundings.

If we consider an isolated system or a closed system without entropy flux ($d_e S = 0$), it follows that the entropy increases until it reaches a maximum at equilibrium [36, 86, 87]. The equilibrium state is asymptotically stable and forms a global attractor. This satisfies the second law and thus the general phase equilibrium criteria: $\frac{dS}{dt} = \frac{d_i S}{dt} = \sigma_s \geq 0$ and

$$\frac{d^2 S}{dt^2} = \frac{d^2_i S}{dt^2} = \frac{d\sigma_s}{dt} \leq 0 \quad (3.1/3.2)$$

Eq. (3.1) and **Eq. (3.2)** are comparable with the stability of the equilibrium state expressed in **Table 3.1**, and are used to validate the new approach in **Section 3.3**.

To summarize an intensive review of calculation methods to determine phase equilibrium, a schematic diagram is given (**Fig. 3.1**), in which two current branches as well as the new approach expressed in this chapter are classified. The evolutions of objective functions in detail are presented in **Table 3.2**.

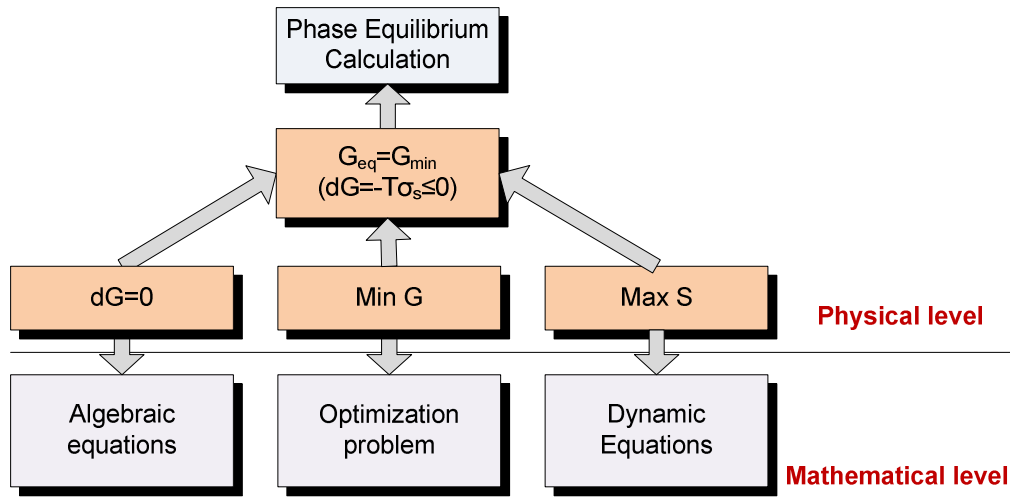


Figure 3.1: A schematic review of phase equilibrium calculation

Table 3.2: A brief review of objective function for current two approaches

Approach to algebraic equations	
Objective function	Reference
Equivalence of fugacity	Examples [36, 85, 88-90]
RRE	Original work [91]
Modified RRE	Instances [92-98]
Approach to optimization problem	
Objective function	Reference
Min. G	Original works [99, 100], recent works [101-104], review [105].
Min. TPDF	Original works [106-108], evolutions [105, 109-116], review [117].
Min. modified TPDF	Original works [118-122].
Area method	Original works [123, 124], evolutions [125-127].
τ method	Original works [128], evolutions [129-132]

Note:

- RRE is the abbreviation of Rachford-Rice equation;
- TPDF is the abbreviation of Tangent plane distance function.

First of all, algebraic equations can be formulated in accordance with the equivalences of fugacity for each constituent in each phase. As a matter of fact, this approach is formulated concerning the equilibrium state as the starting state. To solve the algebraic equations of equilibria, three popular methods are used, i.e., substitution methods [36, 88], Newton or

Quasi-Newton methods [95-98, 133] (see review [102]), and homotopy continuation method [117, 134-138] (see review [139, 140]). However, as an illustration, although the direct substitution method converges fast, this method is limited and can only be used for calculating simple ideal systems, where the fugacity coefficients are only weakly dependent on the phase composition [108]. The application of the Newton method and Newton based methods is limited due to the critical requirements that the initialization must be close enough to the solution.

In contrast to the algebraic equations, another approach starts from non-equilibrium state. As a consequence, an objective function is minimized, i.e., minimum G, minimum TPDF, minimum modified TPDF, maximum Gibbs free energy surface integration (also named area method) and τ method. On the whole, the minimum Gibbs free energy and the minimum TPDF are the most popular two, and they are a necessary and sufficient condition for the phase equilibrium. Other objective functions have downsides. For example, in spite of several derivations of minimum modified TPDF, they are applied rarely. Whereas, for the area method and the τ method, there is no guarantee to prove that they are necessary and sufficient conditions for phase equilibrium. With the goal to find the optimal solutions, A variety of optimization methods can be employed. For that, Kangas has classified two global methods, i.e., stochastic optimization methods and global deterministic optimization methods [117].

Steyer et al. [141] used a rate-based approach to determine liquid-liquid equilibrium (LLE), which starts also from non-equilibrium state. Through four cases, the high efficiency of the approach is confirmed in comparison with homotopy. However, the approach cannot be used to determine other phase behaviors apart from LLE, and the work did not attest the necessary and sufficient conditions of phase equilibrium of this approach.

Quite a number of popular methods for calculating phase equilibrium still face challenges when used for solving engineering problems.

- The first challenge comes from intrinsic thermodynamic models themselves. Most of the models applied regressed parameters from pure components, binary mixtures or low scale multicomponent mixtures and there is great uncertainty when employing these parameters with specific mixtures [114]. Moreover, the models have non-uniqueness of minima and maxima in the Gibbs energy surface, which is directly used to determine thermodynamically stable, metastable and unstable equilibrium states [142]. Therefore, the objective function consists in the highly non-linear and non-convex form, which gives no rigorous guarantee that the global minimum will be found [101, 109, 111];
- The second challenge comes from the prior determination of the number of phases [105, 113, 131, 142]. Usually a small number of phases are assumed. If they are not stable, phases will be split adding a new phase to reformulate the mathematical objective

function and the phase equilibrium calculation is repeated. This process continues until the appropriate number of phases is found. The phase equilibrium can then be identified numerically. However, if too many phases are assumed, numerical problems may arise, or cause the solution to converge to a trivial or local extrema [105, 113, 131].

- The third challenge regards the numerical difficulties encountered using numerical techniques [114, 142], which sometimes are very complex.

3.2 Dynamic Equations

A closed system with constant temperature and pressure is investigated in accordance with other works as reviewed in **Section 3.1**. If a phase, namely phase α , is considered as an object, the mass balance of the phase α is expressed (in molar quantities):

$$dn^{(\alpha)}/dt = \text{Inflow} - \text{Outflow} \pm \text{sources/sinks} \quad (3.3)$$

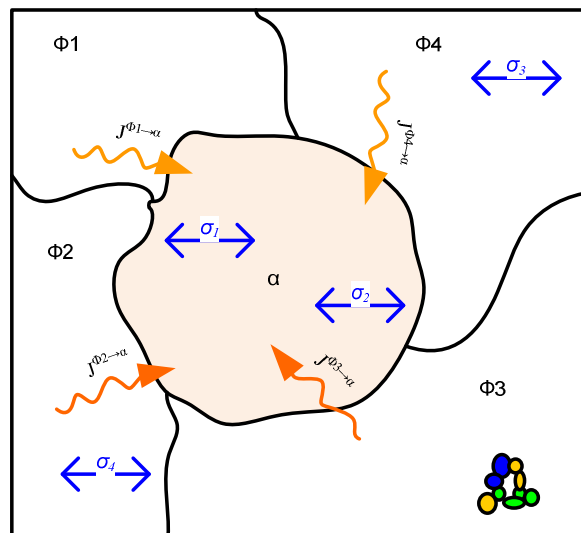


Figure 3.2: Schematic diagram of mass transfer and reaction in a closed system

If the system is not homogeneous, then there are other phases (one or more), which surround the specific phase α (**Fig. 3.2**). In addition with the reactions in each phase with respect to each constituent, thus it follows: $dn_{ic}^{(\alpha)}/dt = \sum_{k=1}^{NP} J_{ic}^{(k \rightarrow \alpha)} + \sigma_{r,ic}^{(\alpha)}$ (3.4)

In accordance with linear dissipative thermodynamics, the mass fluxes \mathbf{J} are driven by conjugated mass transfer forces \mathbf{X} , and the forces are chemical potential differences with respect to each component between the phase α and the phase surrounding the phase α [86,

$$87]: J_{ic}^{(k \rightarrow \alpha)} = \frac{kA}{RT} \cdot X_{ic}^{(k \rightarrow \alpha)} = \frac{kA}{RT} \cdot (\mu_{ic}^{(k)} - \mu_{ic}^{(\alpha)}) \quad (3.5)$$

Coupling the definition of the chemical potential based on the ideal gas:

$$\mu_{ic}(T, p, \{x\}) = \mu_{ic}^{ig}(T, p) + RT \ln(f_{ic}/p) \quad (3.6)$$

With regard to **eqs. (3.5) (3.6)**, the **eq. (3.4)** is derived as:

$$\frac{dn_{ic}^{(\alpha)}}{dt} = kA \ln \left[\prod_{k=1, k \neq \alpha}^{NP} f_{ic}^{(k)} / (f_{ic}^{(\alpha)})^{NP-1} \right] + \sigma_{r,ic}^{(\alpha)} \quad (3.7)$$

This equation is a schematic equation, which figures out the relationship of each component in a specific phase and fugacity of the component in all phases. The meaning of the symbols expressed above is listed here.

$n_{ic}^{(\alpha)}$	stands for the mole of constituent ic in the phase α ;
$J_{ic}^{(k \rightarrow \alpha)}$	stands for the flux from phase k to phase α with respect to component ic ;
$\sigma_{r,ic}^{(\alpha)}$	stands for the source or sinks with respect to component ic in the phase α .
$X_{ic}^{(k \rightarrow \alpha)}$	stands for the force from phase k to phase α with respect to component ic ;
$\mu_{ic}^{(k)}$	stands for the chemical potential of the constituent ic in phase k ;
kA	stands for the product term of mass transfer coefficient k and the interfacial area A ;
$\mu_{ic}(T, p, \{x\})$	stands for the chemical potential of a mixture under T, p condition with composition $\{x\}$;
$\mu_{ic}^{ig}(T, p)$	stands for the chemical potential of a pure ideal gas under T, p condition;
$f_{ic}^{(k)}$	stands for the fugacity of the constituent ic of mixture in phase k , which is a function of $T, p, \{x\}$;
$\prod_{k=1, k \neq \alpha}^{NP}$	k is phase ID, which counts from 1 to NP , but k cannot be equal to α ;

A closed system without any reactions is the specific interest of this thesis. Therefore, the **eq. (3.7)** is simplified as:
$$\frac{dn_{ic}^{(\alpha)}}{dt} = kA \ln \left[\prod_{k=1, k \neq \alpha}^{NP} f_{ic}^{(k)} / (f_{ic}^{(\alpha)})^{NP-1} \right] \quad (3.8)$$

However, the **eq. (3.8)** cannot to be solved directly, because the number of equations is less than the number of unknowns ($\{x\}, \{n\}$). There are $NC*NP$ equations, whereas, the unknowns are $2NC*NP$. For this reason, the number of unknowns has to be reduced.

Here $\theta_{ic}^{(\alpha)}$, which denotes the phase partitioning coefficient of the constituent ic in the fluid phase α with respect to all constituents, is implemented. With regard to the definition of $\theta_{ic}^{(\alpha)}$, it follows:
$$\theta_{ic}^{(\alpha)} = n_{ic}^{(\alpha)} / n_{ic}^{tot}, \quad \sum_{k=1}^{NF} \theta_{ic}^{(k)} = 1 \quad \text{and} \quad n_{ic}^{(\alpha)} = \theta_{ic}^{(\alpha)} \cdot n_{ic}^{tot} \quad (3.9)$$

Since the reaction is not involved here, so $n_{ic}^{tot} = n^{tot} \cdot z_{ic}^{tot}$, and
$$n_{ic}^{(\alpha)} = \theta_{ic}^{(\alpha)} \cdot n^{tot} \cdot z_{ic}^{tot} \quad (3.10)$$

$$\text{It follows } x_{ic}^{(\alpha)} = n_{ic}^{(\alpha)} / \sum_{ic=1}^{NC} n_{ic}^{(\alpha)} = \theta_{ic}^{(\alpha)} \cdot z_{ic}^{tot} / \sum_{ic=1}^{NC} (\theta_{ic}^{(\alpha)} \cdot z_{ic}^{tot}) \quad (3.11)$$

Thus, the relationship among $\{\theta\}$, $\{x\}$ and $\{n\}$ can be established concerning the **eqs. (3.9-3.11)**. The unknowns ($\{x\}, \{n\}$) are replaced by the new unknowns $\{\theta\}$. In this way, the number of unknowns is reduced to a value equal to the number of equations. Consequently, the dynamic equations can be solved in principle.

Inserting the **eq. (3.10)** into **eq. (3.8)**, an equation is yielded:

$$\frac{d\theta_{ic}^{(\alpha)}}{dt} = \frac{kA}{n^{tot} \cdot z_{ic}^{tot}} \ln \left[\frac{\prod_{k=1, k \neq \alpha}^{NP} f_{ic}^{(k)}}{(f_{ic}^{(\alpha)})^{NP-1}} \right] \quad (3.12)$$

These are the dynamic equations which cover a closed system without any reactions, and they are used to determine the most practical phase behaviors in the field of chemical engineering in this thesis, i.e., VLE, LLE, VLLE and LLLLE. The calculation of solid solubility is not particular interest, because the scale of the mathematical equation (e.g., SLE) is only one and current methods, e.g., Newton method, can handle it efficiently. Therefore, the development of a specific approach is not necessary. Moreover, two facets are summarized for the calculation in detail.

- Firstly, the reduction of the scale of the ordinary differential equations (ODEs) is reasonable in accordance with $\sum_{k=1}^{NF} \theta_{ic}^{(k)} = 1$. Thereby, only $NP-1$ fluid phases are investigated with regard to the $\theta_{ic}^{(k)}$;
- Secondly, several parameters can be fixed as constant values. For example, $n^{tot} = 1$. Similarly, the value of k and A is set as 1 in this thesis, because they do not affect stable solutions once ODEs reach equilibrium state in principle, but just affect the calculation time to approach the steady-state. However, they cannot be too large or too small; otherwise, the ODEs will be stiff if kA is too large or the calculation needs a long time if kA is too small.

Here are several detailed equations for calculating the phase equilibria of VLE, VLLE, LLE, and LLLLE in this thesis (**Table 3.3**).

Table 3.3: Dynamic equations for calculating the phase equilibria

Type	Investigated phases	Simplified dynamic equation
VLE	Liquid	$d\theta_{ic}^L/dt = \ln(f_{ic}^V / f_{ic}^L) / z_{ic}^{tot}$

LLE	One liquid	$d\theta_{ic}^{L2}/dt = \ln(f_{ic}^{L1}/f_{ic}^{L2})/z_{ic}^{tot}$
VLLE	Two liquid phases	$\left\{ \begin{array}{l} d\theta_{ic}^{L1}/dt = \ln[f_{ic}^V \cdot f_{ic}^{L2}/(f_{ic}^{L1})^2]/z_{ic}^{tot} \\ d\theta_{ic}^{L2}/dt = \ln[f_{ic}^V \cdot f_{ic}^{L1}/(f_{ic}^{L2})^2]/z_{ic}^{tot} \end{array} \right.$
LLLE	Two liquid phases	$\left\{ \begin{array}{l} d\theta_{ic}^{L1}/dt = \ln[f_{ic}^{L3} \cdot f_{ic}^{L2}/(f_{ic}^{L1})^2]/z_{ic}^{tot} \\ d\theta_{ic}^{L2}/dt = \ln[f_{ic}^{L3} \cdot f_{ic}^{L1}/(f_{ic}^{L2})^2]/z_{ic}^{tot} \end{array} \right.$

Note:

- The fugacity of vapor (or gas) phase is usually calculated using this equation:
 $f_i^V = p \cdot \phi_i^V$, ϕ_i^V denotes the fugacity coefficient of component i in the vapor phase;
- The fugacity of liquid phase(s) is usually calculated either using this equation:
 $f_i^L = p \cdot \phi_i^L$ or using activity coefficient: $f_i^V = p_i^s \cdot x_i \cdot \gamma_i$, here p_i^s denotes the saturated pressure of component i and γ_i denotes the activity coefficient of component i .

3.3 Validation and Evaluation

The previous section has formulated the dynamic equations, whereas, in this section, the validation of the dynamic equations will be discussed using results collected from 17 examples, which cover different multicomponent, multiphase and different thermodynamic methods.

The 17 cases presented in **Table 3.4** are shown in more detail in **Table A4.1, Appendix 4**. It clearly shows that the investigated instances in this thesis cover the phase behaviors from low component scale to high component scale. Only two cases are discussed as representatives in this section to avoid repetition. It is well-known that if the system is not ideal when it contains more than one liquid phase, such as in LLE, VLLE, LLLE, etc. systems. The equilibrium phase behaviors for two complex cases are depicted in **Fig. 3.3** and **Fig. 3.4** in which phase behavior calculations are usually extremely difficult to solve owing to the highly non-ideal behavior. Random initial values were generated for these two systems. More results are presented in **Table A4.2**, the consistency of all calculated results for all investigated systems confirms the feasibility of the dynamic equations to determine the phase equilibria.

Table 3.4: A review of investigated systems and phase types in this work

NC	Type of equilibrium (No. of case, default=1)			
	VLE	VLLE	LLE	LLLE
1	--	--	--	--
2	×	--		--
3	×	×(2)	×	× (3)
4	×			
5	×	×	×	
6	×			
7			×	
10	×	×	×	

'--' denotes: unavailable flash type calculated by this method due to the phase law.

'×' denotes: the case of phase equilibrium is involved in this work.

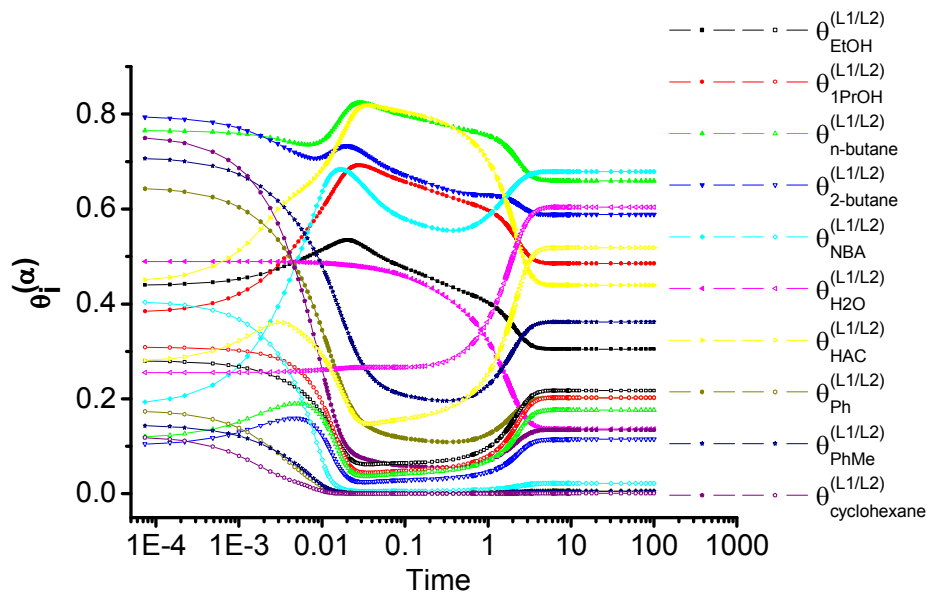


Figure 3.3: Calculation of the ten component VLLE case with random initialization (system ID (SID)=14)

Note:

- The time used in the diagrams of this chapter and the **Appendix 4** is the specified time for the ODE solver (ode45 and ode15s) in MATLAB, but it is not real running time of the computation.

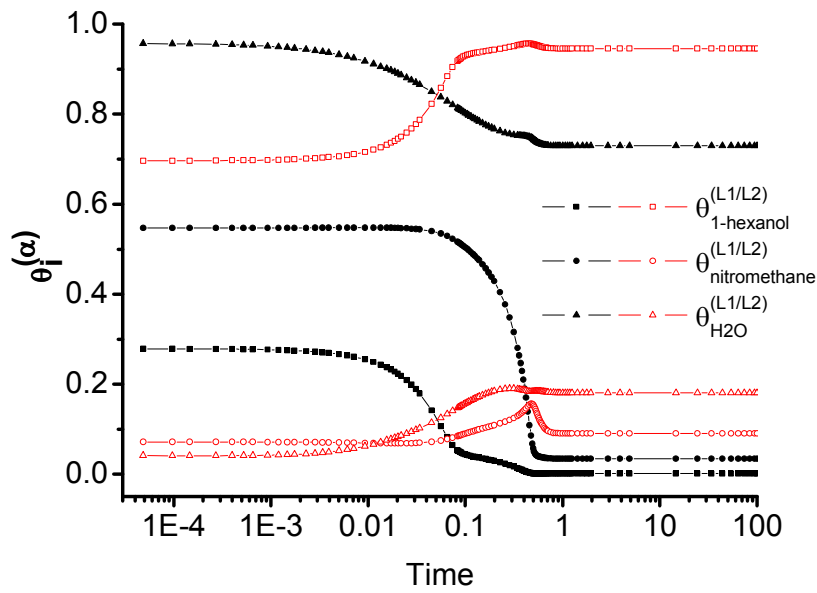


Figure 3.4: Calculation of the three component LLE case with random initialization (SID=15)

To evaluate whether the dynamic equations follow the phase equilibrium criteria, **eq. (3.1)** and **eq. (3.2)** are calculated using **eq. (3.5)** for four selected complex systems. One can see in **Fig. 3.5** how the entropy production rate (σ_s) decreases and eventually reaches zero. Meanwhile, the first derivative of the entropy production rate ($d\sigma_s/dt$) increases simultaneously, also reaching zero (**Fig. 3.6**). It can then be said that the dynamic equations have satisfied the phase equilibrium criteria ($\sigma_s \geq 0$ and $d\sigma_s/dt \leq 0$).

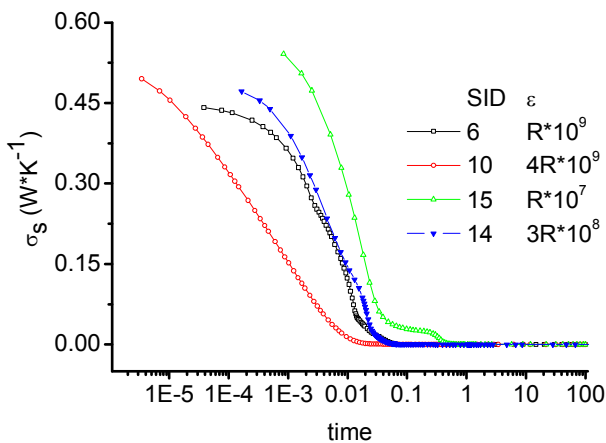


Figure 3.5: Entropy productions of four systems (divided with ϵ)

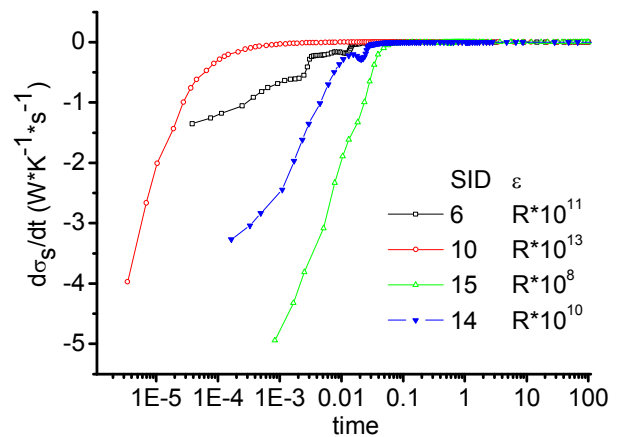


Figure 3.6: First derivation of entropy production of four systems (divided with ϵ)

Note:

- A factor, namely ε , is used in the diagrams to adjust the profiles in the same scale for the reason of easy reading;
- In accordance with linear dissipative thermodynamics [86, 87], the entropy production rate (σ_s) can be calculated using: $\sigma_s = \sum_k J_k X_k$, and there is only one kind of forces

involved in this work: $X_{ic}^{(k \rightarrow \alpha)} = \frac{\mu_{ic}^{(k)} - \mu_{ic}^{(\alpha)}}{T}$.

3.4 Towards Engineering Problems

The previous section describes the excellent performance of the dynamic equations to determine the phase equilibria and their adherence to phase criteria. Two specific problems (the prior determination of phase number and numerical difficulties) relevant to engineering aspects of phase equilibrium determination (as discussed in **Section 3.1**) are discussed.

When using the dynamic method presented in this work, a high number of phases should be chosen at the onset of the problem, because how many phases will coexist at the equilibrium state is unknown. Due to the thermodynamic constraints, the constituents in unstable phases will incorporate into other phases. As a result, the extra, virtual phases will disappear, leaving only those phases that are necessary for equilibrium. This can also be explained physically, in that it is not possible to exist in a non-equilibrium phase if there is no external influence. To evaluate the feasibility of this method, several additional phases were added to complex systems (**Appendix 4**), of which two are shown here. For example, two additional liquid phases were assumed for a system of VLE (**Fig. 3.7**) and LLLE (**Fig. 3.8**), such that they could be represented as VLLLE and LLLLE systems, if desired. Random initializations were used for all calculations. The consistency of the results shows the adherence to the physical nature of the problem and confirms the powerful ability of this approach. Other implementations using the homotopy and Newton methods failed.

Looking at the case of LLLE in more detail (**Fig. 3.8**), this normally three phase system was modeled with five liquid phases. In accordance with the phase rule (Freedom=Component number-Phase number+2), it is obvious that the maximum phase number is three with the known temperature and pressure. The dynamic equations start in an unstable state with virtual phases and continuously approach the equilibrium condition, which features three phases. The driving force of the chemical potential difference drives the non-equilibrium system to approach the stable equilibrium state. Therefore, the objective function (the dynamic equations presented here) adheres to the physical constraints during simultaneous calculation. This is in contrast to other current methods that are not able to handle this problem. The other methods

require the objective function to be strongly dependent on the initialization (such as initial values for phase number and phase composition). Also, once this function is fixed, it does not allow for simultaneous feedback with the physical limitations of the system. Instead, the artificial feedback of increasing the phase number as mentioned above must be undertaken. As a consequence, the mathematical calculation does not have any physical meaning once the initialization of the phase number is incorrect and will fail as a result.

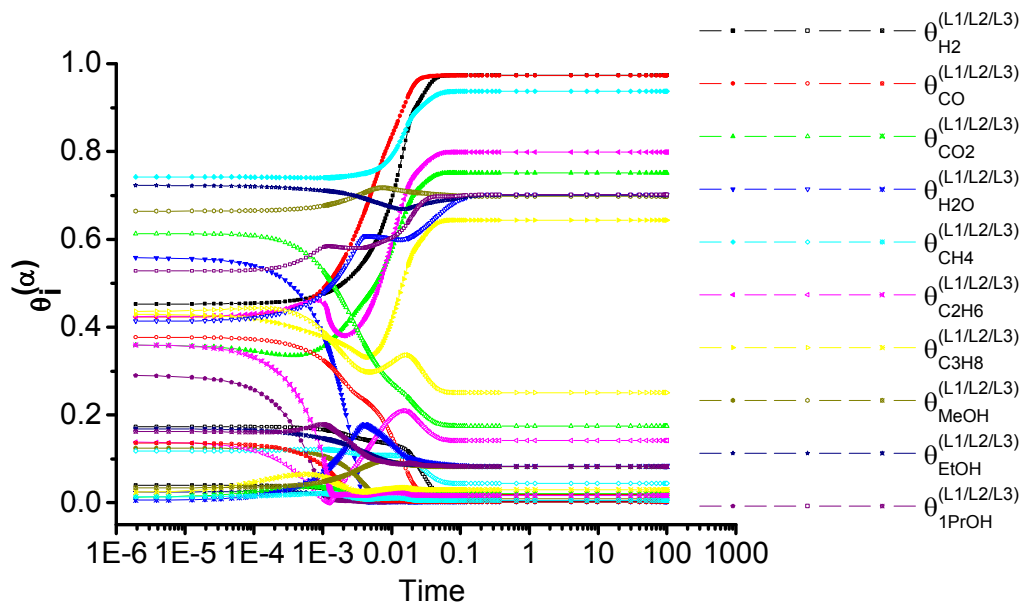


Figure 3.7: The VLE (SID=6, NC=10) calculated by a VLLLE (30 unknowns) with random initialization cases

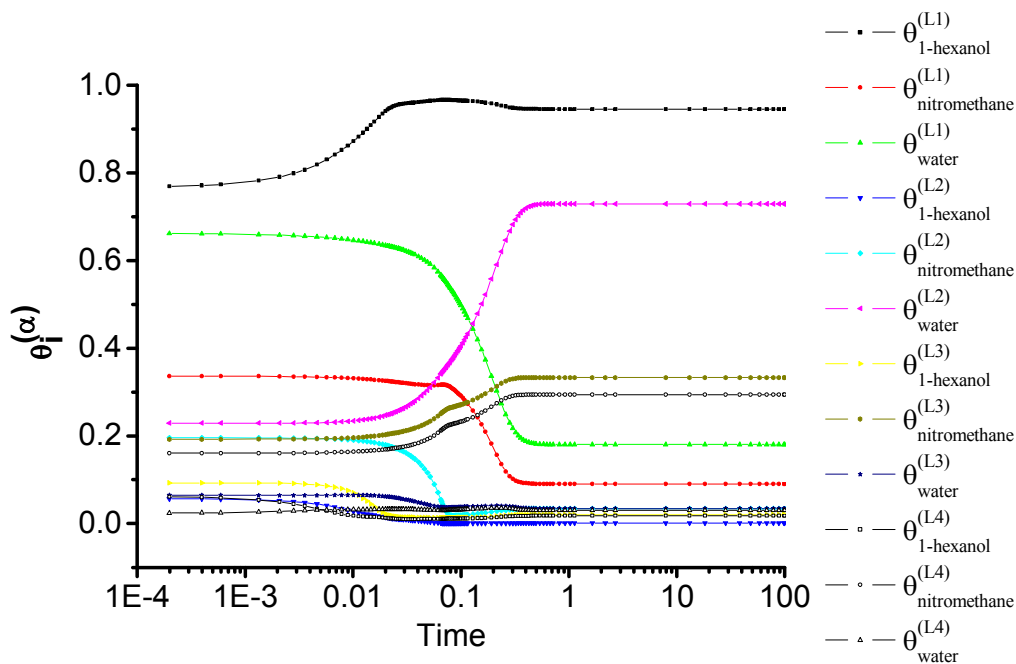


Figure 3.8: The LLLLE (SID=15, NC=3) calculated by a LLLLLLE (12 unknowns) with random initialization cases

In addition to the benefits gained from using this method, there are still several other important aspects to be considered.

- The first of these is the simpler programming required for the dynamic equations. This eliminates the numerical difficulties usually encountered in phase equilibrium calculations. As a consequence, current approaches feature a multitude of specific algorithms which are not easy to handle. In contrast, the method presented here focusses on the physical level with respect to the chemical knowledge and is thus easier to implement than other methods.
- Another aspect is the calculation speed. For example, it costs only seconds for solving the VLLE system with 30 unknowns (Windows XP professional, CPU i3-2100, 3.10GHz, RAM 3.23GB, Matlab 2010b, ODE solvers: ode45 or ode15s), and the calculation of the ten component VLLE case in Matlab is nearly as fast as the calculation in the commercial software Aspen Plus (flash3 module) for the same conditions. Of course, the computation depends not only on the methodology, but also the hardware, programming platform, programming technology, etc. For this object, Steyer et al. [141] have confirmed that the method is more efficient when compared to other methods for LLE calculation.
- A good initialization is usually extremely important to calculation, whereas the achievement of good initialization is difficult. In this work, random initial values were used. The one exception is that the initial values should not all have the same value; otherwise the assumption of equal composition in all phases is performed and causes quasi-equilibrium state without any force and flux.

3.5 Chapter Summary

The dynamic equations are formulated using a novel approach concerning the mass transfer among all phases. This method has been studied for 17 cases and evaluated by the phase equilibrium criteria. This method can be used to determine the complex phase equilibrium of multi-component systems in multiple phases in a closed system with constant temperature and pressure. These equations follow the phase equilibrium criteria to maximize the entropy of a closed system simultaneously to numerical calculation. Starting from a non-equilibrium state using virtual phases it is possible to calculate the equilibrium conditions by considering the mass transfer among all phases. This is unique feature of this new approach compared to the other classical approaches (**Fig. 3.9**).

In summary, this method is well suited for multi-component systems with quite a number of chemical species and phases. It can distinguish between real and virtual phases, it is independent of the thermodynamic model, it is easy to understand for practical use by engineers, it is highly efficient, and can use random initialization.

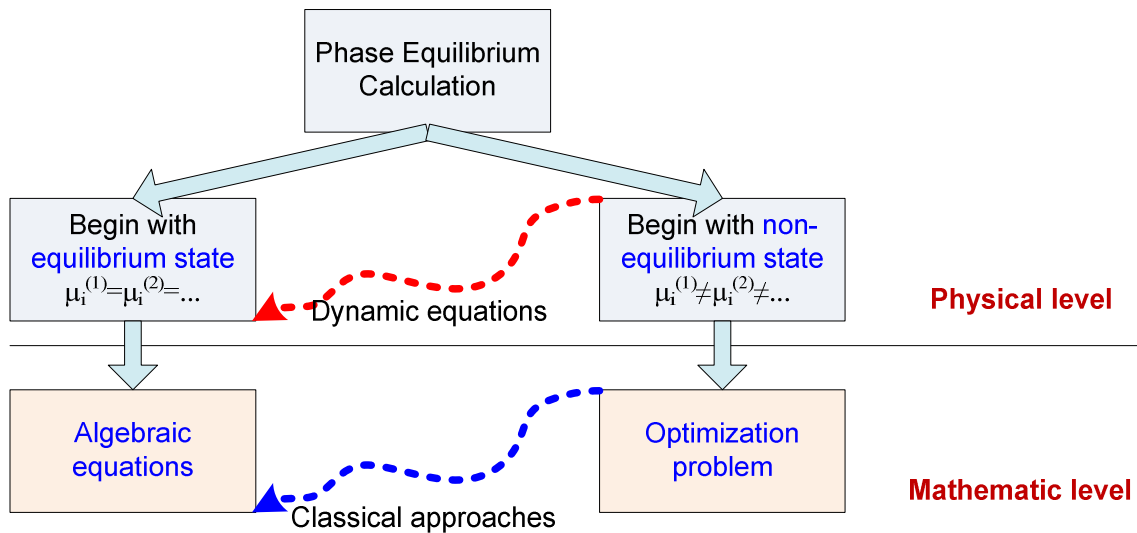


Figure 3.9: A view of link between non-equilibrium and equilibrium state for different approaches of phase equilibrium

Part II

Applications

The separation of chemical mixtures into their constituents has been practiced, as an art, for millennia.

J. D. Seader, et al.
Separation Process Principles, 1998

Chapter 4

Azeotropic Mixture Separation Using CO₂

The last two chapters in Part I focus on the identification of phase behavior, in particular with CXLs. With this basis, the application of CXLs in separation processes and reaction processes will be illustrated in the coming two chapters (Part II), respectively. The effect of phase behavior variation in the phase level on the higher hierarchical levels will be investigated comprehensively.

In this chapter, a particular separation concept for the azeotropic mixture separation by phase behavior tuning using pressurized CO₂ is proposed, and then corresponding process variants are founded and validated in the process simulation. The significant potential of the new process is indicative of an economic alternative to separate azeotropic mixtures using this concept.

4.1 Introduction

The most popular application of CO₂ is the supercritical extraction [143]. The principle is that substances are able to be dissolved in scCO₂ dramatically. In another word, CO₂ plays a role of 'extractor' as scCO₂. There is another concept of separation using CO₂, and the principle is that CO₂ can change miscibility. An interesting experimental phenomenon has been discovered in the 1950s [144, 145]. It is illustrated as follows. Homogeneous aqueous solutions of alcohols or other polar solvents can be split into two liquid phases by pressurized gases, so called 'salting out' agents [35, 145]. In this regard, CO₂ is one of the most popular 'salting out' agents. The liquid can be split into two liquids as a VLLE phase behavior by pressurizing CO₂, and the transition occurs at the lower critical solution pressure (LCSP). The liquid splits into an organic-rich liquid phase and a water-rich liquid phase. If the pressure is

increased further, the upper critical solution pressure (UCSP) may be reached, at which point, the organic-rich phase merges with gas phase [5] (**Fig. 4.1**).

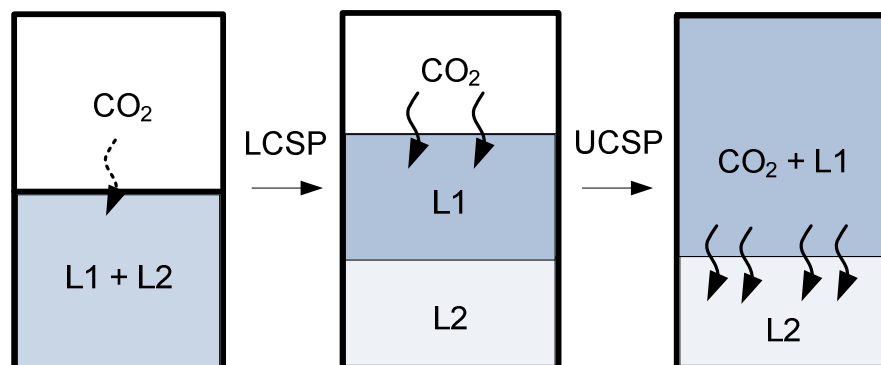


Figure 4.1: The phase changes observed upon expanding a mixture of two miscible liquids past a LCSP and a UCSP

In the past, quite a number of research works focused on the experimental investigation of such interesting thermodynamic phenomena, e.g., as reviewed by Adrian et al. [35]. Also, the hypothetical potential of applying ‘salting-out’ agents for the technical separation purposes in a chemical process has been mentioned in several publications [145-149]. Even, CO₂ can be used to separate the homogeneous catalyst based on the ‘salting out’ principle [150, 151]. The review of the experimental works with ‘salting-out’ performance of the organic-water system is shown in **Table 4.1**. However, the application of other gases is not feasible, with the exception of CO₂. For instance, the C₂H₄, C₂H₆, C₃H₈, and C₄H₁₀ are not safe on account of flammability. The chlorofluorocarbon (here including CClF₃, CHF₃) has destructive effects on the ozone layer [152], and therefore has been banned in many areas. N₂O is a greenhouse gas with a tremendous global warming potential, since it has 298 times more impact 'per unit weight' than CO₂ [153].

However, almost all contributions focus on experimental work to understand the complex phase behavior, but there are only a few works involving thermodynamic modeling. To the best of our knowledge as of today there is no rigorous modeling and simulation study dealing with the prediction and evaluation of such a ‘salting-out’ approach for technical relevant mixtures and process streams. In particular, there is no publication which applies the special phase behavior tuning using pressurized CO₂ in a technical separation process and quantitatively compares the separation costs of this concept.

For this reason, the focus of this work is the validation of the fundamental idea to separate azeotropic mixtures by phase behavior tuning using pressurized CO₂ at the technical process level, and on the quantitative investigation and evaluation of the potential of the novel process.

Table 4.1: Review of investigated water- hydrophilic solvent systems involved in the concept

Solvent	CO ₂	C ₂ H ₄	C ₂ H ₆	C ₃ H ₈	C ₄ H ₁₀	CClF ₃	CHF ₃	N ₂ O
MeOH ^{ZS, M}	x						□	
EtOH ^{AS, M}	x		□	□				
1PrOH ^{AS, M}	x	x	x			x	x	
2PrOH ^{AS, M}	x	□			□			
1BuOH ^{AS, PS}	x							
MePOH ^{AS, M}	x							
tBuOH ^{AS, M}		□						
ACE ^{ZS, M}	x	x	□					
BUE ^{AS, M}	x	x	x			x		
HAC ^{ZS, M}	x	x						
HPA ^{ZS, M}	x	x						
HBA ^{AS, PS}	x							
MeCN ^{AS, M}	x	x						x
DIOX ^{AS, M}	□							
THF ^{AS, M}	□							
DMSO ^{ZS, M}	□							

Note:

x: summarized result by Adrian et al. 1998 [35];

□ : new systems reviewed after 1998 in this thesis.

ZS: zeotropic system.

AS: substance can form azeotropic system with water under atmospheric pressure.

PS: partial soluble in water at 25°C, atmosphere pressure.

M: miscible with water at 25°C, atmosphere pressure.

In **Section 4.2**, the new separation concept is illustrated and two process variants are developed based on the new separation concept. After that, two azeotropic mixture representatives are exemplified in **Section 4.3-4.4**, and further discussion is provided in **Section 4.4**.

4.2 Process Concept

The separation of azeotropic mixtures is a task that is often encountered in the chemical process industries. Azeotropic mixtures are typically separated by homogeneous azeotropic distillation, heterogeneous azeotropic distillation, distillation using salt effects, or pressure-swing distillation (PSD). Among these four methods, the PSD process is the least

applied [154] as it provides several advantages over conventional distillation processes [155, 156].

The basic principle of the PSD process is that the azeotropic point can be shifted by the pressure variation (**Fig. 4.2**). To illustrate the process principle: the component A-rich mixture is separated in the low pressure (LP) distillation, and the azeotropic mixture (P_1) can be separated in extra high pressure (HP) distillation, where component B is the product, and azeotropic mixture (P_2) under HP will be recovered. As a result, the process has only two outputs, and the mixture is separated continuously. However, the potential of the PSD process is determined by the distance between P_1 and P_2 . And usually the distance is not long.

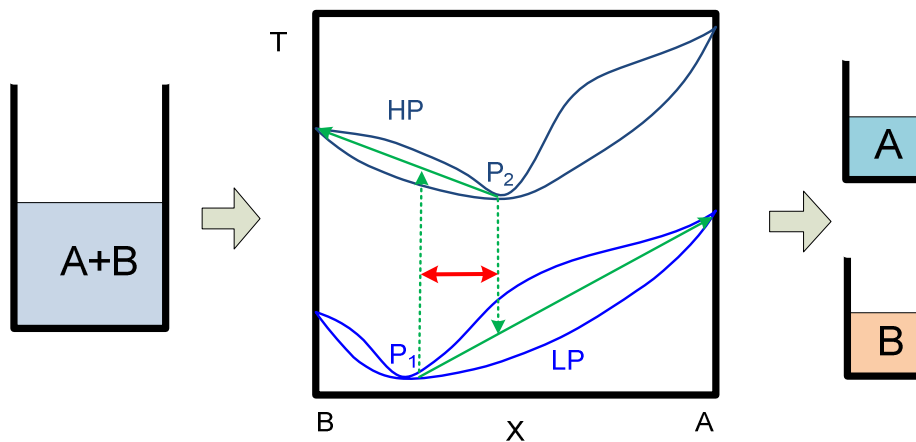


Figure 4.2: Separation principle of the PSD process

To realize the new process concept described in **Section 4.1**, two process variants as representatives for two classes of azeotropic systems were developed. For the purpose to illustrate clearly, two figures (**Figs. 4.3-4.4**) are plotted similar to **Fig. 4.2**. Both process variants apply the 'salting-out' concept of pressurized CO₂ at first, and then two liquids (L_1 and L_2 , CO₂ free basis in **Figs. 4.3-4.4**) are obtained. The huge distance between the resulting liquids L_1 and L_2 is the reason for the huge potential to the whole separation process.

For process variant 1, two additional LP columns are used to achieve the product A and B from L_2 and L_1 correspondingly, and the condensed mixtures will be recycled. As a consequence, the process has only two outputs and the two components are separated. However, for some systems, P_1 is too close to L_1 . As a consequence, only a small fraction of product B can be obtained in the LP distillation column, but most will be recycled along with the azeotropic mixture in accordance with the lever rule, which reduces the separation efficiency for the whole process.

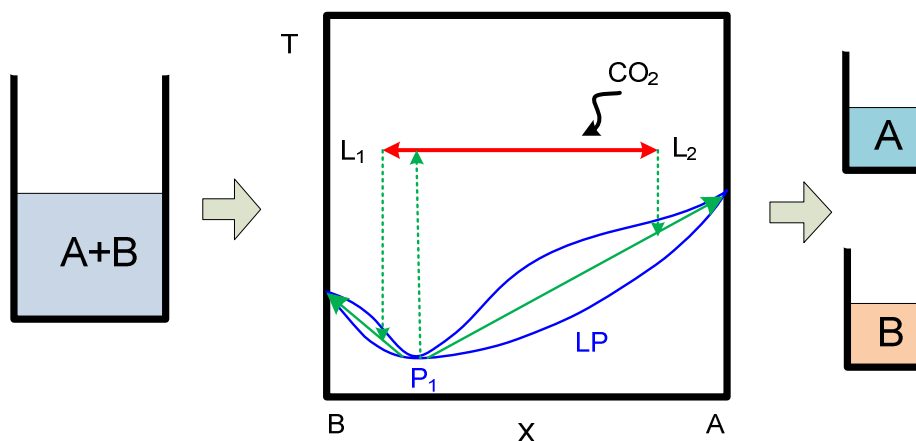


Figure 4.3: Separation principle of process variant 1

To conquer this problem, process variant 2 applies an additional HP column instead of LP to separate L_1 (**Fig. 4.4**). Under HP, the azeotropic point P_2 is shifted, and the horizontal distance between L_1 and P_2 is larger than L_1-P_1 . As a matter of course, this operation will benefit the distillation in accordance with the lever rule and a larger fraction of component B can be separated. Thus, process variant 2 offers a better performance for such pressure-sensitive system than process variant 1 in principle.

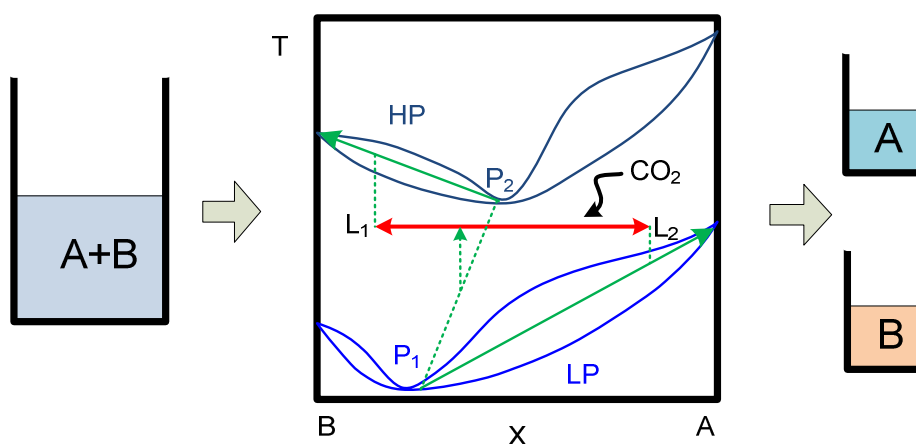


Figure 4.4: Separation principle of process variant 2

To evaluate the two process variants described above, two classes of azeotropic systems are investigated, including a modest asymmetric system: acetonitrile (MeCN)/water (H₂O) in **Section 4.3**, and a nearly symmetric system: 1,4-dioxane (DIOX)/water in **Section 4.4**. Both of them are pressure-sensitive systems, and the technical relevance of these systems arises from the fact that both solvents are widely used in the chemical industries. For this reason, the investigated systems are suitable choices for the case study from both, a scientific and a practical point of view.

A rigorous thermodynamic modeling is the base of a reliable process simulation. At the beginning, the involved systems are modeled, which is described as follows: The VLE binary systems (MeCN/H₂O, DIOX/H₂O) are predicted by NRTL-IG model (parameters are listed in **Table A2.6**, the VLE diagrams are presented in **Figs. A5.1-A5.4**). In this approach, the NRTL model is used for the description of the liquid phase behavior, and the vapor phase is assumed as the ideal gas. The modeling steps and the performance of the model are highlighted. The specific CEoS/GE model: PRWS is used for predicting the VLLE phase behavior of the ternary systems (MeCN/H₂O/CO₂, DIOX/H₂O/CO₂). In this approach, all phases are described by PRWS. The performance of the thermodynamic modeling is shown in **Section 2.3**.

The proposed process variants and a conventional PSD process are simulated using the commercial process simulation software Aspen Plus (V7.1). The VLLE phase behaviors are predicted for a constant temperature (40°C) and modest pressures (pressure range 25bar-65bar for MeCN/H₂O/CO₂ system, 30bar-50bar for DIOX/H₂O/CO₂ system). The rigorous equilibrium stage model is used for simulating the distillation. Nine different feed compositions ($x_{\text{H}_2\text{O}}=0.1-0.9$ mol/mol, increasing increment 0.1) are investigated to evaluate the potential composition range for the application of the new process variants. The feed flow is always set to 100kmol/h; and the product quality is specified to $x_{\text{MeCN or DIOX}}=99.5\%$ (mol/mol) and $x_{\text{H}_2\text{O}}=99.9\%$ (mol/mol) for all cases.

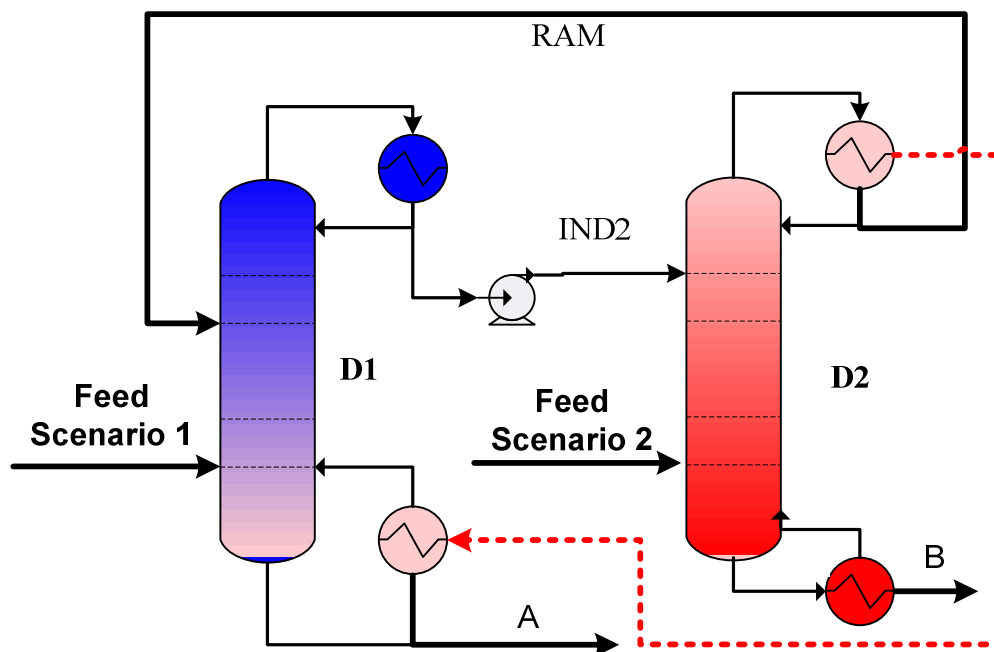


Figure 4.5: Schematic of a conventional PSD process

The flowsheet of the conventional PSD process is shown in **Fig. 4.5** and its specifications of two systems are listed in **Table 4.2**. The feed is dependent on the azeotropic point location

of different systems. In this work, two feed scenarios are used. The product A is obtained from the first column bottom (D1) under low pressure (LP) and the mixture close to azeotropic mixture is condensed on the top at the same time. The condensate is pumped to the second column (D2) under high pressure (HP). Under the HP, the azeotropic point is shifted to another position, and product B is achieved from the bottom. Again the mixture close to the azeotropic mixture is condensed on the top, and returned back to the first column.

Table 4.2: Simulation specifications of the conventional PSD process for the two systems

Specifications	Scenario 1		Scenario 2	
Column	D1	D2	D1	D2
Pressure	LP, 1.01bar	HP, 10bar	LP, 1.01bar	HP, 10bar
Stages	30	30	30	30
MeCN/H ₂ O system	$x_{H_2O} > 0.4$		$x_{H_2O} \leq 0.4$	
Feed stage (stream)	20 (Feed), 5 (RAM)	10 (IND2)	5 (RAM)	15 (Feed), 5 (IND2)
Product	A=H ₂ O	B=MeCN	A=H ₂ O	B=MeCN
DIOX/H ₂ O system	$x_{H_2O} > 0.6$		$x_{H_2O} \leq 0.6$	
Feed stage (stream)	10 (Feed), 10 (RAM)	15 (IND2)	10 (RAM)	10 (Feed), 15 (IND2)
Product	A=H ₂ O	B=DIOX	A=H ₂ O	B=DIOX

There is significant difference of the flowsheet of the new process variants compared to the conventional PSD process. Thereby, a legible interpretation is given at first. Here three scenarios are used in order to cover wide feed composition range. The operation range is determined by the 'salting-out' performance and the azeotropic point locations of different systems and different pressures (**Figs. 4.3-4.4**). **Figs. 4.6-4.7** display the flowsheets of two process variants. For scenario 1, the feed has low concentration of component A; and for scenario 3, it is rich in component B. The feed stream cannot be split directly using pressurized CO₂, and both scenarios need to feed to distillation column (D1 or D2) to obtain condensate at first. However, in scenario 2, the feed, which has an appropriate concentration range and is split with pressurized CO₂, is fed into the flash directly. Two liquids are formed and go into two corresponding columns (D1 and D2) after releasing the CO₂ under low pressure. Finally the products are achieved at the bottom, and the condensed mixture will be recycled back again. The difference between **Fig. 4.6** and **Fig. 4.7** is the pressure of the two columns, which are connected the **Figs. 4.3-4.4**, respectively. The specifications of the two process variants for two systems are listed in **Table 4.3**.

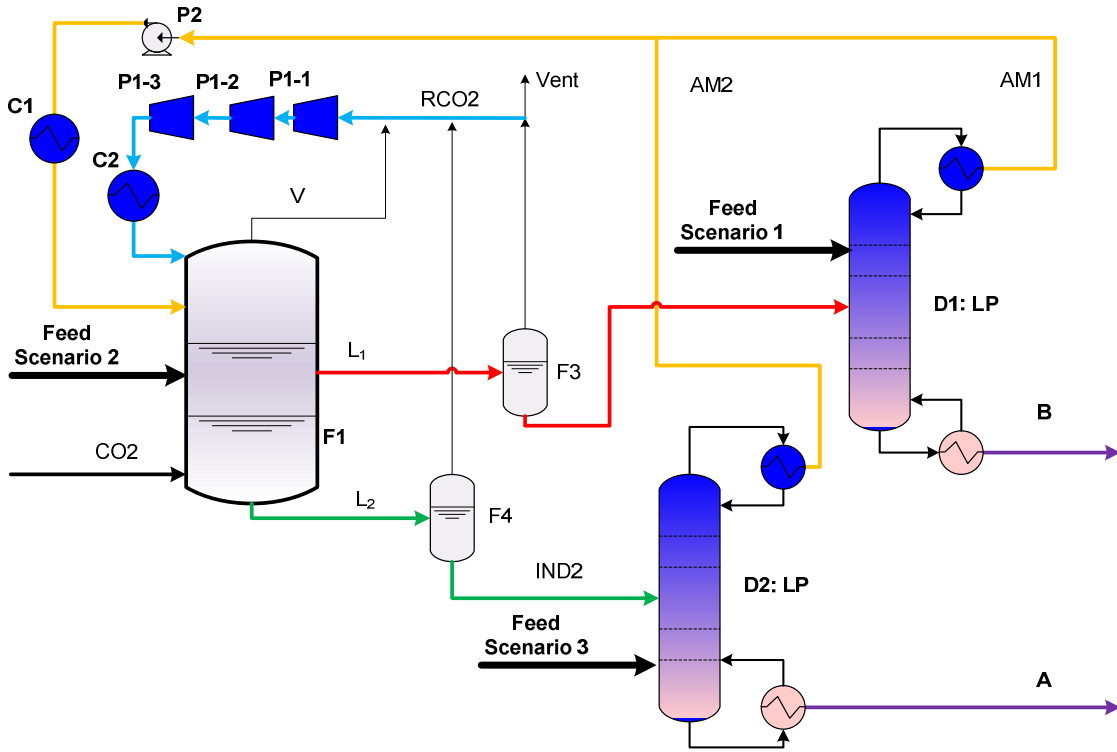


Figure 4.6: Schematic flowsheet of process variant 1

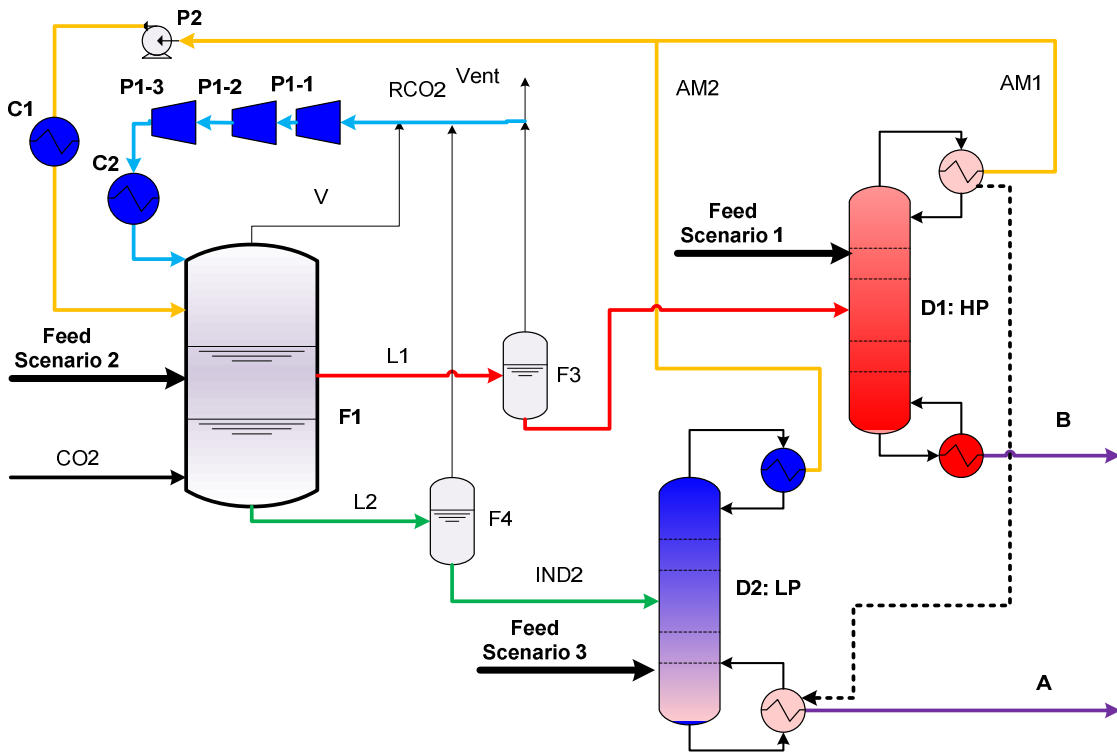


Figure 4.7: Schematic flowsheet of process variant 2

Since the release of CO₂ out of the liquid involves a decompression step, a fraction of the decompression energy can be recovered and used e.g., for driving a turbine. Therefore, in

order to check the potential costs reduction, both process variants for MeCN/H₂O system are investigated for both subcases, with a turbine and without a turbine.

Table 4.3: Specification of simulation of new process

Term	Specification for both systems
F1	25bar-65bar (increase stage 5bar), 40°C (isothermal operation)
F2, F3, F4	Ideal flash, 1.01bar, 40°C
P1-1/2/3	3 stages' isentropic compressor Outflow pressure setting is dependent on the pressure in F1. isentropic efficiency = 1 (default), mechanical efficiency = 1 (default)
P2	Liquid pump, pump efficiency = 0.95, drive efficiency = 0.95. Outflow pressure setting is dependent on the pressure in F1.
C1, C2	Cooler, 40°C (outflow), isobaric
Specification only for MeCN/H ₂ O system	
Process variant 1	Scenario 1: $0 < x_{H_2O} \leq 0.2$; Scenario 2: $0.3 \leq x_{H_2O} < 0.9$; Scenario 3: $0.9 \leq x_{H_2O} < 1$ D1: LP, 1.01bar, D2: HP, 3.0bar. Both 30 stages, feed stage: 10 RadFrac module, Murphree efficiency of each stage = 0.4
Process variant 2	Scenario 1: $0 < x_{H_2O} < 0.3$; Scenario 2: $0.3 \leq x_{H_2O} \leq 0.9$; Scenario 3: $0.9 < x_{H_2O} < 1$ D1: HP, 10bar, D2: LP, 1.01bar. Both 30 stages, feed stage: 10 RadFrac module, Murphree efficiency of each stage = 0.4
Turbine	Isentropic turbine, isentropic efficiency = 0.8, mechanical efficiency = 0.95, outflow pressure = 1.01bar
	Note: <ul style="list-style-type: none"> The boundary of 'salting-out' performance of MeCN/H₂O system is around $x_{H_2O}=0.2-0.9$. So in the range of $x_{H_2O}=0.2-0.9$, the mixture can be split directly; for the mixture with $x_{H_2O}<0.2$ or $x_{H_2O}>0.9$, direct split using pressurized CO₂ is not possible. It follows that the feed needs to be distilled at first; Process variant 1 for MeCN/H₂O system does not cover the composition range with $0.2 < x_{H_2O} < 0.3$, because the x_{H_2O} range is too close to the azeotropic point ($x_{H_2O}=0.3218$, 1.01bar) and the lower boundary of 'salting-out' performance. In this range, the process potential is too small by either scenario 1 or scenario 2. However, process variant 2 is not limited in this range, because the azeotropic point was shifted to $x_{H_2O}=0.4867$ under 10bar; With regard to the heat integration to save energy, process variant 1 still uses 3bar column.

Table 4.3 (continuous): Specification of simulation of new process

Specification only for DIOX/H ₂ O system	
Process variant 1	Scenario 1: $0 < x_{H_2O} \leq 0.4$; Scenario 2: $0.4 \leq x_{H_2O} < 0.7$; Scenario 3: $0.7 \leq x_{H_2O} < 1$ D1 & D2: LP, 1.01bar. Both 30 stages, feed stage: 10 RadFrac module, Murphree efficiency of each stage = 0.4
Process variant 2	Scenario 1: $0 < x_{H_2O} \leq 0.4$; Scenario 2: $0.4 \leq x_{H_2O} < 0.7$; Scenario 3: $0.7 \leq x_{H_2O} < 1$ D1: HP, 10bar, D2: LP, 1.01bar. Both 30 stages, feed stage: 10 (D2), 15 (D1) RadFrac module, Murphree efficiency of each stage = 0.4
	Note: <ul style="list-style-type: none"> The boundary of 'salting-out' performance of DIOX/H₂O system is around $x_{H_2O}=0.2-0.7$. So in the range of $x_{H_2O}=0.2-0.7$, the mixture can be split directly; for the mixture with $x_{H_2O} < 0.2$ or $x_{H_2O} > 0.7$, direct split using pressurized CO₂ is not possible. It follows that the feed needs to be distilled at first; Turbine is not included for the DIOX/H₂O system, because it does not provide a significant reduction of the separation costs as discussed in the case of the MeCN/H₂O system, which will be explained in Section 4.3.

Since this work is focusing on evaluating the potential of the application of a fundamental separation idea for a technical process concept, the capital costs are not considered at this point. Instead, the running separation costs as operational costs are evaluated. The price of the used utilities is listed in **Table 4.4**. The recycle ratio of the mixture and CO₂ and the energy requirement for the separation (electricity and steam) are also calculated to analyze the processes using the following equations:

$$\text{Separation costs (USD/kmol)} = \frac{\text{Costs (USD/h)}}{\text{Feed (kmol/h)}}$$

$$\text{Recycle ratio} = \frac{\text{Recycled mixture flow (kmol/h)}}{\text{Feed (kmol/h)}}$$

$$\text{Energy requirement (kWh/kmol)} = \frac{\text{Duty (kW)}}{\text{Feed (kmol/h)}}$$

Table 4.4: The price of used utilities

Utility	Quality	Price	MeCN case	DIOX case
Electricity	--	0.084 (USD/kWh)	Pumps and compressor	
Water	18-40°C	0.06 (USD/ton)	Cooling	Cooling
Steam 1	100°C	17.00 (USD/ton)	Heating: LP in PSD; LP in process variant 1	
Steam 2	120°C	17.82 (USD/ton)	Heating: LP in process variant 2	Heating: LP in PSD & process variant 1, LP is process variant 2.
Steam 3	150°C	20.15 (USD/ton)	Heating: HP in PSD; By-product in process variant 2	By-product of HP is PSD & process variant 2
Steam 4	190°C	26.68 (USD/ton)	Heating: HP in PSD; HP in process variant 2	
Steam 5	210°C	32.20 (USD/ton)	Heating: HP in PSD; HP in process variant 2	

Note:

- The price of utilities is under same investigated level [158]. The electricity price is 1.3-3.1 times as expensive as steams with respect to same energy (kWh).

4.3 Case: Acetonitrile/H₂O

The operation of the conventional PSD process on a Y-X diagram of MeCN/H₂O is shown in **Appendix 5**. Several recent articles [155, 157-160] have reported that the PSD process is an outstanding alternative to separate MeCN/H₂O. For this reason, it is a suitable and technically relevant system, which is used to evaluate the potential of the new proposals. The result of the conventional PSD process has been evaluated, and the results achieved in this thesis are consistent with the results in an earlier publication [161]. The operation of the two process variants in Y-X diagrams are displayed in **Appendix 5**.

To explain the key results systematically out of the huge amount of simulation results obtained, an overview of the separation costs is shown firstly to choose an appropriate direction. Afterwards, more details related to the process performance are given, and reasons are discussed and analyzed. This section is focusing on describing the potential, performance and the analysis of the new process variants.

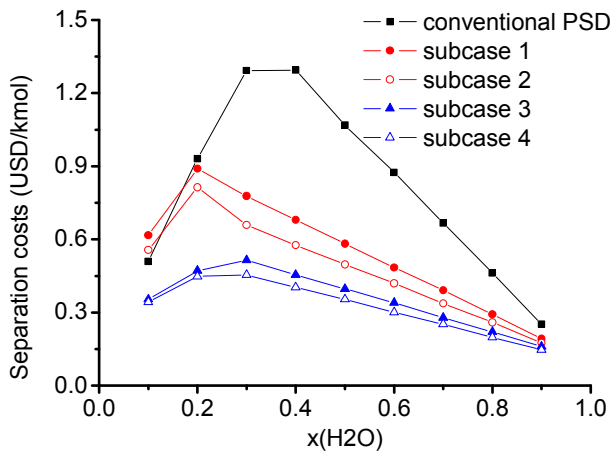


Figure 4.8: Separation costs contrasting the conventional PSD process and the two process variants

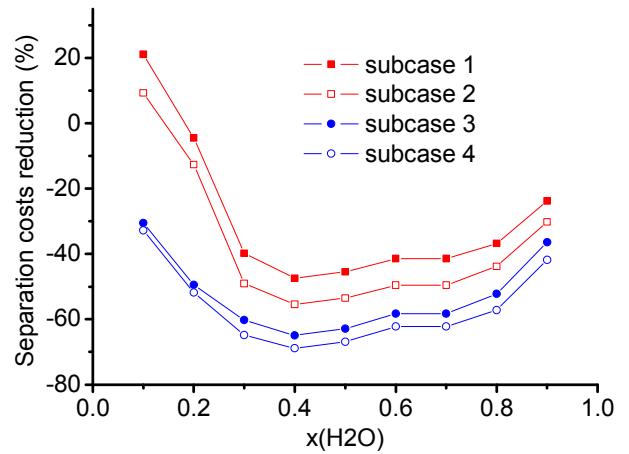


Figure 4.9: Separation costs reduction of the two process variants based on the conventional PSD process

Note:

- Subcase 1: process variant 1 without turbine;
- Subcase 2: process variant 1 with turbine;
- Subcase 3: process variant 2 without turbine;
- Subcase 4: process variant 2 with turbine;
- PSD does not apply gas, and therefore no case with turbine is investigated.

Fig. 4.8 shows the overview of the separation costs contrasting the conventional PSD process and the two process variants (case with the minimum separation costs among investigated pressures). Two important results are summarized.

Firstly, the trend of the separation costs in the two process variants is similar, and both are lower in comparison with the conventional PSD process for almost all cases. Thus, both of the new process variants generally have potential to cut down the separation costs. **Fig. 4.9** illustrates the separation costs reduction of the two process variants based on the conventional PSD process. The process variant 1 offers a cost reduction of 23.8%~53.5% for the feed composition range of $0.3 \leq x_{\text{H}_2\text{O}} \leq 0.9$. With process variant 2 a cost reduction of 30.5%~68.9% is realized for a feed composition range of $0.1 \leq x_{\text{H}_2\text{O}} \leq 0.9$. At lower water fractions in the feed, however, process variant 1 features only little cost reduction potential (at $x_{\text{H}_2\text{O}}=0.2$), and even higher costs are involved at $x_{\text{H}_2\text{O}}=0.1$. As a result, process variant 2 is superior to process variant 1 regarding the separation costs.

As a second important result, the profiles of the separation costs with and without the turbine are similar. Thus, the application of a turbine does not affect the energy costs significantly; it only saves less than 5% for process variant 2 in general (**Fig. 4.8**).

As for all the investigated cases in this work the performance with and without a turbine is similar, the results of the process variant subcases with turbine are not further discussed in the following. While both process variants show a similar qualitative performance, process variant 2 features a quantitatively better performance than process variant 1. To this case, the following text only discusses the results of process variant 2 of the MeCN/H₂O system, while the results of process variant 1 of the MeCN/H₂O system are given in **Appendix 5**.

If details in the process performance are investigated, another exceedingly important point is found: the operating pressure of the VLLE flash, named the operating pressure in short in the following text, has a big influence on the separation costs, and the impact is not monotonous (for a fixed feed composition) (**Fig. 4.10**).

Fig. 4.11 shows the operating pressure influence on the separation costs of process variant 2. Clearly, there exists an optimal operating pressure range: 35bar-45bar. This diagram indicates that the process is in fact dominated by the operating pressure. This can be illustrated by two main contribution terms, i.e., the recycled CO₂ flow and the recycled condensate mixture flow, which contribute to the separation costs in terms of electricity and heating energy consumption, respectively.

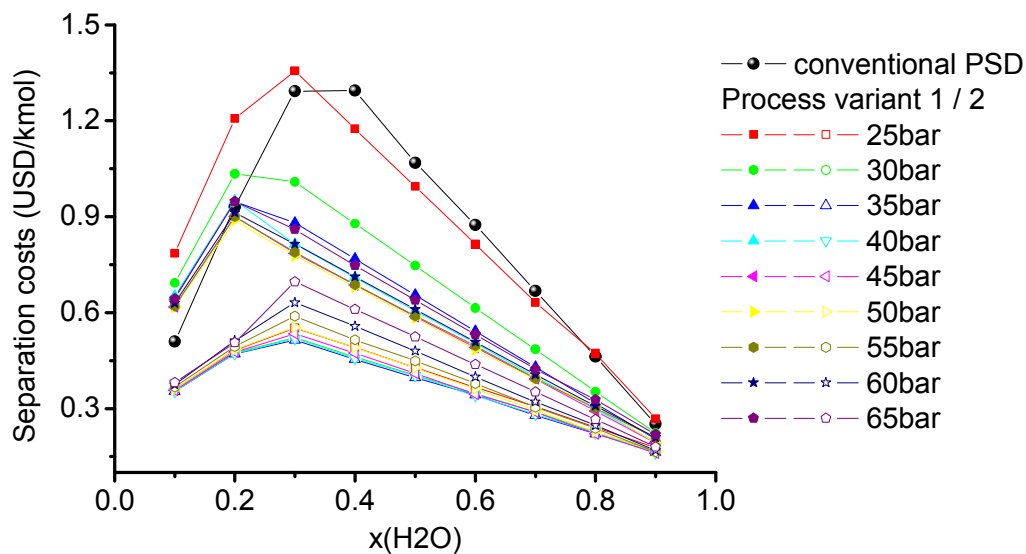


Figure 4.10: Separation costs contrast among the conventional PSD process and new process

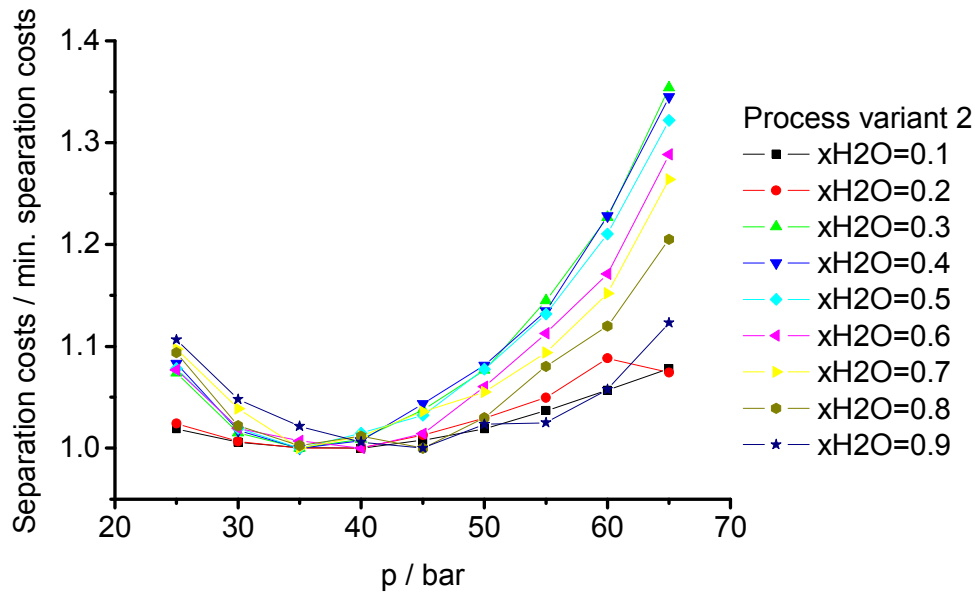


Figure 4.11: Operating pressure influence on the separation costs of process variant 2

Fig. 4.12 displays the recycle ratio of CO₂ flow in process variant 2. The figure indicates that the pressure has a monotonous impact on the recycled CO₂ flow. Taking the recycle ratio of CO₂ flow as an example, it is increased by a factor of 3-4 when the pressure rises from 25bar to 65bar at $x_{H_2O}=0.3$. This dominant influence of the operating pressure has a clear physical background: the higher operating pressure, the more CO₂ is pressed into the liquid.

As a matter of cause, more electricity is required to compress more CO₂ and to provide and maintain the higher pressure level. **Fig. 4.13** highlights the electricity requirement of process variant 2. The electricity requirement increases by a factor of 4-5 when the operating pressure is increased from 25bar to 65bar. This trend is quantitatively similar to the increase of the recycle ratio of the CO₂ flow. Apparently, the operating pressure has a direct impact the CO₂ flow, and both the operating pressure as well as the CO₂ flow have direct influence on the electricity requirement.

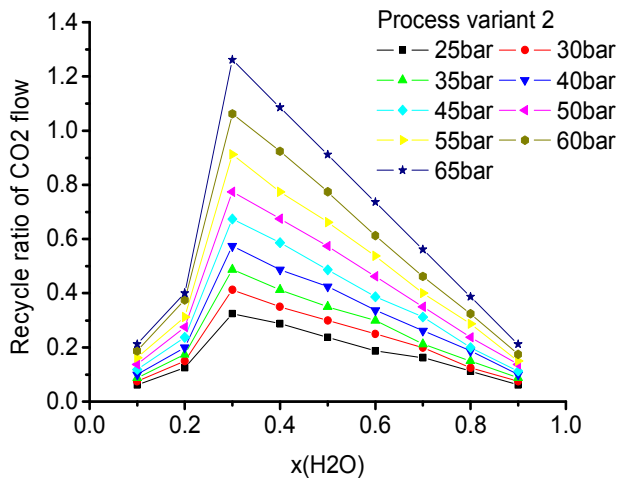


Figure 4.12: Recycle ratio of CO₂ flow in process variant 2

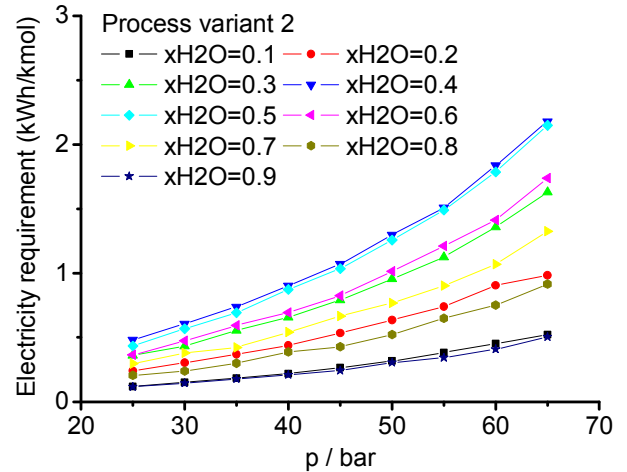


Figure 4.13: Electricity requirement of process variant 2

As observed above, process variant 2 inevitably requires more electricity in contrast with the conventional PSD process due to more CO₂ compressing. Thus, at first it seems astonishing that process variant 2 still offers a significant potential to reduce the separation costs. The reason for this is caused by another key factor: the reduction of the condensate recycle flow.

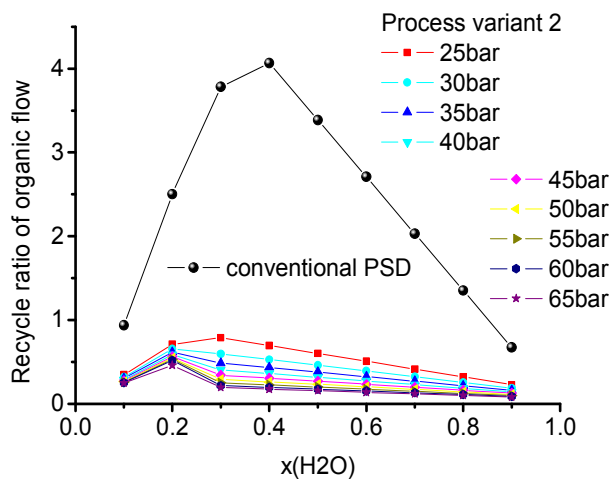


Figure 4.14: Recycle ratio of condensate flow in process variant 2

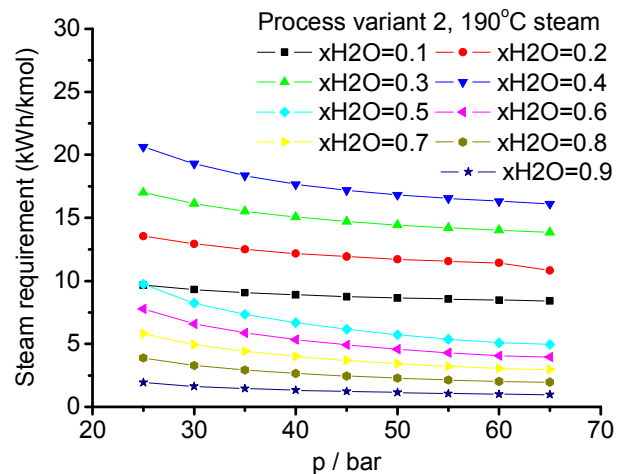


Figure 4.15: Steam requirement of process variant 2

Fig. 4.14 illustrates the significant reduction of the recycle ratio of the condensate flow in process variant 2 in comparison to the conventional PSD process. The huge reduction is attributed to the synergistic effects resulting from the 'salting-out' performance and the pressure-swing strategy. The minimum reduction is 73.6% and the maximum reduction

achieves 95.7% for the best case among all feed composition ranges. All the best cases for each feed composition are the ones at the highest investigated pressure (65bar), which indicates that the high operating pressure can enhance the 'salting-out' performance. By increasing the distance of the two liquids in the composition space, the distillations and thereby the separation efficiency of the whole process is significantly improved. As a consequence, the total recycled condensate mixture flow reduces. This significant flow reduction provides several benefits to distillation. On the one hand, the steam requirement for heating is reduced, which is seen directly in **Fig. 4.15**. Additionally, also the required size of the columns is reduced, which will result in a significant reduction of the capital costs.

The analysis above reveals the inherent reason of the optimal operating pressure range in **Fig. 4.11**. The opposite impacts of the operating pressure on the electricity requirement and the steam requirement gives rise to an arc-shaped performance curve. The electricity requirement is only around one tenth of the steam requirement (**Fig. 4.13** and **Fig. 4.15**), but the costs for electricity are much higher than for the steam considering same energy amount (see utility costs in **Table 4.4**). As a result, the separation costs are dominated by steam only in the low pressure range while for higher pressures the electricity is increasingly dominating the separation costs.

4.4 Case: 1,4-Dioxane/H₂O

The operation of the conventional PSD process and two process variants in Y-X diagram of DIOX/H₂O are shown in **Appendix 5**, respectively. The results of the DIOX/H₂O system are similar to the results of the MeCN/H₂O system. For this reason, in this section it is not necessary to repeat the detailed discussion of similar results compared to **Section 4.2**. Instead of the analysis of the new process variants, the different performances between the MeCN/H₂O system and the DIOX/H₂O system are evaluated and the reasons for the differences are discussed in particular. Eventually, a general guideline will be proposed to apply this separation concept consequently. The other results are also recapitulated in **Appendix 5**.

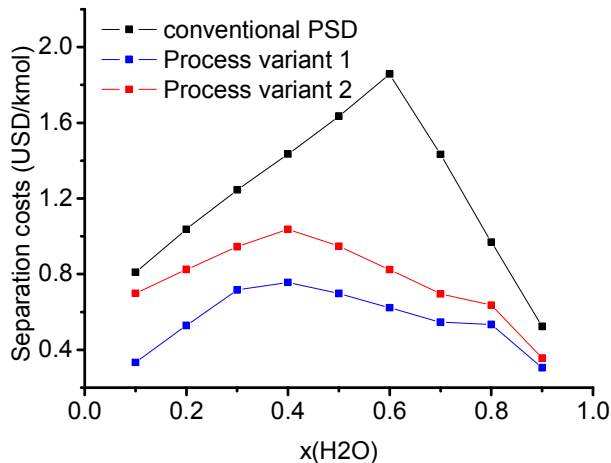


Figure 4.16: Separation costs contrast among the conventional PSD process and the new process variants

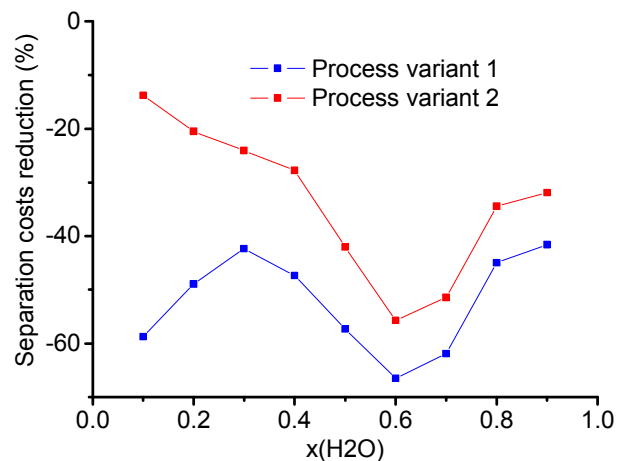


Figure 4.17: Separation costs reduction of the two process variants based on the conventional PSD process

Likewise, an overview on the separation costs of the conventional PSD process and the two process variants (for the case with the minimum separation costs among investigated pressures) is investigated in **Fig. 4.16**. Primarily, the two process variants again yield less separation costs than the conventional PSD process. Based on the conventional PSD process, the separation costs reductions of two process variants are calculated (**Fig. 4.17**). The separation costs of the two process variants are reduced for the DIOX/H₂O system significantly in the same way as for the MeCN/H₂O system; whereas, process variant 1 shows an even better performance than process variant 2 for the DIOX/H₂O system. On account of the better performance of process variant 2 than process variant 1 of the MeCN/H₂O system, the performance of the two process variants of the DIOX/H₂O system is totally opposite. With the DIOX/H₂O system, process variant 1 reduces the separation costs by 41.6%~66.5% for the best case among all feed composition ranges, while process variant 2 cuts down the separation costs by 13.8%~55.7% for the best case among all feed composition ranges.

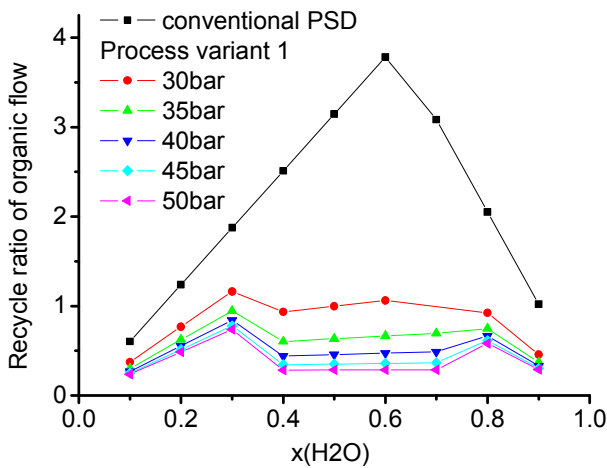


Figure 4.18: Recycle ratio of condensate flow in process variant 1

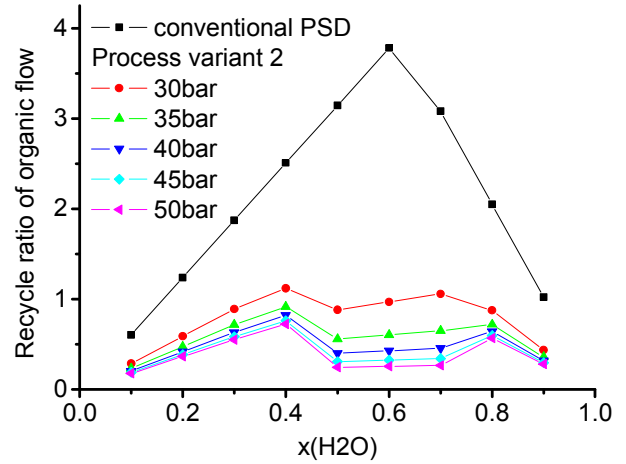


Figure 4.19: Recycle ratio of condensate flow in process variant 2

To understand the reason for this behavior, the recycled condensate mixture flows of the two process variants and of the conventional PSD process have to be analyzed (**Figs. 4.18-4.19**). Two important results are found. The first result is that both process variants reduce the recycled condensate flow significantly. Similar as concluded in **Section 4.3**, the reduction of recycled condensate mixture flow is still the key factor to reduce the separation costs for this system. However, the former two diagrams show a very similar reduction of recycle ratio of organic flow. This indicates that the condensate mixture flow is likely independent with the process variant. For example, for the DIOX/H₂O system, a reduction of 60.6%~92.4% is achieved for the best case among all feed composition ranges by process variant 1 and 70.6%~93.3% for the best case among all feed composition ranges by process variant 2. While, this trend is more distinguishable for the MeCN/H₂O system, a reduction of 54.6%~92.8% is achieved by process variant 1 and 73.6%~95.7% by process variant 2. Concerning the high quality steam for HP distillation in process variant 2, process variant 2 can be even more expensive than process variant 1 if the condensate flow cannot be reduced more remarkably. And this is the visible reason for the fact that process variant 1 offers a better performance than process variant 2 for the DIOX/H₂O system.

The inherent reason of that is attributed to the system properties: the position of azeotropic point of the respective azeotropic systems. The first system class (see **(1)** in **Fig. 4.20**) has the azeotropic point P_1 close to the side B (or A) at atmospheric pressure, which is too close to L_1 (or L_2 if P_1 is close to A). In accordance with the lever rule, the LP distillation has to recycle a huge amount of condensate mixture, which gives rise to large energy consumption and low efficiency. On the other hand, the P_2 within HP is shifted farther away from L_1 (or L_2 if P_1 is close to A). In other words, the HP distillation increases the efficiency remarkably. The MeCN/H₂O system is exactly representative of this system class, while the DIOX/H₂O system

is a specific representative of another system class (see **(2)** in **Fig. 4.20**). For this system class, the azeotropic point P_1 under atmospheric pressure is in the middle approximately, and the distance between L_1 and P_1 is still large. As a result, the separation efficiency is still adequate to separate L_1 by LP distillation. Nevertheless, HP distillation still can increase the separation efficiency by enlarging the distance between L_1 and P_2 , the rise is not too significant. Moreover, the higher quality steam is required for HP distillation, which counteracts the potential of process variant 2, as demonstrated by the DIOX/H₂O case.

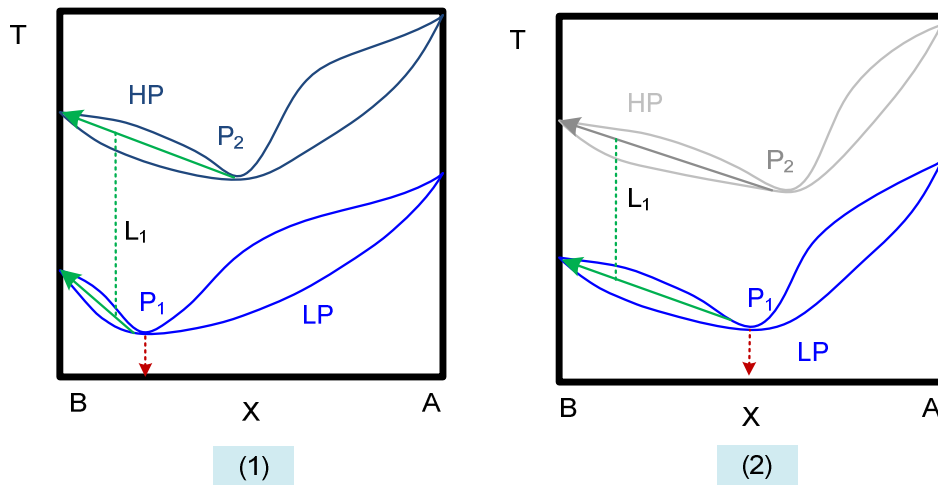


Figure 4.20: Two system classes of a binary azeotropic system considering the position of the azeotropic point under low pressure

4.5 Discussion

The previous two sections (**Section 4.3-4.4**) demonstrate the significant potential to reduce the separation costs for azeotropic mixture separation using the novel separation concept. Meanwhile, they also demonstrate the different favorites of the two process variants for the different systems. To expression of this separation concept, a schematic diagram (**Fig. 4.21**) is proposed to summarize a more general guideline for this separation concept. It comprises four classes of azeotropic systems:

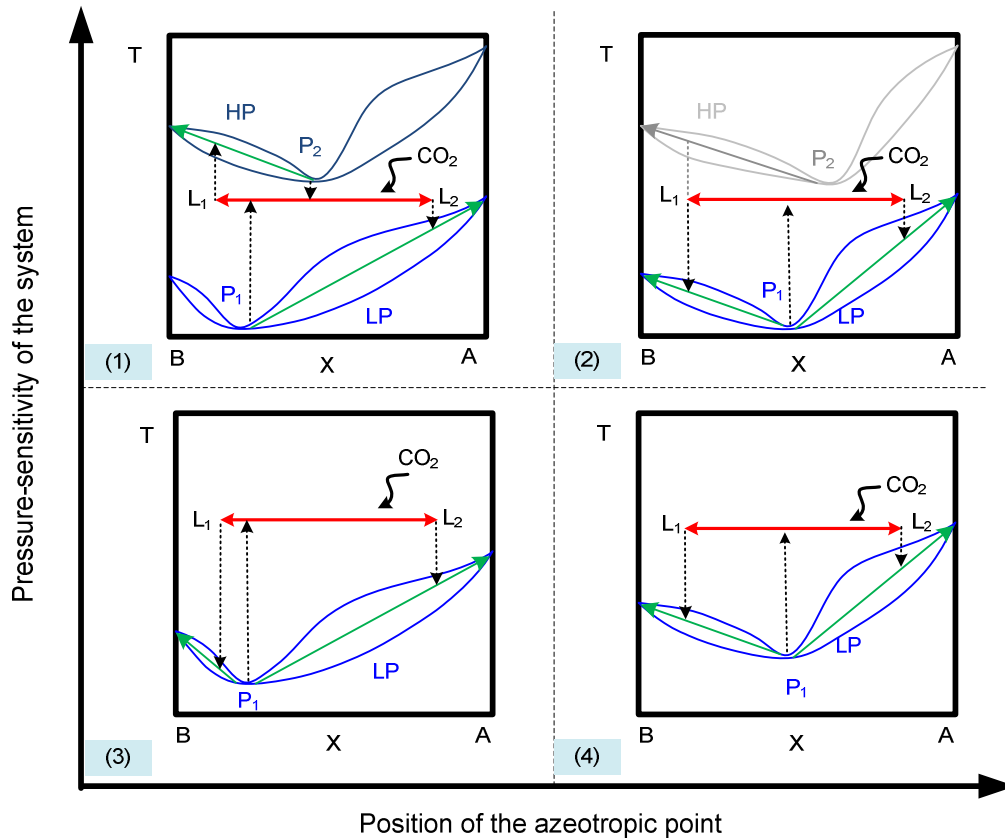


Figure 4.21: Classification of azeotropic mixture separation using 'salting-out' concept

Class (1) has the pressure-sensitive property of the system with the position of the azeotropic point close to one side. The MeCN/H₂O system is a classical representative as investigated in **Section 4.3**. For this system class, process variant 2 offers a higher potential to reduce separation costs than process variant 1. The dominating factor is that the combination of 'salting-out' performance and pressure-swing strategy improves the separation efficiency of the whole process significantly.

The system of Class (2) is also pressure-sensitive, but the position of the azeotropic point lies in the middle approximately. The DIOX/H₂O system is a typical representative as analyzed in **Section 4.4**. For this system class, process variant 1 has superiority to process variant 2. The main reason for that is attributed to its particular property of azeotropic point, which leads to reduce the separation costs for process variant 1 in terms of the lower quality steam. Additionally, the high-pressure column can be avoided and therefore lower capital costs can be achieved. At the same time, process variant 1 still can achieve relatively similar separation efficiency to that achieved by process variant 2.

Class (3) and class (4) are pressure-insensitive. For this reason, the application of process variant 2 is not possible. The only choice is process variant 1 and it is still very efficient for Class (4). The reason has been described as the same as for Class (2). However, this separation concept may not be efficient for Class (3), especially when the azeotropic point

(P_1) is too close to L_1 . The smaller the distance between P_1 and L_1 , the lower the separation efficiency of the whole system. Moreover, once the azeotropic point (P_1) does not lie between L_1 and L_2 , this separation concept cannot be used any longer for such extremely azeotropic systems. A possible system could be e.g., the water and ethanol system, since the azeotropic point is highly rich in ethanol (~90% ethanol (mol/mol)).

It should be noted that the feed composition considered in this thesis varies in a broad range, which yields also a large variation with regard to the size of equipment. In this fundamental study, it is not yet the aim to estimate capital costs quantitatively. However, a qualitative analysis can be still performed at this point. The new process variants require a higher number of equipment components compared to the conventional PSD process (i.e., flash tanks, coolers, and compressors), however, the significant reduction of recycled condensate mixture flow (e.g., 73.6%~95.7% reduction for the best case among all feed composition ranges by process variant 2 for MeCN/H₂O system) decreases the distillation column size drastically. As a consequence, the capital costs of the new process can potentially be even lower than the capital costs of the conventional PSD process, because the distillation columns are usually a main factor being much more expensive than other equipment components.

4.6 Chapter Summary

This chapter demonstrates a conceptual idea to transfer the phase tuning information from the phase level to the higher hierarchical process levels. In detail, pressurized CO₂ is used to change the miscibility of homogeneous mixtures on the phase level, while on higher levels, a technical approach for azeotropic mixture separation based on the phase behavior tuning is performed.

For validating the separation concept, two process variants are proposed and developed. After that, the performance of the new process variants is evaluated. Two azeotropic systems, i.e., the MeCN/H₂O system and the DIOX/H₂O system, which are representatives for Class (1) and Class (2), in particular, are investigated in case studies by means of process simulation. The results are compared to that of the technical reference process scheme, i.e., a conventional PSD separation process. A significant reduction of the separation costs when compared to the conventional PSD process for both systems can be achieved, although the new process variants consume more electricity than the conventional PSD process. The main reason for the achievement of the significant reduction as analyzed is that the significant increase of separation efficiency through the phase behavior tuning leads to a remarkable reduction of the recycled condensate mixture. Thus, these results clearly turn out that the novel fundamental separation approach by phase behavior tuning using pressurized CO₂ is a

promising alternative to the conventional processes for the separation of azeotropic mixtures. The major findings can be recapitulated in **Table 4.5**.

Table 4.5: General results of case studies

The MeCN/H ₂ O system, a representative of Class (1)				
Feed	Reduction of separation costs		Reduction of recycled condensate mixture flow	
x_{H_2O}	Process variant 1	Process variant 2	Process variant 1	Process variant 2
0.1	-54.2%~-21.1%	25.1%~30.5%	-11.8%~54.6%	63.2%~73.6%
0.2	-29.6%~4.5%	45.0%~49.4%	13.9%~65.1%	71.7%~81.6%
0.3	-4.9%~39.8%	46.1%~60.2%	33.6%~91.5%	79.2%~94.9%
0.4	9.2%~47.5%	52.8%~64.9%	46.5%~92.8%	82.9%~95.7%
0.5	6.9%~45.5%	50.9%~62.9%	45.7%~92.3%	82.2%~95.4%
0.6	7.0%~41.5%	49.9%~58.3%	44.5%~91.4%	81.2%~94.9%
0.7	5.3%~41.5%	47.3%~58.3%	42.7%~90.1%	79.6%~94.1%
0.8	-2.3%~36.8%	42.4%~52.2%	38.8%~87.3%	76.3%~92.6%
0.9	-6.5%~23.8%	28.5%~36.4%	20.9%~67.7%	66.2%~87.9%
The DIOX/H ₂ O system, a representative of Class (2)				
Feed	Reduction of separation costs		Reduction of recycled condensate mixture flow	
x_{H_2O}	Process variant 1	Process variant 2	Process variant 1	Process variant 2
0.1	55.3%~58.7%	10.3%~13.8%	38.0%~60.6%	52.4%~70.6%
0.2	44.0%~48.9%	15.4%~20.5%	38.0%~60.6%	52.5%~70.6%
0.3	36.2%~42.4%	17.5%~24.1%	38.0%~60.6%	52.5%~70.6%
0.4	32.9%~47.3%	19.9%~27.8%	62.8%~88.7%	55.4%~71.2%
0.5	48.9%~57.3%	33.3%~42.0%	68.3%~90.9%	72.0%~92.2%
0.6	58.4%~66.5%	48.5%~55.7%	71.9%~92.4%	74.4%~93.3%
0.7	58.6%~61.9%	38.4%~51.4%	77.4%~90.6%	65.7%~91.4%
0.8	39.9%~65.6%	29.1%~34.4%	55.0%~71.6%	57.3%~72.3%
0.9	37.0%~41.6%	27.0%~31.9%	55.0%~71.6%	57.3%~72.3%

Note:

- The reduction of recycled condensate mixture flow is pressure-dependent, and therefore a reduction range yielded by the different operation pressures is shown in this table. For the MeCN/H₂O system, the operation pressure range is 25bar-65bar; and for DIOX/H₂O system, the operation pressure range is 30bar-50bar;
- All cases involved in this table are investigated without turbine.

Besides, the selection of a suitable process variant is dominated by the properties of the pressure-sensitivity and the position of the azeotropic point. The potential of using the new separation concept is generalized and four classes of azeotropic systems are classified.

Concerning the negative environmental impact from quite a number of the traditional organic solvents that are used in a wide application range and at large scale, the new separation technology presented in this thesis using the benign solvent CO₂ seems attractive and may help to pave the way towards more sustainable separation processes.

Reactor design uses information, knowledge, and experience from a variety of areas -thermodynamics, chemical kinetics, fluid mechanics, heat transfer, mass transfer, and economics.

Octave Levenspiel
Chemical Reaction Engineering, 3rd ed., 1999

Chapter 5

Reaction Intensification Using CO₂

The previous chapter describes a new process for the separation of azeotropic mixtures by phase behavior tuning using CO₂, and this chapter will investigate reaction intensification using CO₂, following a brief review on reactions in CXLs (**Section 5.1**). Because of the active research in the field of long-chain alkene hydroformylation, it is selected and reviewed briefly as an example for further research.

Following this, in **Section 5.2**, the four factors of solvent type, solvent quantity, temperature, and pressure, are investigated, and their influence on a 1-octene hydroformylation system with respect to H₂ solubility, CO solubility, the H₂/CO ratio, and CO₂ solubility is thermodynamically evaluated. In **Section 5.3**, a proposal to combine two solvent concepts for long-chain alkene hydroformylation is also discussed.

5.1 Introduction

Recently, three reactions carried out in CXLs, i.e., oxidation, hydrogenation, and hydroformylation, have received particular attention, since all of them involve several permanent gases, H₂, CO, and O₂. One feature of CXLs is their ability to increase the solubility of permanent gases. Furthermore, CXLs favor homogeneous as well as heterogeneous reactions in terms of improving mass transfer and strengthening safety through fire suppression. This is especially important for systems involving hydrogen and oxygen. A brief review of these three reaction classes in CXLs is given in **Table 5.1**.

Table 5.1: A review of reactions in CXLs

Reaction	Year	Pub. No.	Representative works
Oxidation	2002-2012	15	[30, 162-164]
Hydrogenation	2001-2012	11	[29, 165-172]
Hydroformylation	2002-2012	10	[173-176]

Note: The total publication number is inquired from SCOPUS.

This chapter focuses on the hydroformylation. The hydroformylation reaction is one of the most important homogeneously catalyzed reactions in the chemical industry [177]. **Fig. 5.1** describes the scientific research since 1950 on hydroformylation reactions. There is a notable interval after 1995, in which the number of relevant publications in this area has significantly increased. Among these publications, a considerable number focus on hydroformylation reaction in CO₂ atmosphere (i.e., scCO₂ and/or CXLs). In principle, several catalysts can catalyze hydroformylation, but only two of them are extensively used in industry, rhodium-based catalysts and cobalt-based catalysts. Rhodium-based catalysts are most popular due to their high activity and selectivity [177]. As a consequence, rhodium-catalyst based hydroformylation processes have received intensive attention.

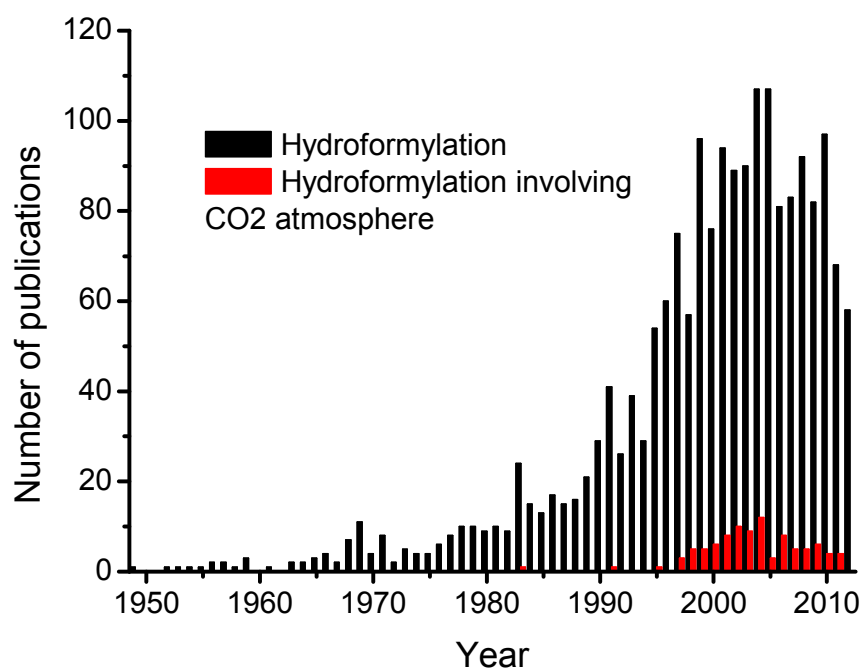


Figure 5.1: Publication review of hydroformylation (inquired by SCOPUS with carbon dioxide, hydroformylation in title or abstract or keyword)

For short-chain alkenes ($C \leq 4$), there is a mature hydroformylation process, i.e., the Ruhrchemie-Rhône Poulenc process [177], in which water is used as solvent to dissolve

catalyst and alkenes. However, this process concept is not applicable to long-chain alkene hydroformylation due to limited solubility of long-chain alkenes in water. Long-chain aldehydes, the hydroformylation products of long-chain alkenes, are usually used for plasticizers, detergents, and surfactants. They share approximately 8% of the world's overall alkene hydroformylation capacity [177]. Extensive efforts, e.g., within the SFB Transregio 63 project funded by the DFG (German Research Foundation) [178], are made in developing energy-efficient and sustainable processes for long-chain alkene hydroformylation.

In these various rhodium-catalyst studies, the most challenging aspects are associated with enhancing the hydroformylation reaction and sustainably separating/recovering the extremely expensive rhodium catalyst (with the ligand) and aldehydes from raw products. Two recycling approaches have been demonstrated [177]; one, such as in the Union Carbide Corp. (UCC) process, is based on gas recycling to remove the aldehydes from the catalyst solution; the second, such as in the Low Pressure Oxo (LPO) process, is based on liquid recycling to remove the aldehydes from the catalyst solution. Although the liquid-recycling approach conquers some downsides of the gas-recycling approach, i.e., high gas recycling and compression costs, high temperature and high gas flow in the stripping process, and accumulation of heavy ends, it is still limited for long-chain hydroformylation because of harsh distillation conditions that result in thermal stress on the rhodium catalyst [177, 179]. To address this issue, several novel concepts have recently been proposed, including a biphasic ionic liquid system [180-184], a supported ionic liquid system [185, 186], a micellar solvent system [187-189], a fluoruous biphasic system [190-193], a thermomorphic solvent system [194-197], a gas expanded liquid system [28, 164, 198, 199], a supercritical fluid system [200-202], and a supercritical fluid-ionic liquid biphasic system [203, 204]. Among these novel concepts, CXLs were first reported in 2002 [176] as reaction media of long-chain alkene hydroformylation, and the research group of Prof. B. Subramaniam from Kansas University has made significant progress in this area during the last ten years [28, 164, 198, 199]. The experimentally demonstrated several attractive features, i.e., mild reaction condition (30-60°C, <120bar), high turnover frequencies (4-fold higher than those in either neat organic solvent or neat CO₂), high n/iso- ratio (~17.5) of products with a rhodium catalyst [198].

In addition to approaches for enhancing the hydroformylation reaction and recovering the rhodium catalyst in sustainable processes, another important aspect for hydroformylation is to achieve a high ratio of linear aldehydes (n-aldehydes) that are, unlike iso-aldehydes, the target products. As a matter of fact, the high selectivity of hydroformylation in producing a high n/iso-ratio of aldehydes is desirable with respect to the energy-intensive downstream separation as well as to the non-biodegradability of branched surfactants [179].

To understand the hydroformylation reaction and further achieve high aldehyde n/iso-ratios in process design and development, hydroformylation reaction kinetics must be studied. Because there are several types of reaction mechanisms with many reaction steps [177], a full kinetics analysis is relatively complicated. Also, the combination of rhodium and ligand is manifold. Consequently, most published works on hydroformylation kinetics are often based on simplified models without detailed discussions on the relationship of the n/iso-ratio of aldehydes and the H₂/CO ratio. Only a few publications have mentioned the n/iso-ratio of aldehydes in the discussion of kinetics, and even fewer, including Sharma et al. (ionic liquid) [205] and Koeken et al. (scCO₂) [206], have considered benign solvents [205-210]. Although the publications on kinetics are currently not comprehensive, it is well-known that high CO solubility reduces catalyst activity and a high H₂/CO ratio increases catalysis performance [179]. This explains why almost all published works report a positive order for H₂ and a negative order for CO in the rate expressions.

There are a number of unresolved issues remaining with respect to long-chain alkenes hydroformylation. One important aspect is the phase behavior representation. From the perspective of hydroformylation processes, phase behavior plays an important role for reaction (e.g., provide accurate gas solubility and H₂/CO ratio for long-chain alkene hydroformylation) and downstream separation (e.g., quantitatively estimate the separation costs). However, this direction has not yet been systematically studied because of theoretical difficulties, diversity of the benign solvents, and experimental expense. Consequently, the development of a suitable pathway for comprehending CXLs through thermodynamic modeling work is strongly desirable.

Section 5.2 presents a thermodynamic analysis of CXLs based on the thermodynamic modeling work with capability of fully predicting the VLE phase behavior of CXLs using the PSRK model of **Section 2.2**. Through simulations corresponding to 'experimental work' conditions, useful information can be obtained and its impact on CXLs are clarified. The 1-octene hydroformylation system is selected.

Section 5.3 describes a novel idea, a so-called 'CO₂-expanded TMS (CXTMS)', for combining CXLs and thermomorphic (or temperature-dependent) multi-component solvent (TMS) systems in accordance with the CXL features. A minor but important modeling exercise related to a TMS composed of dimethyl formamide (polar solvent), decane (non-polar solvent), and other components involved in the hydroformylation system as reactants or products is also carried out.

5.2 Features of CXLs

Four main factors, i.e., temperature, pressure, solvent proportion, and solvent type, are discussed with respect to their capability and impact to change the concentration of gases and the H₂/CO ratio. Ten conventional solvents are tested, including acetone (ACE), methanol (MeOH), acetonitrile (MeCN), toluene (PhMe), methyl cyclohexane (MeCE), n-pentane (PNE), 1,4-dioxane (DIOX), dimethyl formamide (DMF), tetrahydrofuran (THF), and ethyl acetate (EA). The investigated system contains six constituents: H₂, CO, CO₂, 1-octene, n-nonanal, and a solvent given above. The technical process has normally a temperature-range of 60°C-100°C and a pressure-range of 10bar-40bar. To obtain more information on phase behavior, a wider temperature-range of 10°C-100°C and a wider pressure-range of 10bar-100bar is investigated in this thesis. The composition varies depending on individual cases. Detailed models are shown in **Section 2.1** and **Appendix 1-2**. The specific CEoS/GE model is PSRK.

Table 5.2: Specification of cases

Case	Variables	T/°C	p/bar	Total quantity (mol/mol) H ₂ /CO/CO ₂ /OCT/NAL/solvent
Case 1	Solvent proportion	50	50	1/1/2/2/2/n
Case 2	Temperature	50-100	50	1/1/2/2/2/2
Case 3	Pressure	50	10-100	1/1/2/2/2/2

The first case investigates the impact attributed to solvent type and solvent addition. The specification can be found in **Table 5.2**. The solvent quantity n is variable with a maximum x_{solvent} (mol/mol) of 0.8. The results are displayed in **Figs. 5.2-5.5**.

Fig. 5.2 shows the impact of different solvents on the H₂ concentration in the liquid phase. Obviously, different solvents can have significantly different impact on the H₂ concentration. The more solvent ($x_{\text{solvent}} < 0.8$), the higher the H₂ concentration in the liquid. For example, the H₂ concentration is enriched by more than twice in the range $0 < x_{\text{PNE}} < 0.8$, a possible advantage for the hydroformylation reaction in CXLs. In **Fig. 5.3**, CO concentrations remain similar for most of the solvents with the exception of DMF, which dissolves much more CO than other solvents. The addition of solvent does not yield a monotonic effect with respect to the CO concentration in the liquid phase.

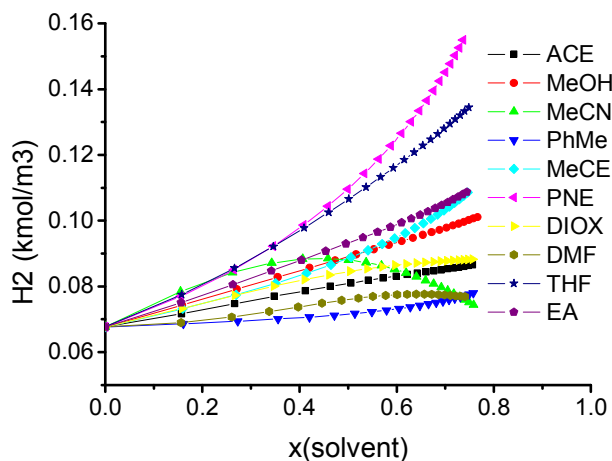


Figure 5.2: H₂ concentration in liquid dependent on solvent quantity and type

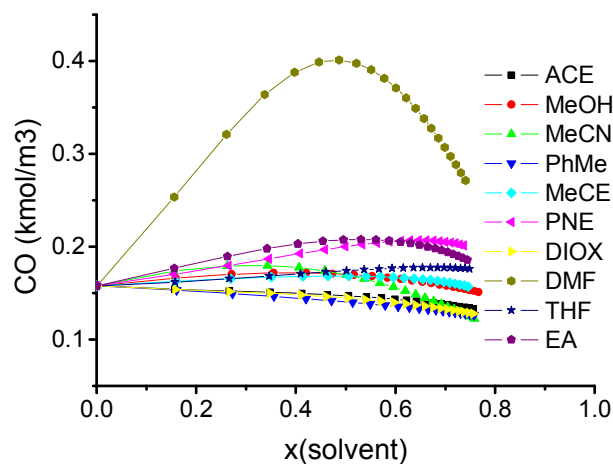


Figure 5.3: CO concentration in liquid dependent on solvent quantity and type

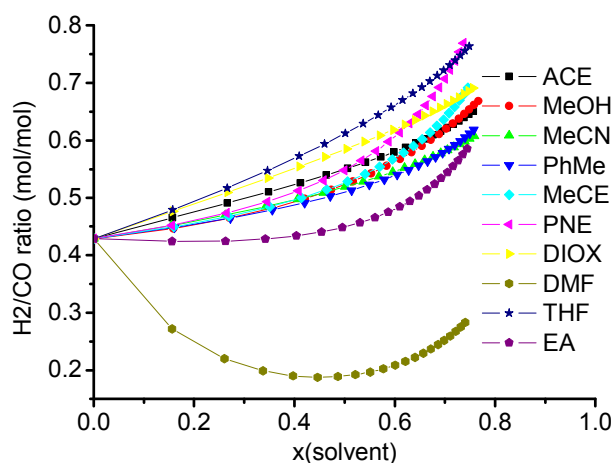


Figure 5.4: H₂/CO ratio in liquid dependent on solvent quantity and type

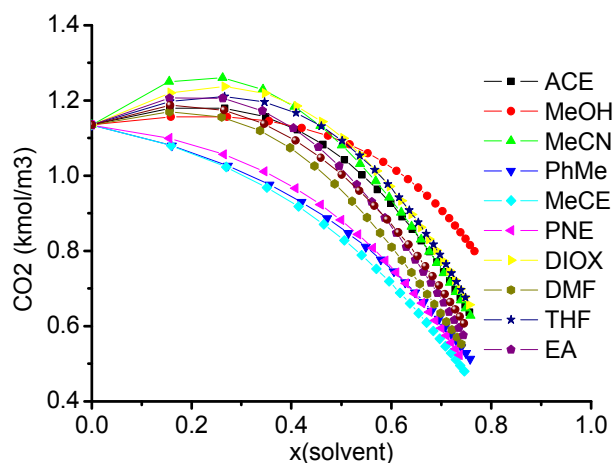


Figure 5.5: CO₂ concentration in liquid dependent on solvent quantity and type

The H₂/CO ratio dependent on the solvent is highlighted in **Fig. 5.4**. It indicates that a solvent quantity increase ($x_{\text{solvent}} < 0.8$) results in a higher H₂/CO ratio in CXLs except for the case of DMF. Taking the H₂/CO ratio as an illustration, with THF, it rises by a factor of 2 at $x_{\text{THF}} = 0.8$ over that for $x_{\text{THF}} = 0$. **Fig. 5.5** shows that the CO₂ concentration is decreased in the liquid phase when solvent is added.

The results from the first case lead to the conclusion that the addition of solvent ($x_{\text{solvent}} < 0.8$) will benefit hydroformylation in CXLs in two respects:

- The reaction rate can be increased by increasing H₂ concentration through addition of solvents. However, the addition of solvent will also dilute the concentration of the reactant 1-octene.

- The n/iso-aldehyde ratio can be improved by increasing the H₂/CO ratio with addition of solvents.

The second case investigates the impact of temperature on CXLs. The specification can be found in **Table 5.2**. The results are shown in **Figs. 5.6-5.9**.

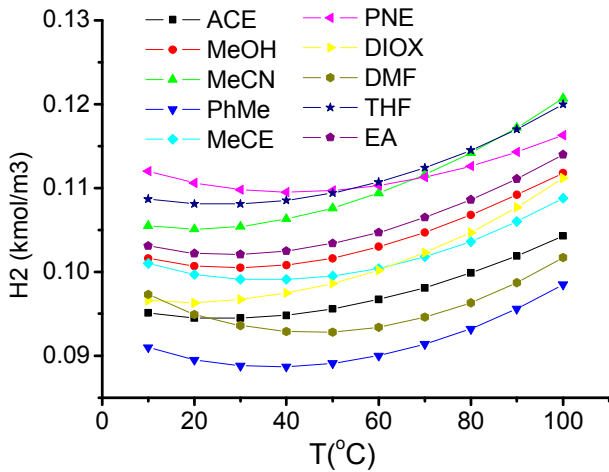


Figure 5.6: H₂ concentration in liquid dependent on temperature

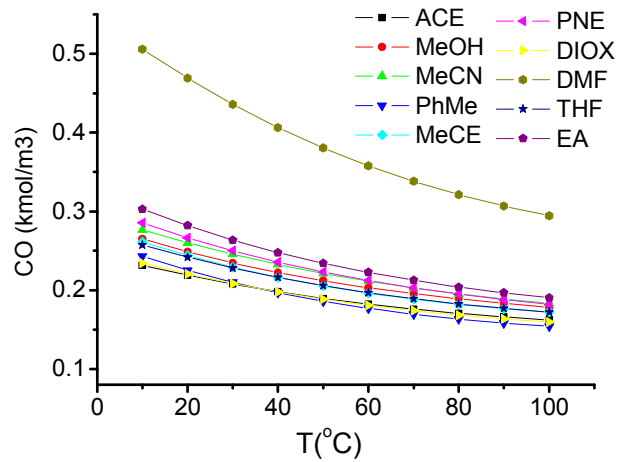


Figure 5.7: CO concentration in liquid dependent on temperature

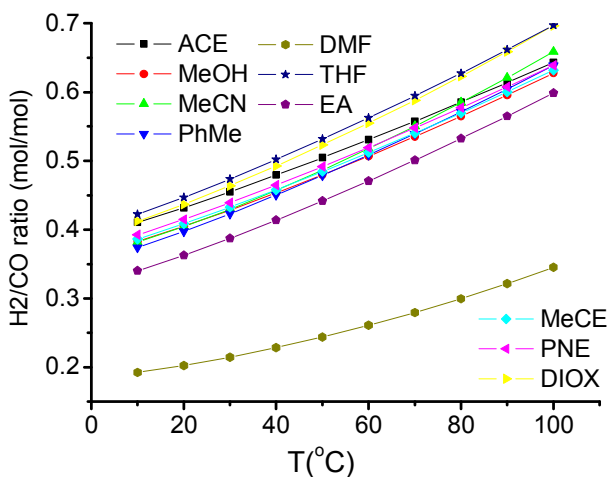


Figure 5.8: H₂/CO ratio in liquid dependent on temperature

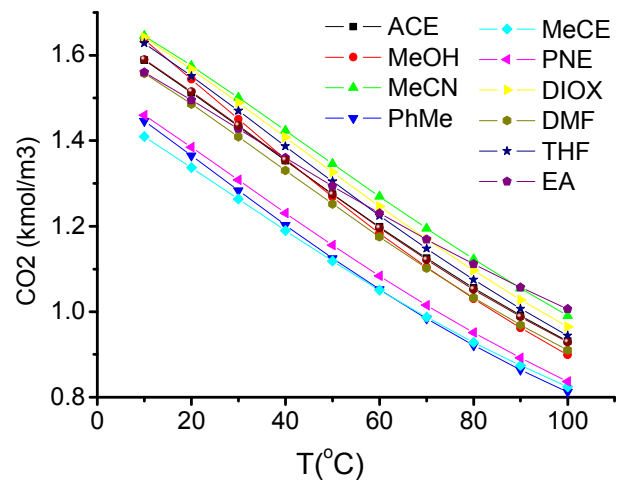


Figure 5.9: CO₂ concentration in liquid dependent on temperature

The temperature has only a slight influence on the H₂ concentration in the liquid, and the profiles are slightly arc-shaped, with their lowest points occurring between 30°C-50°C dependent on the solvent type (**Fig. 5.6**). In contrast to H₂, the temperature always has a negative influence on the CO concentration in the liquid. From 10°C to 100°C, the reduction of the CO concentration varies from 30% to 50% (**Fig. 5.7**). Such significant reduction helps to

increase the H₂/CO ratio in the liquid phase (**Fig 5.8**). The H₂/CO ratio is increased by a factor of two. **Fig. 5.9** displays the negative impact of temperature on CO₂ solubility.

From the results of the second case, several features due to the temperature variation can be observed:

- The n/iso-aldehyde ratio will be improved due to the increase of the H₂/CO ratio;
- The reaction rate of course increases as temperature rises due to the Arrhenius temperature dependency of the reaction.

The third case investigates the impact of pressure. The specification can be found in **Table 5.2**. The results are shown in **Figs. 5.10-5.13**.

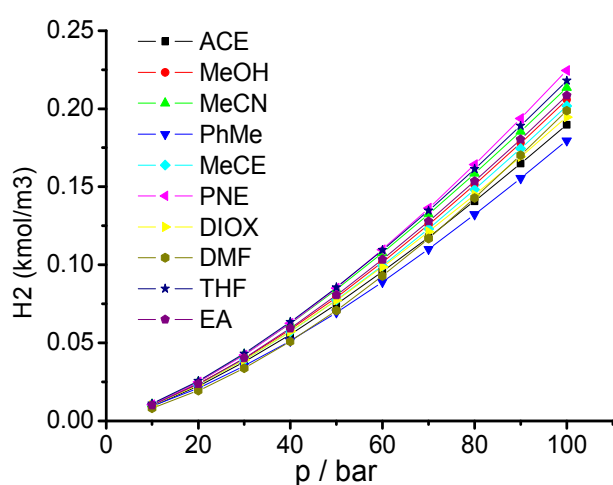


Figure 5.10: H₂ concentration in liquid dependent on pressure

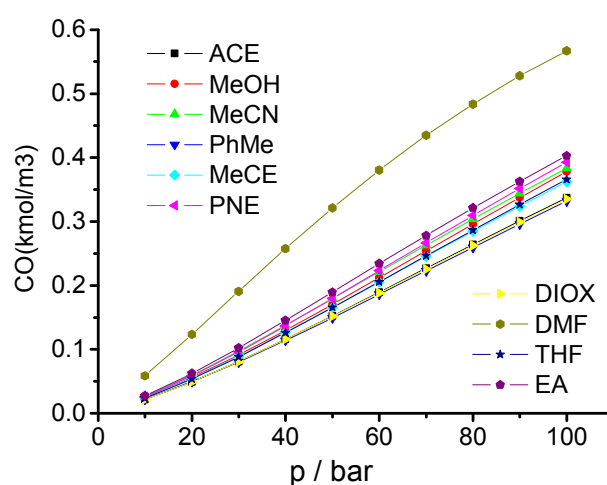


Figure 5.11: CO concentration in liquid dependent on pressure

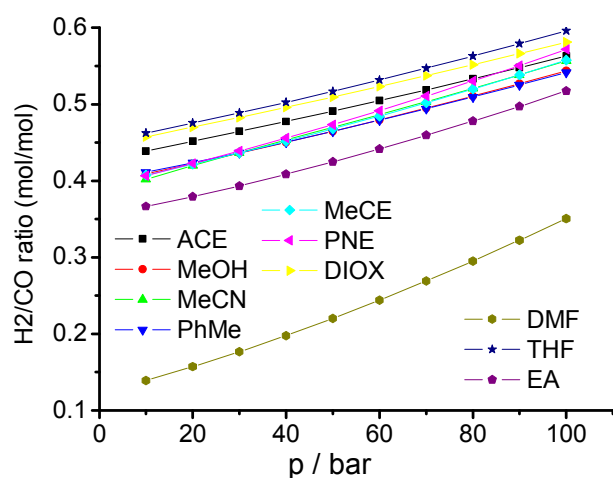


Figure 5.12: H₂/CO ratio in liquid dependent on pressure

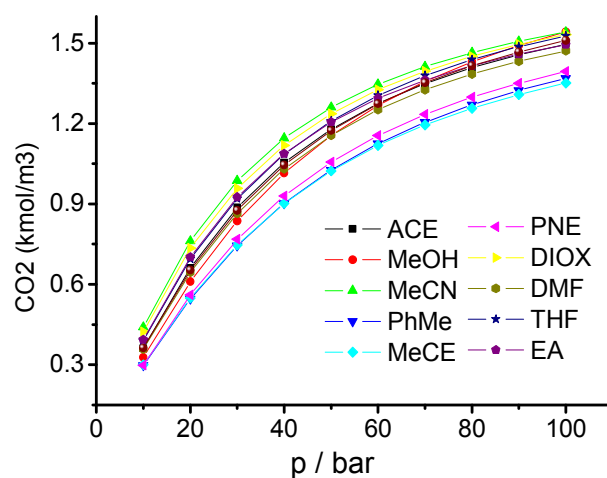


Figure 5.13: CO₂ concentration in liquid dependent on pressure

Under pressure increase, the H₂ concentration and the CO concentration are increasing significantly (**Figs. 5.10-5.11**), and the impact is nearly linear. Pressure has a positive influence (around 0.1-0.15 H₂/CO ratio increase is obtained from 10bar-100bar) on the H₂/CO ratio in the liquid (**Fig. 5.12**), although the impact is not as dramatic as that due to temperature increase. **Fig. 5.13** illustrates that the CO₂ concentration in the liquid phase is dependent on pressure changes. For this reason, while pressure can enhance the hydroformylation rate significantly, its impact on the n/iso-aldehyde ratio is not as great as that of temperature and solvent type.

Table 5.3 A table for qualitative illustrating the impacts of CXLs and the appropriate actions for hydroformylation.

Qualitative behavior	Appropriate actions for hydroformylation
Solvent type has very significant influence on gas solubility. DMF is considered to be a weak solvent for hydroformylation in CXLs;	Select solvent type carefully before the experiment;
Solvent addition ($x_{\text{solvent}} < 0.8$) has positive influence on the H ₂ /CO ratio;	Solvent addition favors a high n/iso-aldehyde ratio, but attention should also be paid to the dilution of alkene with addition of solvent;
Temperature rise can increase the H ₂ /CO ratio significantly;	Increase reaction temperature if temperature rise does not generate more by-products and consider catalyst stability;
High pressure not only increases gas solubility, but also benefits a high H ₂ /CO ratio.	Select high pressure for hydroformylation, but also consider costs of providing and maintaining a high pressure level.

At this time, the impact on the H₂/CO ratio remains unclear if the compositions vary along with the reaction. In the following discussion, we will investigate the variation of the H₂/CO ratio along with the reaction with specified temperature and pressure. Two cases will be considered. The first case applies ACE as a solvent and the second case applies THF as a solvent. Both cases assume a total amount of 100 kmol, and the initial compositions (mole ratio) are 0.2, 0.2, 0.15, 0.15, 0, and 0.2 for H₂, CO, CO₂, 1-octene, nonanal, and solvent (ACE or THF). It is assumed that there is no side reaction and all 1-octene will be consumed in the end. Thus, in such a case pure n-nonanal will be the product. The stoichiometric quantity of H₂, CO, and 1-octene will be consumed and nonanal will be produced continuously along the reaction. To account for the change of the components over reaction time, the mixture composition is varied according to the stoichiometric relationship. The variations in H₂/CO ratio in the two cases are shown in **Figs. 5.14-5.15**.

Qualitatively, both figures show similar profiles, but the H₂/CO ratio in CO₂-expanded THF has a higher value than that of CO₂-expanded ACE. Higher temperature and higher pressure also help to increase the H₂/CO ratio along with reaction. These results once again are consistent with previous conclusions. Additionally, the H₂/CO ratio profile features different trends under different conditions. For example, consider the profiles of the H₂/CO ratio with 50°C and 80°C under 50bar in **Fig. 5.14** which seems to be in contrast with each other. During hydroformylation reaction, the H₂/CO ratio profile climbs up at 50°C, yet this profile first decreases and then increases at 80°C. Obviously, both the reaction temperature and pressure have a substantial effect on the H₂/CO ratio along the reaction.

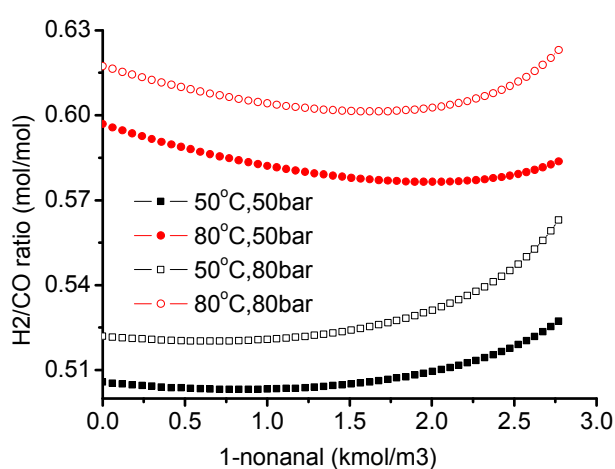


Figure 5.14: The H₂/CO ratio varies along the reaction, solvent is ACE

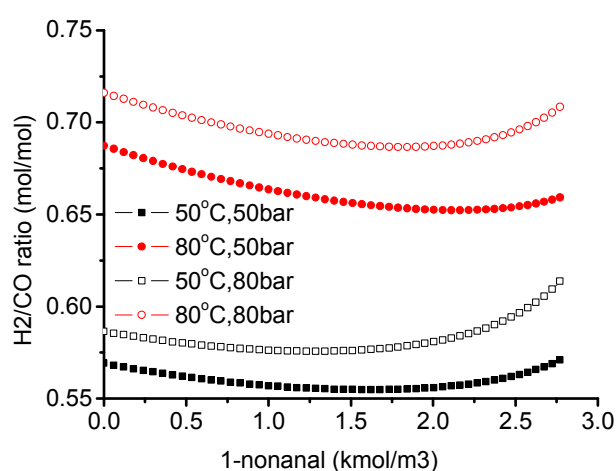


Figure 5.15: The H₂/CO ratio varies along the reaction, solvent is THF

The above analysis shows that the four factors, namely temperature, pressure, solvent type and solvent quantity, have substantial effects on the H₂/CO ratio in CXLs. The comprehensive information obtained by these thermodynamic models is useful for reactor design using the concept of Elementary Process Functions (EPF) [211, 212]. In previous work on optimization of multiphase reaction systems (e.g. [179]) often the thermodynamic models used were rather simple approaches such as, e.g., Henry's law which will not be applicable to more complex systems as considered in this work.

5.3 CO₂-Expanded TMS

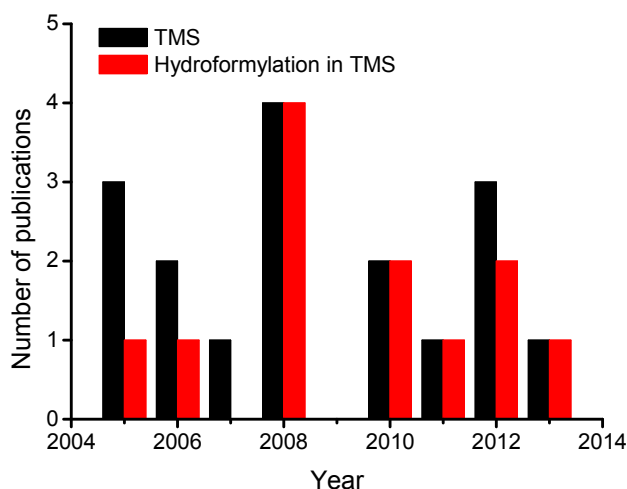


Figure 5.16: Publication review of TMS and hydroformylation in TMS (inquired by SCOPUS with temperature-dependent multi-component solvent or thermomorphic multi-component solvent and hydroformylation in title or abstract or keyword)

Pioneering work on TMS systems has been carried out by the group of Prof. A. Behr from TU Dortmund since 2005 [213]. There are only few publications, a total of 17 (**Fig. 5.16**), and a considerable number of them deal with the application of TMS for a hydroformylation reaction system. Obviously, the TMS system offers specific advantages for product separation as well as for catalyst recovery [214], and, as discussed in **Chapter 1** and **Sections 5.1-5.2**, CXLs provide benefits to the hydroformylation reaction in several aspects (**Table 5.3**). If these two concepts are particularly integrated into the reaction and into separation, the integrated process could be extremely efficient. Technically speaking, this concept is possible, because both constituents of TMS, dimethyl formamide (DMF) and n-decane (C₁₀), can be efficiently expanded [215, 216].

Table 5.4: Features of CXTMS and possible benefits for the hydroformylation process

Feature	Possible benefit
Enhance solubility of gases	Increase reaction rate, reduce reactor size
Increase H ₂ /CO ratio	Increase n/iso-aldehyde ratio in the product
Enhanced transport rates	Increase reaction rate, reduce reactor size
Eco-friendly feature	Reduce pollution

The LLE information may be used to design the operational point between reaction and downstream separation of hydroformylation in TMS. Therefore, the thermodynamic modeling of this complex system is an important part of the SFB Transregio 63 project [178], especially

in clarifying the specific temperature-dependent character. By tuning the phase behavior using temperature as a control variable, the process can be manipulated. In other words, the reaction can be performed under high temperature to approach a homogeneous phase, while the separation can be performed under low temperature to split the phase. The system thus has features of both efficient reaction and separation processes. To design such processes, an understanding of the LLE phase behavior of TMS systems is definitely required.

However, there are only few available publications of phase behavior modeling work, especially for modeling the LLE of TMS systems. To the best knowledge of the author, only one publication has focused on modeling the LLE of TMS using PC-SAFT [214]. In this publication, several binary systems and ternary systems were successfully modeled by PC-SAFT. This model cannot, however, predict comprehensive TMS systems with all components involving 1-dodecene hydroformylation (i.e., DMF, n-decane, 1-dodecene, 2-dodecene, n-dodecane, 1-tridecanal, and 2-methyl-dodecanal) due to lack of parameters. In this work, UNIFAC-Do has been successfully applied to predict the LLE phase behavior of binary systems (**Appendix 6**) and ternary systems (**Figs. 5.17-5.18**). The detailed parameters are listed in **Appendix 2**. With respect to the features of UNIFAC-Do, the extension to a multicomponent system is also possible. Therefore, this work provides an alternative way for quantitatively estimating the composition distribution of LLE, and it can also be used to estimate the separation costs of the hydroformylation processes.

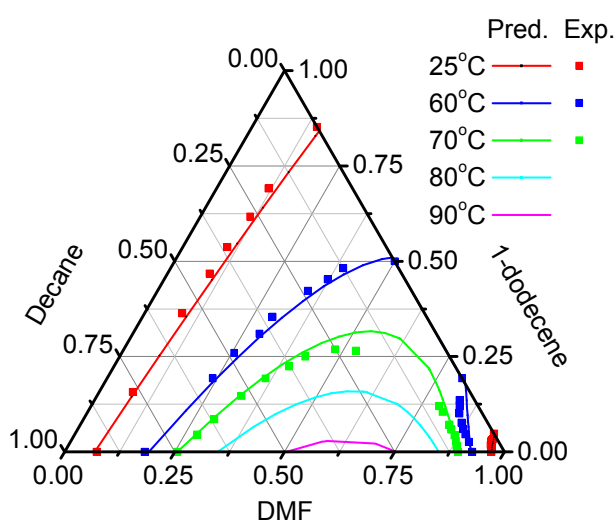


Figure 5.17: The ternary diagram of DMF/1Do/C10 system predicted by UNIFAC-Do with regressed interaction parameters, data reference [214]

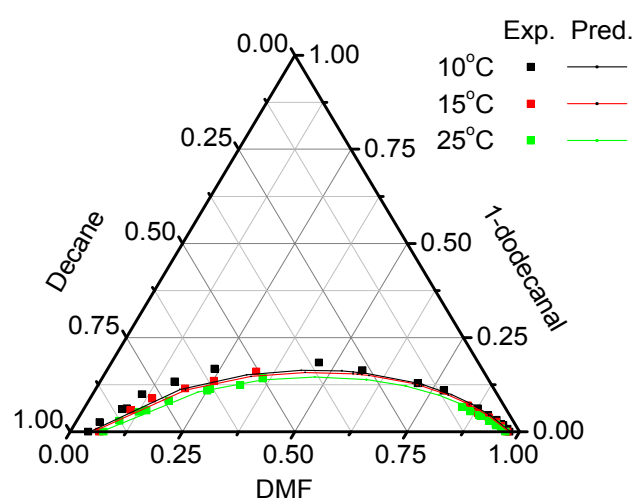


Figure 5.18: The ternary diagram of DMF/NC13/C10 system predicted by UNIFAC-Do with regressed interaction parameters, data reference [214]

5.4 Chapter Summary

In this chapter, a systematic thermodynamic analysis for comprehension of CXLs is first performed. Four factors, namely temperature, pressure, solvent type and solvent quantity are discussed. The various influences are generally sorted in terms of the solubility of gases and the H₂/CO ratio. Several guidelines are generalized for 1-octene hydroformylation in CXLs. The H₂/CO ratio along with the reaction can be tuned. The CEoS/GE model provides a way for representing a comprehensive correlation of temperature, pressure, and composition in CXLs, and this thermodynamic information can therefore be used to investigate in more detail hydroformylation kinetics and further research of reactor design using the concept of EPF. Besides, a fundamental concept, namely CXTMS, is proposed and possible benefits are enumerated for long-chain hydroformylation. The important representation of LLE phase behavior of the 1-dodecene hydroformylation system in TMS is performed using UNIFAC-Do.

Obviously, using such a detailed thermodynamic prediction, more information can be obtained to understand the complex systems better. Based on this information, the long-chain hydroformylation can be manipulated with suitable control variables in a proper manner. Thus, this chapter demonstrates a practical thermodynamic basis that can be used for solvent screening and included into the EPF concept for process intensification.

However, the lack of 'tailor-made' hydroformylation kinetics for CXLs limits a further research in this study. There are extremely comprehensive correlations between the reaction kinetics and the factors discussed above. Several facets are illustrated:

- The solvent affects through transient state and solvation effect the H₂/CO ratio and solubility of gases;
- The temperature has an extraordinary influence on the H₂/CO ratio, and reaction networks through the activation energy of reactions;
- Solvent type and quantity also affects the recovery of the rhodium catalyst.

In short, a number of further efforts, especially in the area of reaction kinetics, are required for long-chain alkene hydroformylation.

Chapter 6

Summary, Conclusion, and Outlook

6.1 Summary

This thesis is devoted to the study of chemical processes based on a benign alternative solvent concept known as CXLs. Two parts, including Fundamentals and Applications, are covered.

In the section titled Fundamentals, it was shown that the thermodynamic aspect helps to quantitatively understand the phase behavior and the aspect of the phase equilibrium calculation helps to efficiently determine the phase equilibrium state. To detail, the CEoS/GE model is applied to model the VLE and VLLE phase behaviors involved in CXLs and its performance is evaluated through abundant exemplifications. The dynamic equations are, at first, developed based on mass balance and, secondly, the phase equilibrium criteria are validated in terms of the maximum entropy theory of a closed system, and finally the performance of the dynamic equations are evaluated using complex cases. Besides, the background of the performance is analyzed and the features of the dynamic equations are summarized.

The Applications part emphasizes the approaches used to manipulate the phase behavior in separation and reaction processes at higher hierarchical process levels. For separation processes, at first, a separation concept is proposed and, secondly, two process variants are developed and validated in process simulation studies, and finally the performance of the new separation concept is evaluated and the potential is highlighted. For reaction processes involving CXLs, a 1-octene hydroformylation case is investigated by thermodynamic analysis with regard to the gas solubility and much information is generalized to comprehend the characteristic features of CXLs. Then, a fundamental idea to combine the features of CXLs and TMS for a hydroformylation process, namely CXTMS, is put forward and the LLE phase behavior of a TMS system involved in the SFB TR/63 project is modeled.

The major contributions of this thesis are summarized as follows:

- Provided practical path to model the phase behavior (VLE and VLLE) of CXLs using the CEoS/GE models, and phase behavior (LLE) of TMS using UNIFAC-Do;
- Established the dynamic equations to determine phase behavior equilibria;
- Designed and validated a new concept to separate azeotropic mixtures;
- Studied the hydroformylation in CXLs using a thermodynamic method.

6.2 Conclusion

After this study, a general conclusion can be drawn that a clear route from the phase level to the unit operation level and/or plant level can be established. The implementation from the phase level to the higher hierarchical levels (unit operation level and/or plant level) is successfully performed.

The Fundamentals part confirms the capacity of the CEoS/GE model to predict the VLE and VLLE phase behaviors of CXLs and the practical characters of dynamic equations to determine phase behaviors. Therefore, this identification of phase equilibria provides a confident basis to implement the phase level to higher hierarchical levels. To detail the thermodynamic modeling work, the CEoS/GE model is practical to provide VLE information of CXLs with regard to the feature of UNIFAC, in case without experimental data. But, a CEoS/GE model with adjustable parameters is required for a good prediction of the VLLE phase behavior. Therefore, experimental data are consequently required for parameter estimation. On another hand, the dynamic equations demonstrated as novel but general approach provide the practical benefits to determine complex phase equilibria.

In the Applications part, the implementation from the phase level to the higher hierarchical levels is exemplified in an azeotropic mixture separation process in particular. The results show that the new chemical process employing the benign alternatives is significantly different in comparison to the conventional chemical processes and that it has significant potential for process intensification. Therefore, the novel separation concept is a promising alternative to the conventional processes for azeotropic mixture separation. For reaction intensification using CO₂, though there is no suitable kinetics to quantitatively implement reaction from the phase level to the higher hierarchical levels as in the separation case, the thermodynamic analysis provides a path to comprehend the 1-octene hydroformylation system in CXLs, and the thermodynamic modeling of 1-dodecene hydroformylation system in TMS expresses the phase behavior tuning between homogeneous reaction and heterogeneous separation quantitatively. Therefore, this provides a suitable path to implement the phase level to the higher hierarchical levels with respect to downstream separation. The hypothesis, CXTMS, is still required to be validated through experiments.

6.3 Outlook

Due to complexity of the benign solvent alternatives, further work is required to expand upon several points not covered in this thesis.

In the first place, more experimental work is required to be able to study the phase behavior of CXLs more in depth. Especially the VLLE phase behavior of CXLs systems cannot be fully predicted without any data. Moreover, only a few binary systems regarding the ‘salting-out’ performance have been published. Unfortunately, this data is still not totally acceptable on accounts of the disagreement in different publications due to difficulty of complex phase behavior measurement. On this point there is still wide open space to explore. In another word, the powerful models are also still necessary to be used for predicting the phase behavior in case of limited data or even no data. For instance, in **Chapter 4**, the PRWS with regressed k_{ij} from isothermal data can have high uncertainties when extrapolated to other temperatures. So currently, only the influence of pressure on the process is clarified; the influence of temperature on the process remains unknown. If the temperature can be included in modeling, the dimension of thermodynamic space for the process is much greater, and better solutions may be found.

Quite a few facets of research on the long-chain alkene hydroformylation have to be comprehensively manipulated, i.e., thermodynamic aspect, reaction kinetics and catalyst recovery. Several bottlenecks still require much effort:

- Prediction of the phase behavior involving benign solvents. It is difficult if ILs or surfactants are involved because there is no credible method for them. If the system is more complex, e.g., scCO_2 + ILs, the research has been only carried out empirically;
- Prediction of the reaction rate with respect to solvents, as solvents may have a non-negligible effect on reaction kinetics;
- Catalyst recovery. The rhodium catalyst is more expensive than gold, and it is not acceptable in industry if the rhodium concentration in the raw product stream is more than 1-10ppb. This is a harsh constraint.

The dynamic approach for determining phase behavior shows practical ability. However, the theoretical basis is based on a closed system with constant temperature and pressure. The possibility to extend this method to the close/open system with reaction, with or without unknown temperatures and pressures, is still an open topic.

Appendix

Appendix 1: CEoS/GE model

All CEoS/GE mixing rules are derived from the basic relationship between GE and φ :

$$\frac{G_{EoS}^E}{RT} - \frac{G_{ref.}^E}{RT} = \ln \frac{\varphi_{m,EoS}(T, p, x_i)}{\varphi_{m,ref.}(T, p, x_i)} - \sum_i^{NC} x_i \ln \frac{\varphi_{i,EoS}^*(T, p)}{\varphi_{i,ref.}^*(T, p)} \quad (\text{a1})$$

Usually, only two reference fluids are used, i.e., ideal fluid and VDW fluid (**Table 2.1**). Most of mixing rules apply ideal fluid as reference, after that the **Eq. (a1)** is derived as:

$$\frac{G_{EoS}^E}{RT} = Z_m - \sum_i^{NC} x_i \left[Z_i - \ln \left(\frac{Z_m - B_m}{Z_i - B_i} \right) \right] - \varepsilon_m C(V_m) - \sum_i^{NC} x_i \varepsilon_i C(V_i) \quad (\text{a2})$$

$$\text{Or } \frac{A_{EoS}^E}{RT} = - \sum_i^{NC} x_i \ln \left(\frac{Z_m - B_m}{Z_i - B_i} \right) - \varepsilon_m C(V_m) - \sum_i^{NC} x_i \varepsilon_i C(V_i) \quad (\text{a3})$$

$$\text{With } C(V) = \frac{1}{u-w} \ln \left(\frac{V+wb}{V+ub} \right), \quad C^* = \frac{1}{u-w} \ln \left(\frac{1+w}{1+u} \right), \quad C_r = -\frac{1}{w-u} \ln \left(\frac{r+w}{r+u} \right), \quad r = \frac{V}{b},$$

$$A = \frac{ap}{R^2T^2}, \quad B = \frac{bp}{RT}, \quad \varepsilon = \frac{a}{bRT} = \frac{A}{B}.$$

Applying the simplifications based on infinite pressure and/or zero pressure theory, the relationships is founded between G_{EoS}^E and G^E , and G^E is calculated by

$$G^E = RT \sum_i^N x_i \ln \gamma_i, \text{ where } \gamma_i \text{ is usually provided by activity models.}$$

Table A1.1: Formula list of EoS/GE mixing rules

Name	b_m	ε_m Or a_m
HVO	$b_m = \sum_i^{NC} x_i b_i$	$\varepsilon_m = \sum_i^{NC} x_i \varepsilon_i + \frac{G^E}{RTC^*}$
KTK	$b_m = \sum_i^{NC} x_i b_i$	$a_m = \sum_i^{NC} \sum_j^{NC} x_i x_j a_{ij} - \frac{b_m}{C^*} G^E$
WS	$b_m = \frac{\sum_i^{NC} \sum_j^{NC} x_i x_j (b - a/RT)_{ij}}{1 - \varepsilon_m}$	$\varepsilon_m = \sum_i^{NC} x_i \varepsilon_i + \frac{G^E}{RTC^*}$
HVOS	$b_m = \frac{\sum_i^{NC} \sum_j^{NC} x_i x_j (b - a/RT)_{ij}}{1 - \varepsilon_m}$	$\varepsilon_m = \sum_i^{NC} x_i \varepsilon_i + \frac{1}{C^*} \left[\frac{G^E}{RT} + \sum_i^{NC} x_i \ln \left(\frac{b_m}{b_i} \right) \right]$
TCO	$b_m = \left(b_{VDW} - \frac{a_{VDW}}{RT} \right) / (1 - \varepsilon_m)$	$\varepsilon_m = \frac{A_{VDW}}{B_{VDW}} + \frac{A^E}{C^* RT}$
CHV1	$b_m = \sum_i^{NC} x_i b_i$	$\varepsilon_m = \sum_i^{NC} x_i \varepsilon_i + \frac{1}{C^*} \left[\frac{A^E}{RT} + (1 - \delta) \cdot \sum_i^{NC} x_i \ln \left(\frac{b_m}{b_i} \right) \right]$
MTC	$b_m = \left(b_{VDW} - \frac{a_{VDW}}{RT} \right) / (1 - \varepsilon_m)$	$\varepsilon_m = \sum_i^{NC} x_i \varepsilon_i + \frac{A^E}{RTC^*}$
EAL	$b_m = \frac{Q}{R} \cdot \frac{1 - \varepsilon_m}{1 + (u + w) \varepsilon_m}$ $Q = \sum_i^{NC} \sum_j^{NC} x_i x_j (b - a/RT)_{ij}$ $R = \sum_i^{NC} \sum_j^{NC} x_i x_j \left[b^2 + (u + w) \frac{ab}{RT} \right]_{ij}$	$\varepsilon_m = \sum_i^{NC} x_i \varepsilon_i + \frac{G^E}{RTC^*}$
HVLP	$b_m = \sum_i^{NC} x_i b_i$	$\varepsilon_m = \sum_i^{NC} x_i \varepsilon_i + \frac{1}{\delta} \left[\frac{G^E}{RT} + \sum_i^{NC} x_i \ln \left(\frac{b_m}{b_i} \right) \right]$
MHV1	$b_m = \sum_i^{NC} x_i b_i$	$\varepsilon_m = \sum_i^{NC} x_i \varepsilon_i + \frac{1}{q_1} \left[\frac{G^E}{RT} + \sum_i^{NC} x_i \ln \left(\frac{b_m}{b_i} \right) \right]$
MHV2	$b_m = \sum_i^{NC} x_i b_i$	$q_1 \cdot \left(\varepsilon_m - \sum_i^{NC} x_i \varepsilon_i \right) + q_2 \cdot \left(\varepsilon_m^2 - \sum_i^{NC} x_i \varepsilon_i^2 \right)$ $= \frac{G^E}{RT} + \sum x_i \ln \left(\frac{b_m}{b_i} \right)$
PSRK	$b_m = \sum_i^{NC} x_i b_i$	$\varepsilon_m = \sum_i^{NC} x_i \varepsilon_i + \frac{1}{q_1} \left[\frac{G^E}{RT} + \sum_i^{NC} x_i \ln \left(\frac{b_m}{b_i} \right) \right]$
Soave	$b_m = \sum_i^{NC} x_i b_i$	$q(\varepsilon_m) = \sum_i^{NC} x_i q(\varepsilon_i) + \frac{G^E}{RT} + \sum_i^{NC} x_i \ln \left(\frac{b_m}{b_i} \right)$
HVT	$b_m = \frac{\sum_i^{NC} x_i (b_i - a_i/RT)}{1 - \varepsilon_m}$	$\varepsilon_m = \sum_i^{NC} x_i \varepsilon_i + \frac{1}{C^*} \left[\frac{G^E}{RT} + \sum_i^{NC} x_i \ln \left(\frac{b_m}{b_i} \right) \right]$

Table A1.1 (continuous): Formula list of EoS/GE mixing rules

LPVP	$b_m = \sum_i^{NC} x_i b_i$	$U_m = \sum_i^{NC} x_i U_i + \frac{G^E}{RT} + \sum_i^{NC} x_i \ln \left(\frac{b_m}{b_i} \right)$
Exact	$b_m = \sum_i^{NC} x_i b_i$	$0 = q(\varepsilon_m) - \frac{G^E}{RT} - \sum_i^{NC} x_i \ln \left(\frac{b_m}{b_i} \right) - \sum_i^{NC} x_i q^e(\varepsilon_i)$
TCB(0)	$b_m = \left(b_{VDW} - \frac{a_{VDW}}{RT} \right) / (1 - \varepsilon_m)$	$\varepsilon_m = \frac{A_{VDW}}{B_{VDW}} + \frac{1}{C_{V0}} \left(\frac{A_0^E}{RT} - \frac{A_{0,VDW}^E}{RT} - \ln \frac{b_{m,VDW}}{b_m} \right)$
CHV2	$b_m = \sum_i^{NC} \sum_j^{NC} x_i x_j b_{ij}$	$\varepsilon_m = \sum_i^{NC} x_i \varepsilon_i + \frac{1}{q_1} \left[\frac{G^E}{RT} + \sum_i^{NC} x_i \ln \left(\frac{b_m}{b_i} \right) \right]$
LCVM	$b_m = \sum_i^{NC} x_i b_i$	$\varepsilon_m = \sum_i^{NC} x_i \varepsilon_i + \frac{\delta G^E}{C^* RT} + \frac{1 - \delta}{q_1} \left[\frac{G^E}{RT} + \sum_i^{NC} x_i \ln \left(\frac{b_m}{b_i} \right) \right]$
TCB(r)	$b_m = \left(b_{VDW} - \frac{a_{VDW}}{RT} \right) / (1 - \varepsilon_m)$	$\varepsilon_m = \frac{A_{VDW}}{B_{VDW}} + \frac{1}{C_r} \left(\frac{A_0^E}{RT} - \frac{A_{0,VDW}^E}{RT} - \ln \frac{b_{m,VDW}}{b_m} \right)$
BLCVM	$b_m = \left(b_{VDW} - \frac{a_{VDW}}{RT} \right) / (1 - \varepsilon_m)$	$\varepsilon_m = \sum_i^{NC} x_i \varepsilon_i + \frac{A^E}{RT} \left(\frac{\delta}{C^*} + \frac{1 - \delta}{q_1} \right) + \frac{1 - \delta}{q_1} \sum_i^{NC} x_i \ln \left(\frac{b_m}{b_i} \right)$

Note:

- The HK and Uniwaals are not given because they are implicit functions owing to the complex structure. Several distinct functions, such as U in LPVP and q function in Soave and Exact, are also not listed, which are shown in corresponding reference (**Table 2.1**).

Appendix 2: Parameters of investigated systems

In this appendix, the parameters of modeling VLE and VLLE behavior of investigated system are given. The detailed modeling steps are shown in [52, 83]. They contain:

- **Table A2.1** shows the property parameters;
- **Table A2.2** shows the interaction parameter k_{ij} of PRWS;
- **Table A2.3-A2.5** shows the parameters of UNIFAC-PSRK and UNIFAC-Lby, which are integrated in CEoS/GE models, see references [52, 83, 161];
- **Table A2.6** shows the parameters for H₂O/MeCN system (NRTL-IG) are obtained from Aspen internal database [217];
- **Table A2.7-A2.8** shows the parameters of UNIFAC-Do., which are used for predicting the temperature dependent phase behavior of TMS system.

Table A2.1: Property parameters for various substances [217]

Component	$T_c/^\circ\text{C}$	P_c (bar)	ω	Component	$T_c/^\circ\text{C}$	P_c (bar)	ω
H ₂ O	373.98	220.55	0.344861	OCT	293.85	26.80	0.392059
MeOH	239.35	80.84	0.565831	NAL	384.85	27.30	0.511744
DME	126.95	53.70	0.200221	ACE	235.05	47.01	0.306527
CO ₂	31.06	73.83	0.223621	MeCN	272.35	48.30	0.337886
H ₂	-239.96	13.13	-0.21599	PhMe	318.60	41.08	0.264012
CO	-140.23	34.99	0.048162	DIOX	313.85	52.081	0.279262
PNE	196.55	33.7	0.251506	MCH	298.95	34.8	0.236055
DMF	376.45	44.2	0.31771	EA	250.15	38.8	0.366409
MeCE	298.95	34.8	0.236055	THF	267	51.9	0.225354

Note:

- The parameters of Mathias-Copeman α function for MSRK and MPS are not given here, details are shown in the article [52] or Aspen internal database [217].

Table A2.2: k_{ij} of PRWS model [52, 83, 161]

System	Comp. i	Comp. j	PRWS, $k_{ij}=k_{ji}$ ($k_{ii}=0$)		
			UNIFAC-PSRK	UNIFAC-Lby	NRTL
H ₂ O/DIOX/CO ₂	H ₂ O	DIOX	--	--	0.088064
	DIOX	CO ₂	--	--	0.278162
	H ₂ O	CO ₂	--	--	0.088064

Table A2.2 (continuous): k_{ij} of PRWS model

H ₂ O/MeOH/DME/CO ₂	H ₂ O	MEOH	0.104396	0.073108	--
	H ₂ O	DME	0.324279	0.314029	--
	H ₂ O	CO ₂	0.232683	-0.041305	--
	MEOH	DME	0.096760	0.117856	--
	MeOH	CO ₂	0.302716	0.249218	--
	DME	CO ₂	0.084515	0.074518	--
H ₂ O/MeCN/CO ₂	H ₂ O	MeCN	0.371298	--	--
	MeCN	CO ₂	0.783218	--	--
	H ₂ O	CO ₂	0.548554	--	--

Note:

- The table with '--' denotes that the model combination is not involved in this thesis.

Table A2.3: Group parameters of the UNIFAC-PSRK and UNIFAC-Lby

Chemical	Main group	Subgroup	Number	UNIFAC-PSRK		UNIFAC-Lby	
				R	Q	R	Q
CO ₂	CO ₂	CO ₂	1	1.3	0.982	2.5920**	2.5220**
H ₂ O	H ₂ O	H ₂ O	1	0.92	1.4	0.9200*	1.400*
MeOH	CH ₃ OH	CH ₃ OH	1	1.4311	1.432	1*	1*
DME	CH ₂	CH ₃ -	1	0.9011	0.848	0.9011*	0.848*
	CH ₃ O-	CH ₃ O-	1	1.145	1.088	1.1450*	0.9*
H ₂	H ₂	H ₂	1	0.4160	0.5710	--	--
CO	CO	CO	1	0.7110	0.8280	--	--
O ₂	O ₂	O ₂	1	0.7330	0.8490	--	--
NAL	CH ₂	CH ₃ -	1	0.9011	0.848	--	--
		-CH ₂ -	7	0.6744	0.5400	--	--
	-CHO	-CHO	1	0.9980	0.9480	--	--
ACE	CH ₃ CO	CH ₃ CO	1	1.6724	1.4880	--	--
	CH ₂	CH ₃ -	1	0.9011	0.8480	--	--
MeCN	CH ₃ CN	CH ₃ CN	1	1.8701	1.7240	--	--
PhMe	-CH=	-CH=	5	0.5313	0.4000	--	--
	-C-CH ₃	-C-CH ₃	1	1.2663	0.9680	--	--

Note:

- The table with '--' denotes that this UNIFAC-Lby is not used to represent the involved chemicals;
- All parameters of UNIFAC-PSRK are from [69];

Table A2.4 (continuous): UNIFAC-PSRK interaction Parameters $a_{ij,1}$, $a_{ij,2}$, $a_{ij,3}$

Group i/j	-CH=	-C-CH ₃	CH ₃ COO-	CO ₂	H ₂	CO	O ₂
CH ₂				919.8	613.3	-78.389	
				-3.9132	-2.5418	1.87270	
				0.004631	0.006638		
-CH=CH ₂				-52.107	585	-241.56	
				1.5473	-0.8727	1.2296	
H ₂ O				-1163.5			
				5.4765			
				-0.002603			
CH ₃ OH				-72.04			
CH ₃ O-				2795.3			
CH ₃ CO-				132.28	679.19	416.9	
				-1.4761			
-CHO					-3401		
				-162	13.11	3017.5574	
CH ₃ CN				307.1		707.2346	434.74
-CH=	0	167		219.25	734.87		
-C-CH ₃				296.88	320		
	-146.8	0		-0.2073			
CH ₃ COO-			0			4334.3347	
CO ₂	-29.4	249.32		0	838.06	161.54	208.14
		-0.9249			-1.0158		
H ₂				3048.9		863.18	
	16.884	126.44		-10.247	0	-12.309	
						0.046316	
CO					494.67		
			-257.3043	4.2038	-8.1869	0	
					0.04718		
O ₂			32.043			0	

Note:

- All parameters are directly taken from PSRK database [69], except for those parameters correlated with experiment data shown as below. The regression procedure using Aspen Properties (maximum likelihood method) is the same as the reference [52].

- The VLE experimental data of the CO-n-nonanal system and the CO-CO₂-n-nonanal system [50] are used for regression of parameters of the CO and –CHO groups;
- The VLE experimental data of CO/CO₂/MeCN from [47, 49] are used for regression of parameters between CO and MeCN groups;
- The VLE experimental data of EA/CO from [219] are used for regression of parameters between CO and CH₃COO- groups;
- Blank entries mean that interaction parameters are not applicable in this thesis and therefore not needed;
- $a_{ij} = a_{ij,1} + a_{ij,2} (T/K) + a_{ij,3} (T/K)^2$.

Table A2.5: UNIFAC-Lby interaction Parameters $a_{ij,1}$, $a_{ij,2}$, $a_{ij,3}$

Group i/j	CH ₃ -	CH ₃ O-	CO ₂	H ₂ O	CH ₃ OH
CH ₃ -		230.5*	123.9**	1857*	1318*
	0	-1.328	-0.4065	-3.322	-0.01261
		-2.476	0	-9	-3.228
CH ₃ O-	369.9*		117.7**	183.1*	295.2*
	-1.542	0	5.759	-2.507	-0.2191
	-3.228		0	0	3.441
CO ₂	-55.69**	82.87**		1067.0**	727.9**
	-0.4904	-2.877	0	-0.4180	-1.331
	0	0		0	0
H ₂ O	410.7*	19.54*	226.6**		265.5*
	2.868	1.293	-0.2410	0	3.54
	9	-8.85	0		8.421
CH ₃ OH	16.25*	-73.54*	-126.6**	-75.41*	
	-0.3005	-1.237	-0.2024	-0.757	0
	0.6924	-2.308	0	-4.745	

Note:

- UNIFAC-Lby, parameters are from [218] with *, and [66] with **.
- $a_{ij} = a_{ij,1} + a_{ij,2} ((T/K) - 298.15) + a_{ij,3} \left((T/K) \cdot \ln \frac{298.15}{(T/K)} + (T/K) - 298.15 \right)$

Table A2.6: NRTL parameters

	Integrated in PRWS model For predicting VLLE under high pressure [46]			Integrated in NRTL-IG model For predicting VLE under low pressure [217]	
Comp. i	CO ₂	CO ₂	DIOX	H ₂ O	H ₂ O
Comp. j	H ₂ O	DIOX	H ₂ O	MeCN	DIOX
a_{ij}	0	0	0	1.0567	6.5419
a_{ji}	0	0	0	-0.1164	-3.3099
b_{ij}	1520.82	492.68	326.61	283.4087	-1699.4196
b_{ji}	554.58	-571.69	444.37	256.4588	1348.1772
α	0.2	0.2	0.267	0.3	0.3

Table A2.7: UNIFAC-Do parameters, part 1: R, Q

Main group	Subgroup	R	Q
CH ₂	CH ₃ -	0.6325	1.0608
	-CH ₂ -	0.6325	0.7081
	-CH<	0.6325	0.3554
DMF	DMF	2.0000	2.0930
-C=C-	-CH=CH ₂	1.2832	1.6016
	-CH=CH-	1.2832	1.2489
-CHO	-CHO	0.7173	0.7710

Table A2.8: UNIFAC-Do Interaction parameters, part 2: $a_{ij,1}$, $a_{ij,2}$, $a_{ij,3}$

Group i/j	CH ₂	CHO	DMF	-C=C-
CH ₂	0	484.947452	871.437927	189.66
			-0.9515929	-0.27232
CHO	-529.29216	0	-599.5557	202.49
DMF	114.342456	46.067926	0	-55.044021
	-0.7540952			-0.3573974
-C=C-	-95.418	476.25	1033.73782	0
	0.061708		-2.1595105	

Note:

- All R and Q in **Tab A2.7-A2.8** are from the published database of UNIFAC-Do [220], except those interaction parameters expressed below. The reason is that the model with original interaction parameters (published database of UNIFAC-Do [220]) cannot predict the TMS system quantitatively (See **Appendix 7**);

- The interaction parameters of DMF/CH₂ are regressed from binary LLE data [214] of DMF/n-decane; the interaction parameters of DMF/-C=C- are regressed from binary LLE data [214] of DMF/1-dodecene; the interaction parameters of CH₂ and CHO, DMF and CHO group are regressed using the ternary LLE experimental data of DMF/1-dodecanal/n-decane [214]. The regression procedure using Aspen Properties (maximum likelihood method) is the same as the reference [52];
- $a_{ij} = a_{ij,1} + a_{ij,2} (T/K) + a_{ij,3} (T/K)^2$.

Appendix 3: Extra Diagrams of Chapter 2

The following are the diagrams predicted using CEoS/GE model, but diagrams involved in **Tables 2.2-2.3** are not displayed all in the **Chapter 3** and this appendix. The full figures and experimental data reference are shown in the article [52, 83].

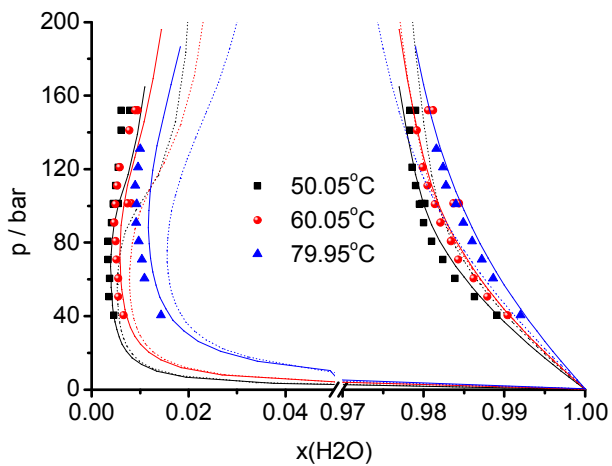


Figure A3.1: Isothermal VLE diagram of $\text{H}_2\text{O}/\text{CO}_2$ system, predicted by PRWS with UNIFAC-PSRK (solid line) and UNIFAC-Lby (dot line)

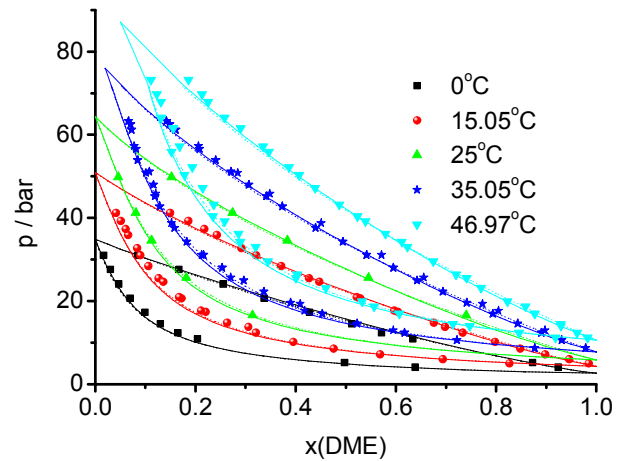


Figure A3.2: Isothermal VLE diagram of DME/CO_2 system, predicted by PRWS with UNIFAC-PSRK (solid line) and UNIFAC-Lby (dot line)

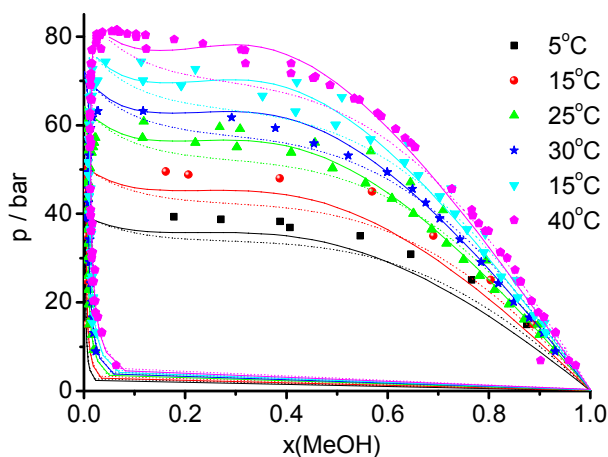


Figure A3.3: Isothermal VLE diagram of MeOH/CO_2 system, predicted by PRWS with UNIFAC-PSRK (solid line) and UNIFAC-Lby (dot line)

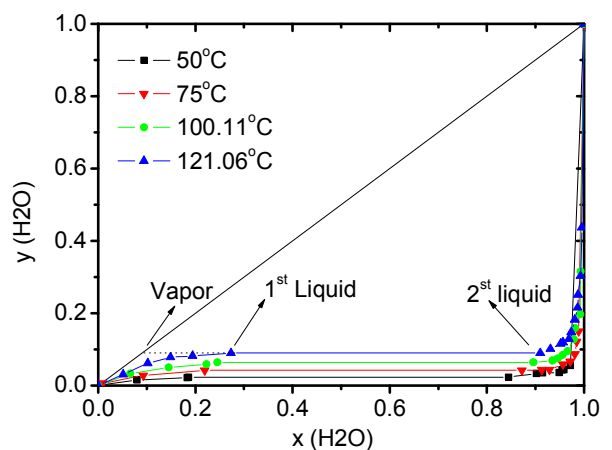


Figure A3.4: Y-X diagram of $\text{H}_2\text{O}/\text{DME}$ system, predicted by PRWS with UNIFAC-PSRK

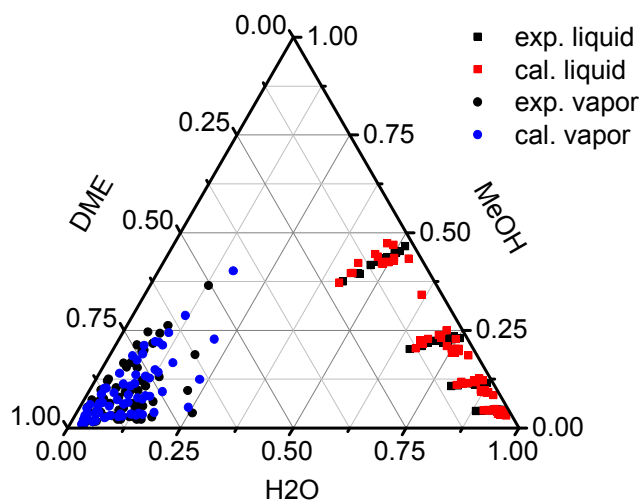


Figure A3.5: VLE diagram of $\text{H}_2\text{O}/\text{MeOH}/\text{DME}$ system for 60°C - 120°C , predicted by PRWS with UNIFAC-PSRK

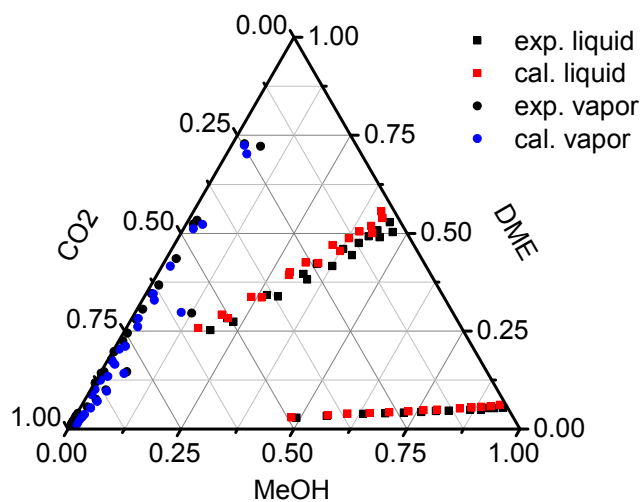


Figure A3.6: VLE diagram of $\text{MeOH}/\text{DME}/\text{CO}_2$ system for 40°C - 60°C , predicted by PRWS with UNIFAC-PSRK

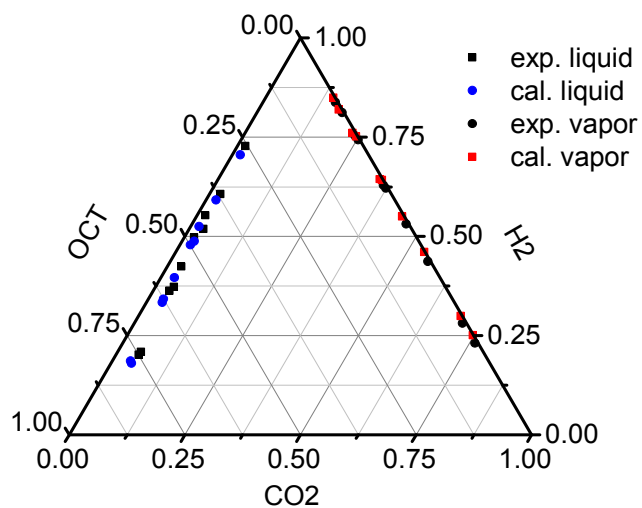


Figure A3.7: VLE diagram of $\text{CO}_2/\text{H}_2/\text{OCT}$ 80bar, 40°C - 60°C , predicted by PSRK

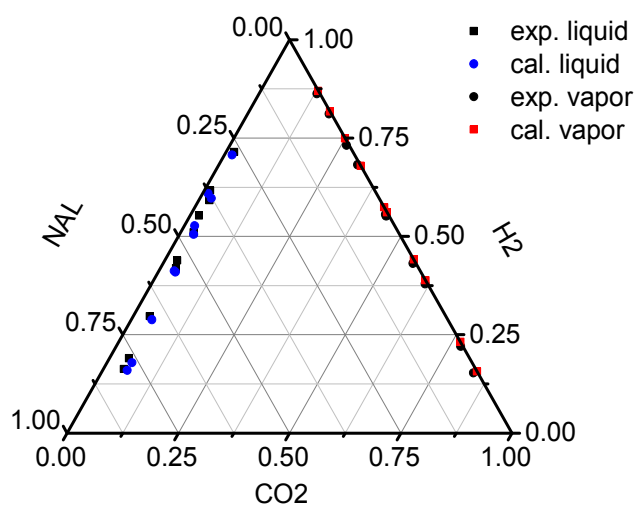


Figure A3.8: VLE diagram of $\text{CO}_2/\text{H}_2/\text{OCT}$ 80bar, 40°C - 60°C , predicted by MSRK-LCVM

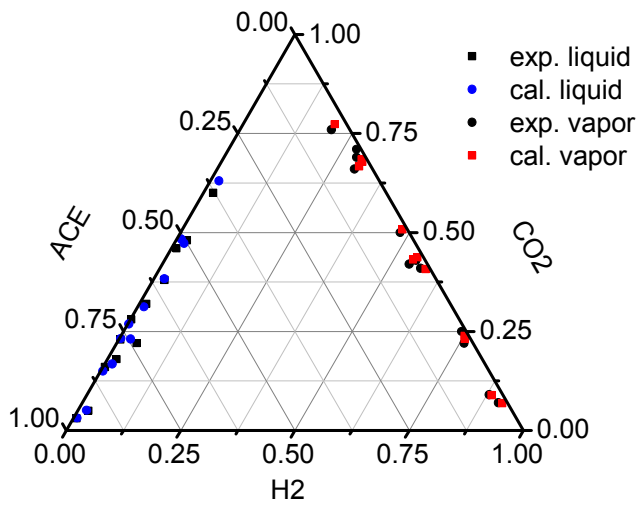


Figure A3.9: VLE diagram of $H_2/CO_2/ACE$ system under 25.1bar-90.1bar, $40^\circ C$, predicted by SRK-HVOS

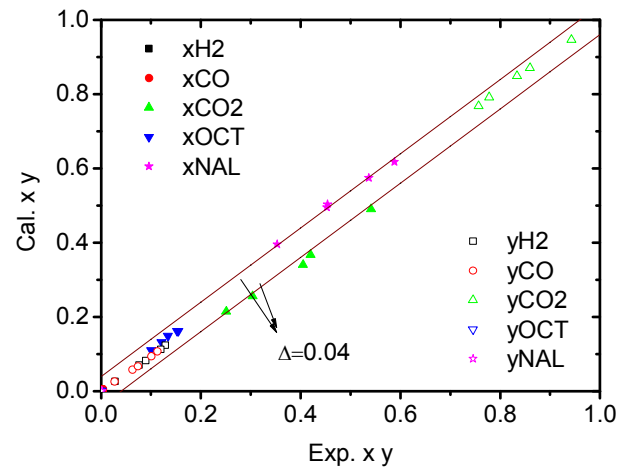


Figure A3.10: VLE parity plot of $H_2/CO/CO_2/OCT/NAL$ system between the experimental results and the calculation at $40^\circ C-50^\circ C$, 22.7bar-39.8bar, predicted by SRK-HVOS

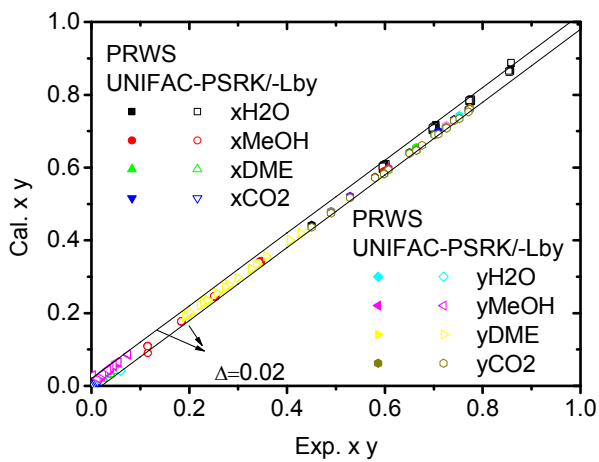


Figure A3.11: VLE parity plot of $H_2O/MeOH/DME/CO_2$ system between the experimental results and the calculation at $80^\circ C$

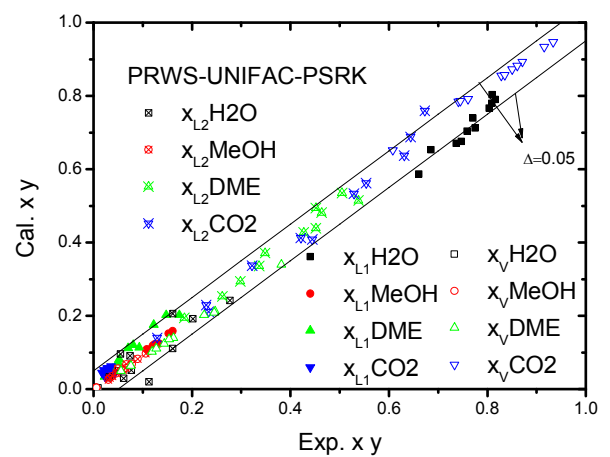


Figure A3.12: VLLE parity plot of $H_2O/MeOH/DME/CO_2$ system between the experimental results and the calculation at $25^\circ C-45^\circ C$

Appendix 4: Extra Tables and Diagrams of Chapter 3

Table A4.1: Detailed information of investigated systems

Type	SID	System	NC	Model	Reference
VLE	1	EtOH, H ₂ O	2	NRTL-IG	Aspen [217] (NRTL)
	2	H ₂ O, MeOH, DME	3	PRWS	Ye [83] (data, model)
	3	H ₂ , CO, CO ₂ , OCT	4	SRK-HVOS	Ye [52] (data, model)
	4	H ₂ , CO, CO ₂ , OCT, NAL	5	SRK-HVOS	Ye [52] (data, model)
	5	H ₂ , CO, CO ₂ , OCT, NAL, ACE	6	SRK-HVOS	Ye [52] (data, model)
	6	H ₂ , CO, CO ₂ , H ₂ O, CH ₄ , C ₂ H ₆ , C ₃ H ₈ , MeOH, EtOH, 1PrOH	10	PSRK	Suzuki [221] (experiment), Patel [222] (studied)
LLE	7	H ₂ O, EtOH, C6	3	NRTL	Aspen [217] (NRTL)
	8	1PrOH, 1BuOH, Ph, EtOH, H ₂ O	5	NRTL	Aspen [217] (NRTL) Tessier [109] (studied)
	9	Dimethyl formamide, n-decane, 1-dodecene, 2-dodecene, n-dodecane, 1-tridecanol, 2-methyl-dodecanal	7	UNIFAC-Do	This work
	10	EtOH, 1PrOH, n-butane, 2-butane, NBA, H ₂ O, HAC, Ph, PhMe, C6	10	UNIQUAC	Aspen [217] (UNIQUAC) Bausa [135] (studied)
VLLE	11	H ₂ O, CO ₂ , DME	3	PRWS	Ye [83] (data, model)
	12	H ₂ O, EtOH, C6	3	NRTL-IG	Aspen [217] (NRTL)
	13	1PrOH, 1BuOH, Ph, EtOH, H ₂ O	5	NRTL-IG	Aspen [217] (NRTL)
	14	EtOH, 1PrOH, n-butane, 2-butane, NBA, H ₂ O, HAC, Ph, PhMe, C6	10	UNIQUAC-IG	Aspen [217] (UNIQUAC)
LLLE	15	1-Hexanol, nitromethane, H ₂ O	3	NRTL	Marcilla [223] (model)
	16	NAL, nitromethane, H ₂ O	3	NRTL	Marcilla [223] (model)
	17	Lauryl alcohol, nitromethane, glycol	3	NRTL	Marcilla [223] (model)

Table A4.2: Results of selected systems in equilibrium state in comparison with reference

Type (SID)	p, T, z	Reference data	Calculation data (this work)
VLE (6)	107.1 bar, 40.25°C $z=0.228/0.087/0.012/0.081/0.160/0.023/0.009/0.303/0.070/0.027]$	Experimental data [221] $x=0.0071/0.0049/0.0057/0.1605/0.0170/0.0068/0.0039/0.6054/0.1359/0.0527$ $y=0.4502/0.1701/0.0192/0.0002/0.3039/0.0384/0.0144/0.0031/0.0005/0.0001$	$x=0.0117/0.0046/0.0059/0.1594/0.0198/0.0091/0.0063/0.5926/0.1374/0.0531$ $y=0.4501/0.1717/0.0183/0.0005/0.3040/0.0373/0.0118/0.0055/0.0007/0.0001$
LLE (9)	1.013bar, 298.15K $z=0.35/0.40/0.05/0.05/0.05/0.05/0.05$	Aspen calculation [217] $x(1)=0.8990/0.0428/0.0069/0.0063/0.0040/0.0204/0.0204$ $x(2)=0.2727/0.4503/0.0561/0.0561/0.0565/0.0542/0.0542$	$x(1)=0.8991/0.0428/0.0069/0.0063/0.0040/0.0204/0.0204$ $x(2)=0.2727/0.4503/0.0561/0.0561/0.0565/0.0542/0.0542$
LLE (10)	1.013bar, 50°C, $z=0.05/0.05/0.05/0.05/0.05/0.05/0.05/0.05/0.05$	Reference[135] $x^{(1)}=0.07/0.09/0.09/0.1/0.18/0.07/0.1/0.1/0.1$ $x^{(2)}=0.03/0.03/0.007/0.009/0.001/0.91/0.03/0.0005/0.0002/0.0009$	$x^{(1)}=0.0656/0.0833/0.0953/0.1010/0.1170/0.1380/0.0459/0.1173/0.1181/0.1185$ $x^{(2)}=0.0386/0.0258/0.0171/0.0130/0.0013/0.8492/0.0530/0.0011/0.0006/0.0003$
VLLE (14)	1.013bar, 80°C $z=0.05/0.05/0.05/0.05/0.05/0.05/0.05/0.05/0.05$	Aspen calculation [217] $x^{(1)}=0.0731/0.0468/0.0226/0.0412/0.0384/0.4275/0.0076/0.1186/0.0923/0.1320$ $x^{(2)}=0.0589/0.0911/0.1221/0.1062/0.1188/0.2863/0.0806/0.0408/0.0670/0.0281$ $y=0.0233/0.0181/0.0122/0.0101/0.0019/0.8738/0.0596/0.0006/0.0005/0.0001$	$x^{(1)}=0.0710/0.0464/0.0244/0.0441/0.0444/0.4235/0.0063/0.1176/0.0939/0.1283$ $x^{(2)}=0.0569/0.0906/0.1230/0.1098/0.1267/0.2806/0.0820/0.0378/0.0675/0.0252$ $y=0.0275/0.0256/0.0223/0.0145/0.0028/0.8402/0.0655/0.0007/0.0007/0.0001$
LLLE (15)	1.013bar, 20.85°C $z=0.1783/0.4024/0.4192$	Experimental data [223] $x^{(1)}=0.6095/0.1387/0.2518$ $x^{(2)}=0.0075/0.0414/0.9511$ $x^{(3)}=0.0239/0.8929/0.0831$	$x^{(1)}=0.6008/0.1295/0.2697$ $x^{(2)}=0.0006/0.0432/0.9561$ $x^{(3)}=0.0236/0.8821/0.0942$

Table A4.3: Results of selected systems in equilibrium state calculated without prior determination of phase number

Real phase (SID)	p, T, z	Initial phase	Calculated result
VLE (6)	107.1 bar, 40.25°C $z=0.228/0.087/0.012/0.081/0.160/0.023/0.009/0.303/0.070/0.027]$	VLLE	$x^{(1)}=x^{(2)}=0.0117/0.0046/0.0061/0.1593/0.0198/0.0089/0.0064/0.5926/0.1378/0.0527$ $y=0.4498/0.1720/0.0190/0.0005/0.3038/0.0365/0.0120/0.0055/0.0007/0.0001$
		VLLLE	$x^{(1)}=x^{(2)}=x^{(3)}=0.0117/0.0046/0.0061/0.1593/0.0198/0.0089/0.0064/0.5926/0.1378/0.0527$ $y=0.4498/0.1720/0.0190/0.0005/0.3038/0.0365/0.0120/0.0055/0.0007/0.0001$
LLE (10)	1.013bar, 50°C, $z=0.05/0.05/0.05/0.05/0.05/0.55/0.05/0.05/0.05/0.05$	LLLE	$x^{(1)}=0.0656/0.0833/0.0953/0.1010/0.1170/0.1380/0.0459/0.1173/0.1181/0.1185$ $x^{(2)}=x^{(3)}=0.0386/0.0258/0.0171/0.0130/0.0013/0.8492/0.0530/0.0011/0.0006/0.0003$
VLLE (14)	1.013bar, 80°C $z=0.05/0.05/0.05/0.05/0.05/0.55/0.05/0.05/0.05/0.05$	VLLLE	$x^{(1)}=x^{(2)}=0.0731/0.0468/0.0226/0.0412/0.0384/0.4275/0.0076/0.1186/0.0923/0.1320$ $x^{(3)}=0.0589/0.0911/0.1221/0.1062/0.1188/0.2863/0.0806/0.0408/0.0670/0.0281$ $y=0.0233/0.0181/0.0122/0.0101/0.0019/0.8738/0.0596/0.0006/0.0005/0.0001$
LLLE (15)	1.013bar, 20.85°C $z=0.1783/0.4024/0.4192$	LLLLLE	$x^{(1)}=x^{(2)}=0.6008/0.1295/0.2697$ $x^{(3)}=0.0006/0.0432/0.9561$ $x^{(4)}=0.0236/0.8821/0.0942$
		LLLLLLE	$x^{(1)}=0.6008/0.1295/0.2697$ $x^{(2)}=0.0006/0.0432/0.9561$ $x^{(3)}=x^{(4)}=x^{(5)}=0.0236/0.8821/0.0942$

Note:

- The references are the same as in **Table A4.2**.

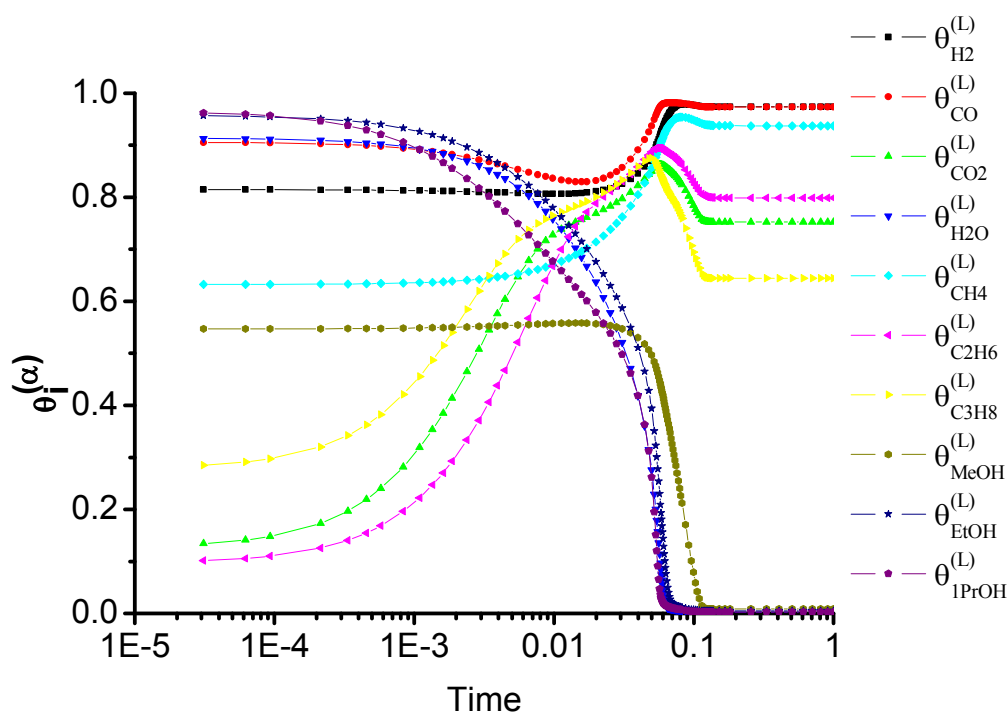


Figure A4.1: Calculation of the VLE case with random initialization (SID=6, NC=10)

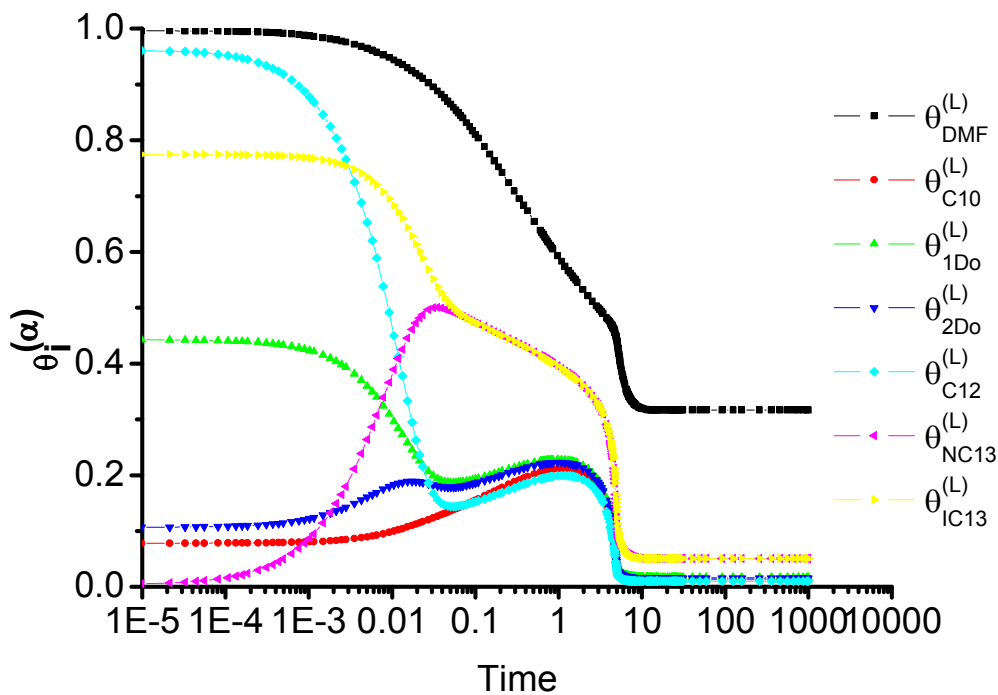


Figure A4.2: Calculation of the LLE case with random initialization (SID=9, NC=7)

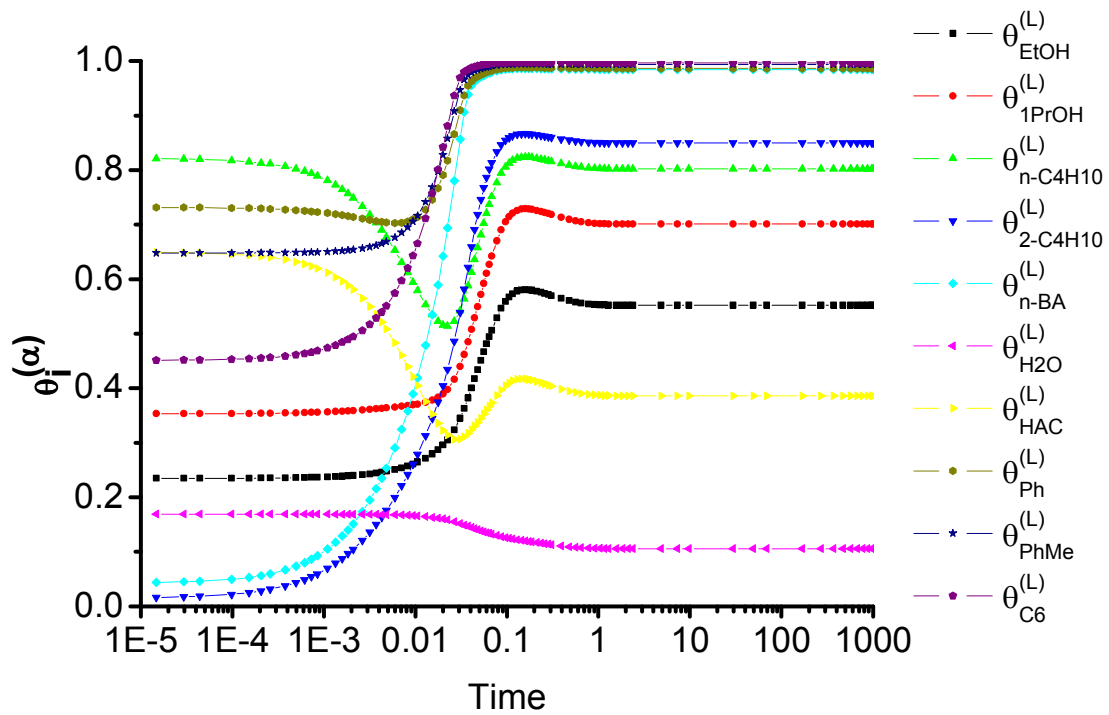


Figure A4.3: Calculation of the LLE case with random initialization (SID=10, NC=10)

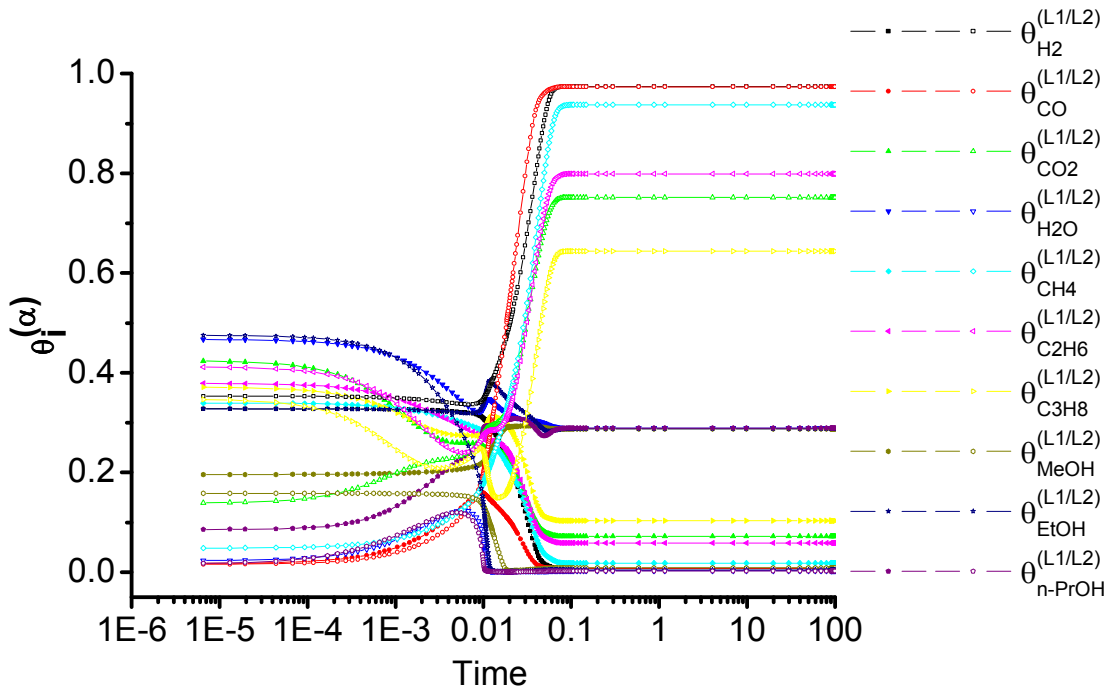


Figure A4.4: The VLE (SID=6, NC=10) calculated by a VLLE (20 unknowns) with random initialization cases

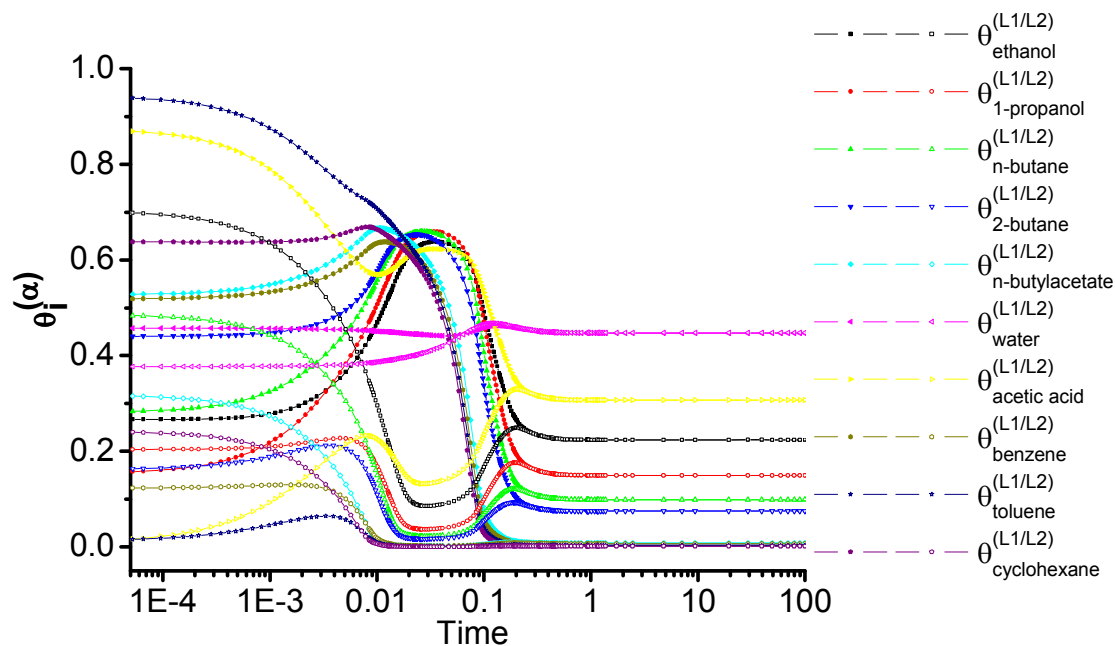


Figure A4.5: The LLE (SID=10, NC=10) calculated by a LLE (20 unknowns) with random initialization case

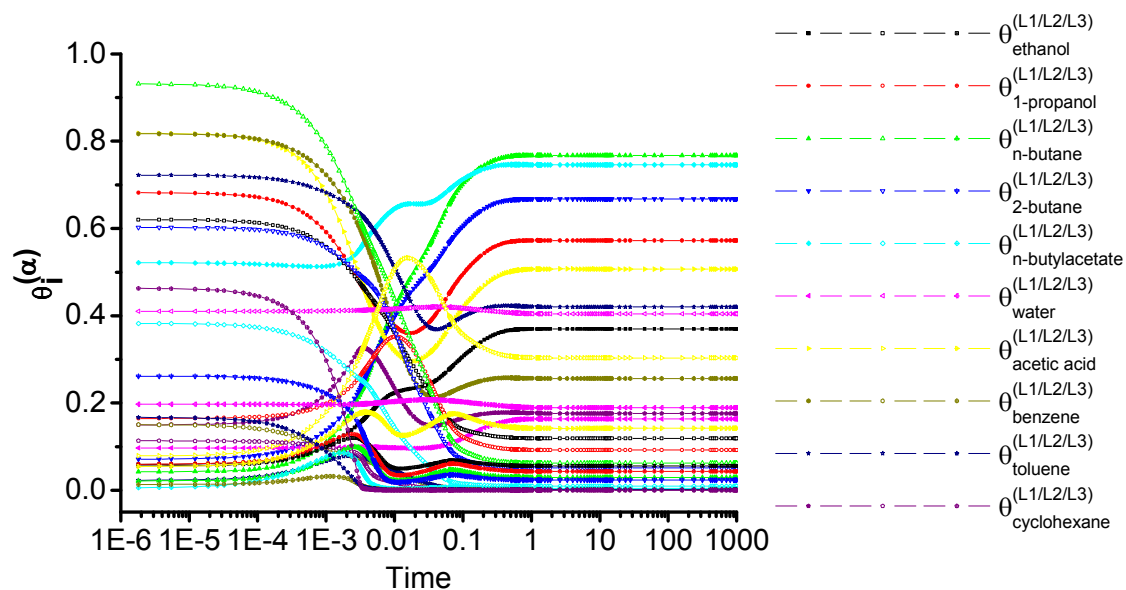


Figure A4.6: The VLLE (SID=14, NC=10) calculated by a VLLLE (30 unknowns) with random initialization case

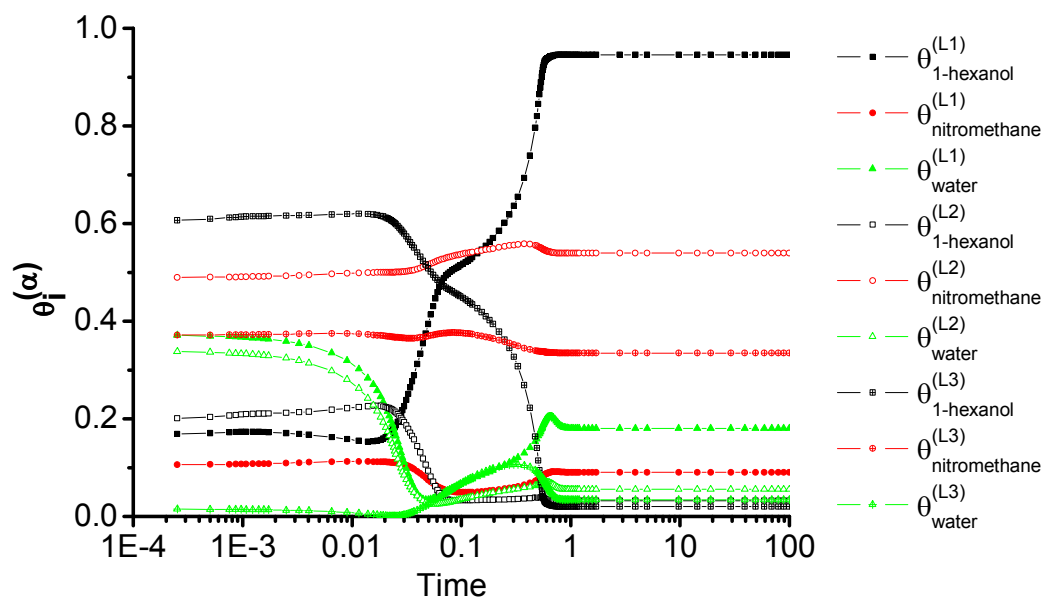


Figure A4.7: The LLLLE (SID=15, NC=3) calculated by a LLLLLE (9 unknowns) with random initialization cases

Appendix 5: Extra Diagrams of Chapter 4

The VLE phase behaviors of H₂O/MeCN and H₂O/DIOX systems are predicted by NRTL-IG model, the involved parameters of NRTL are listed in **Table A2.6**. The H₂O/MeCN system has more experimental data for validating the predications (See **Figs. A5.1-A5.2**) than H₂O/DIOX system (See **Fig. A5.3**). All three cases are well predicted. The extrapolation of H₂O/DIOX system is presented in **Fig. A5.4**.

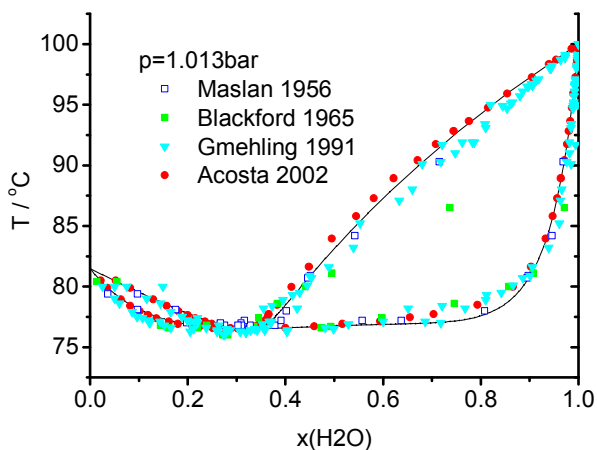


Figure A5.1: Isobaric VLE diagram of H₂O/MeCN system with atmospheric pressure, predicted by NRTL-IG model, data reference [224-227].

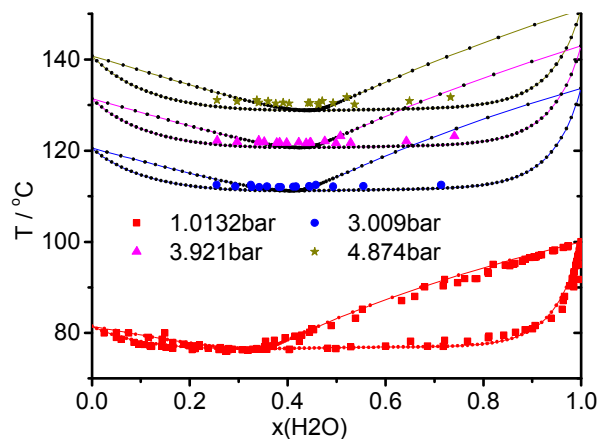


Figure A5.2: Isobaric VLE diagram of H₂O/MeCN system with elevated pressures, predicted by NRTL-IG model, data reference [226].

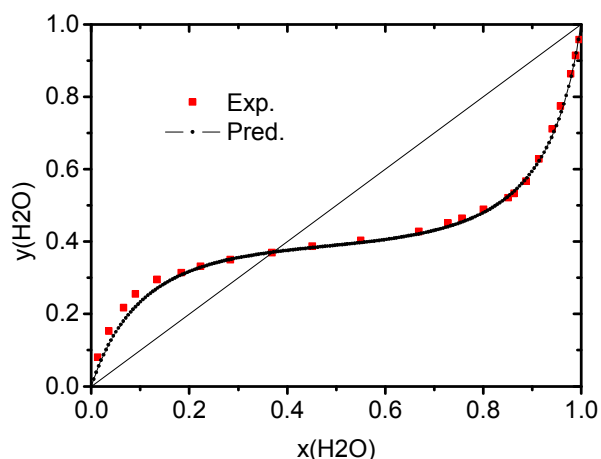


Figure A5.3: Isothermal Y-X diagram of H₂O/MeCN system at 30.35°C, predicted by NRTL-IG model, data reference [228].

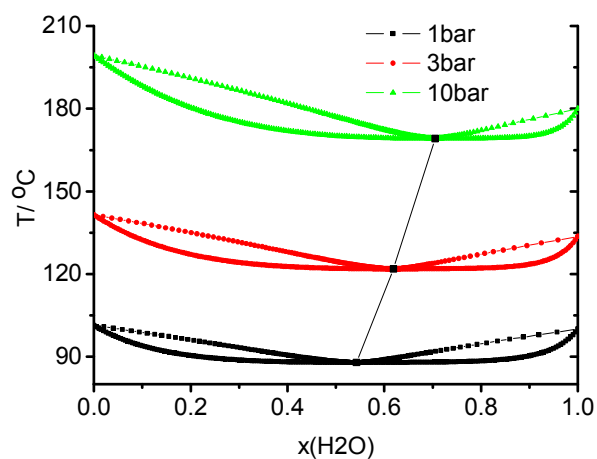


Figure A5.4: Isobaric VLE diagram of H₂O/DIOX system with elevated pressures, predicted by NRTL-IG model.

Figs. A5.5-A5.10 present the detailed operation conditions in process simulation. **Figs. A5.5-A5.6** are the operation diagrams of the conventional PSD for both investigated systems. **Figs. A5.7-A5.8** are the operation diagrams of both process variants for the MeCN/H₂O system, and **Figs. A5.9-A5.10** are the operation diagrams of both process variants for the DIOX/H₂O system.

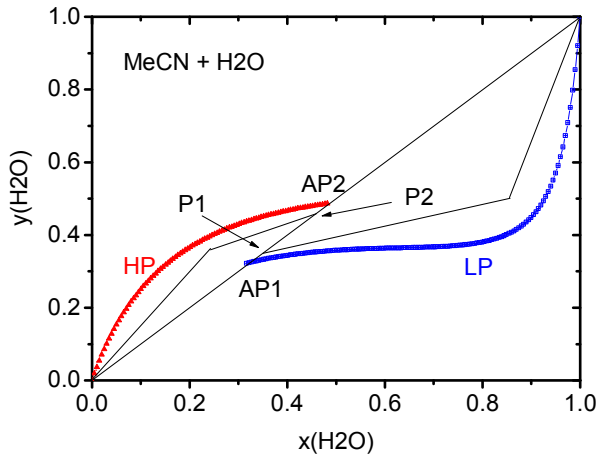


Figure A5.5: Operation of the conventional PSD process in a Y-X diagram of MeCN/H₂O system

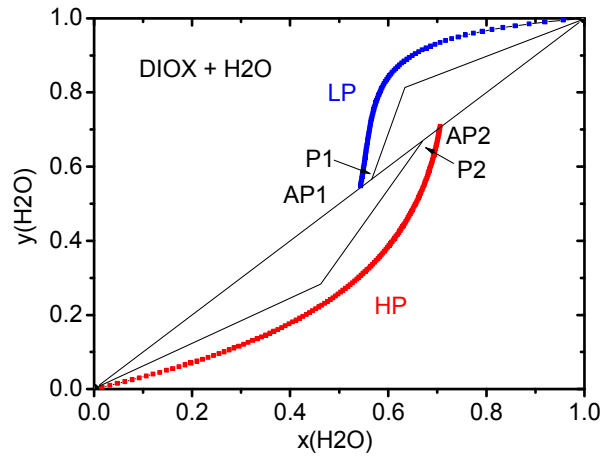


Figure A5.6: Operation of the conventional PSD process in a Y-X diagram of DIOX/H₂O system

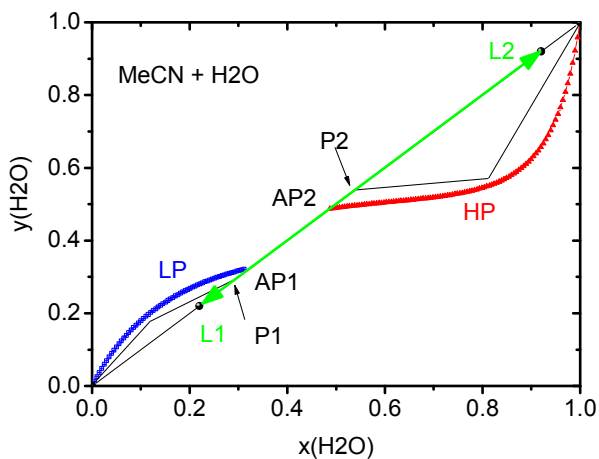


Figure A5.7: Operation of process variant 1 in a Y-X diagram of MeCN/H₂O system

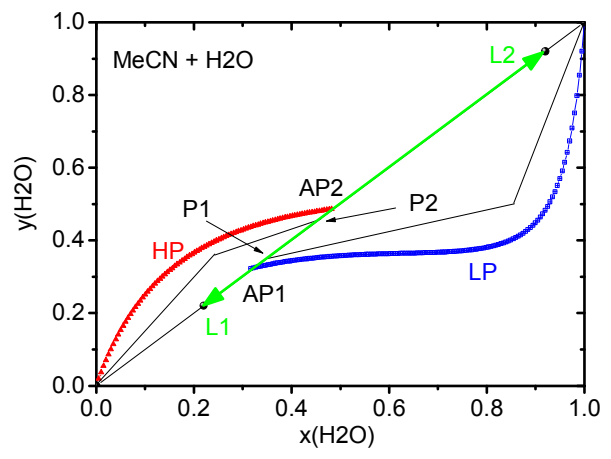


Figure A5.8: Operation of process variant 2 in a Y-X diagram of MeCN/H₂O system

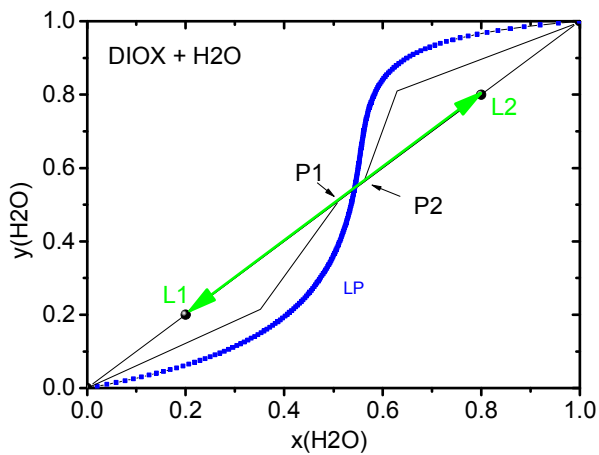


Figure A5.9: Operation of process variant 1 in a Y-X diagram of DIOX/H₂O system

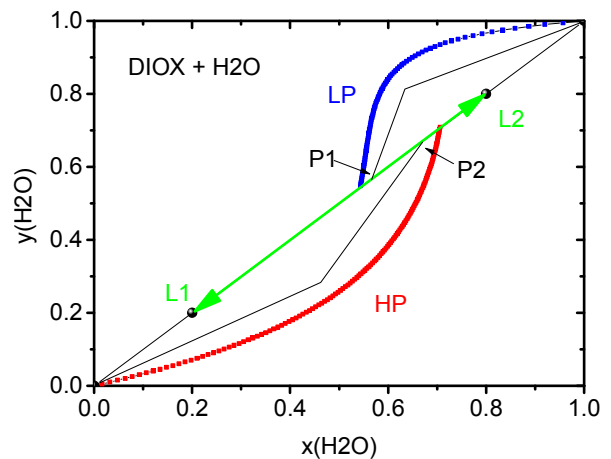


Figure A5.10: Operation of process variant 2 in a Y-X diagram of DIOX/H₂O system

The **Figs. A5.11-A5.15** display quite a few results of process variant 1 for MeCN/H₂O system. Some information is illustrated shortly:

- **Fig. A5.11** shows that there is an optimal pressure range, and it is 45bar-55bar for process variant 1, which is around 10 bar higher than process variant 2;
- **Fig. A5.12** displays the recycled CO₂ flow. The quantity of CO₂ usage in process variant 2 is little lower than in process variant 1. Consequently, the electricity requirement of process variant 1 is also similar to process variant 2 (**Fig. A5.13 & Fig. 5.12**);
- **Fig. A5.14** illustrates how the pressure impacts the recycled organic mixture in process variant 1. The pressure has larger influence for process variant 1 than for process variant 2 (**Fig. 5.13**). The maximum condensate flow reduction for every feed composition is 54.6%~92.8%, which is slightly lower than 73.6%~95.7% of process variant 2. As a consequence, the heating consumption is slightly higher than process variant 2 (**Fig. A5.15 & Fig. 5.14**).

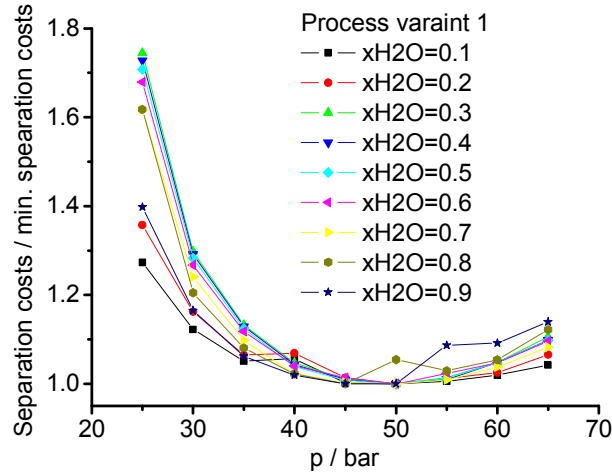


Figure A5.11: Operating pressure influence on the separation costs of process variant 1

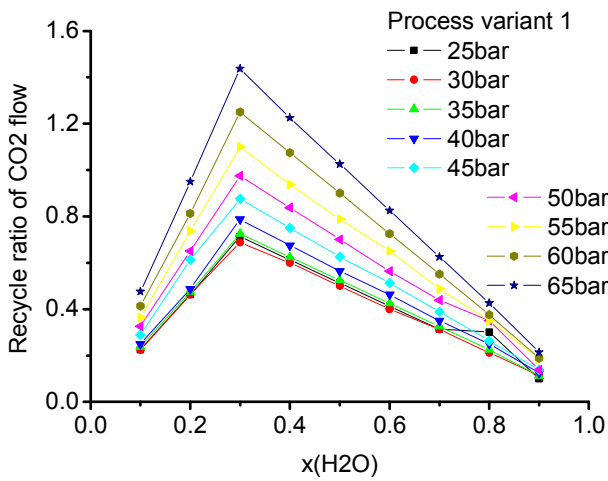


Figure A5.12: Recycle ratio of CO₂ flow in process variant 1

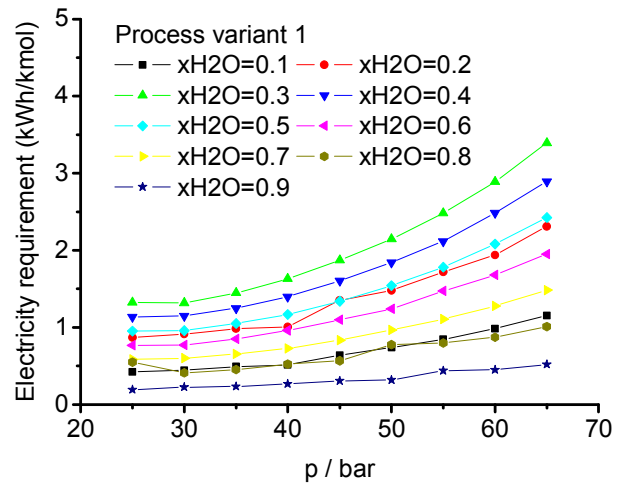


Figure A5.13: Electricity requirement of process variant 1 dependent on pressure and feed

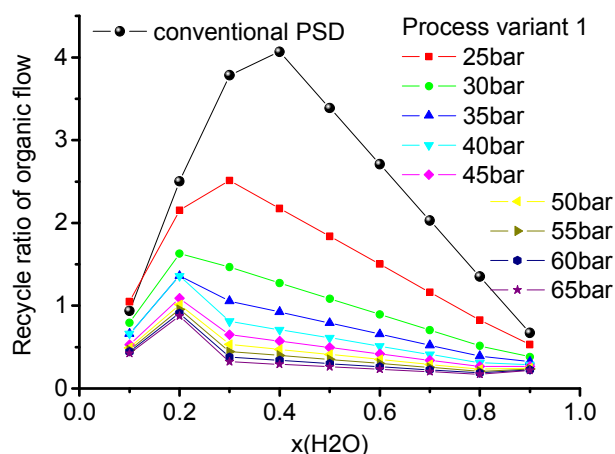


Figure A5.14: Recycle ratio of condensate flow in process variant 1

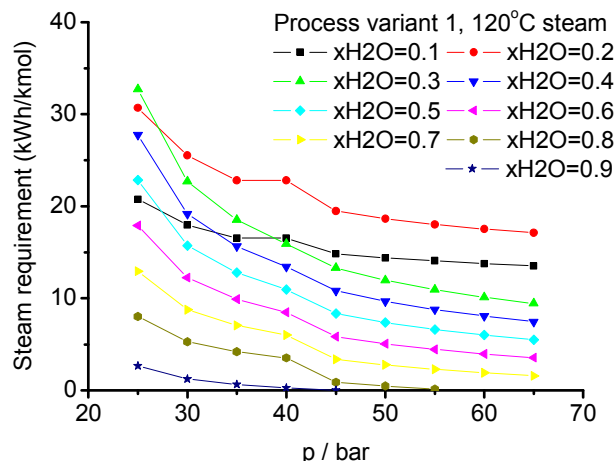


Figure A5.15: Steam requirement of process variant 1

The **Figs. A5.16-A5.25** display quite a few results of process variant 1 for DIOX/H₂O system. Some information is illustrated shortly:

- The **Figs. A5.16-A5.17** have qualitatively similar performance of the separation costs, and the operating pressure of the VLLE flash has less impact on the separation costs in comparison to the impact on the MeCN/H₂O system (**Fig. 4.12**);
- The **Figs. A5.18-A5.19** show that the pressure has similar influence on the two process variants, and there exists an almost the same optimal operating pressure range for both process variants: in the neighbour of 35bar-45bar;
- The **Figs. A5.120-A5.21** display the recycle ratio of CO₂ flow in two process variants. Both are qualitatively and quantitatively similar. As a cause, the electricity requirements are also similar due to the recycle ratio of CO₂ flow (**Figs. A5.22-A5.23**);
- The **Figs. A5.24-A5.25** are the steam requirements of the two process variants.

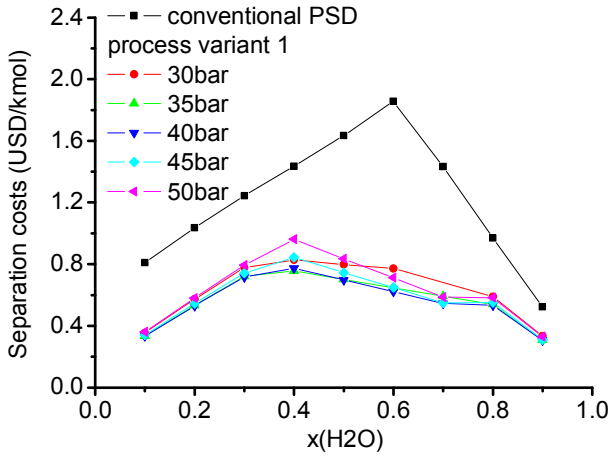


Figure A5.16: Separation costs contrast between the conventional PSD process and process variant 1

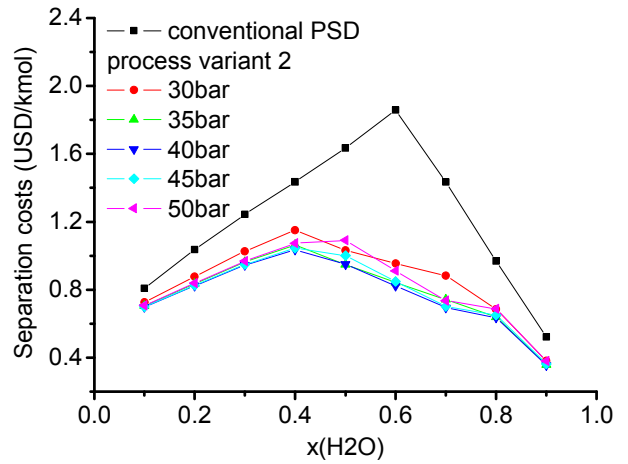


Figure A5.17: Separation costs contrast between the conventional PSD process and process variant 2

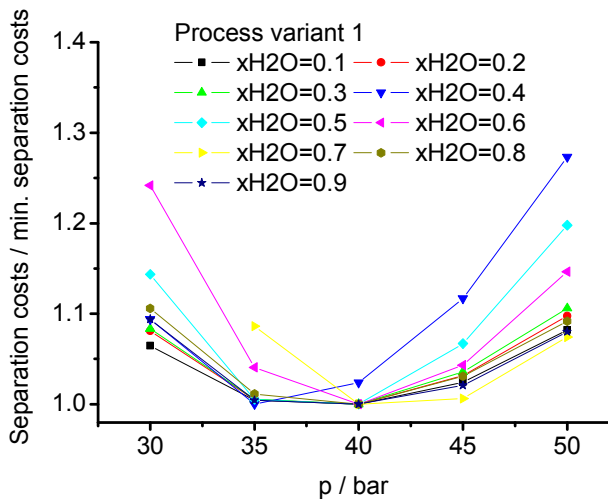


Figure A5.18: Operating pressure influence on the separation costs of process variant 1

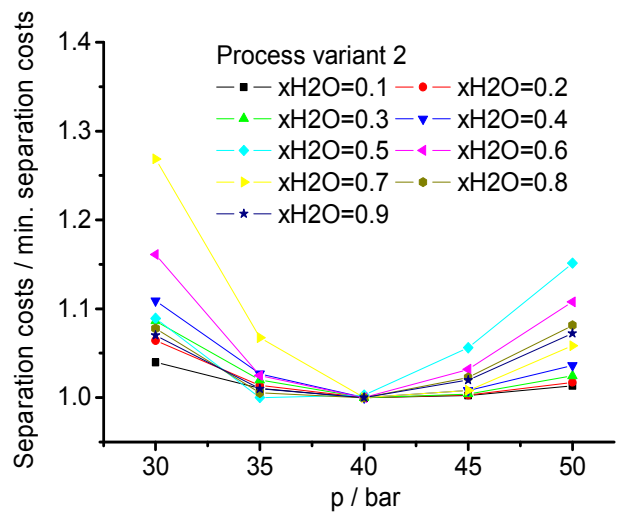


Figure A5.19: Operating pressure influence on the separation costs of process variant 2

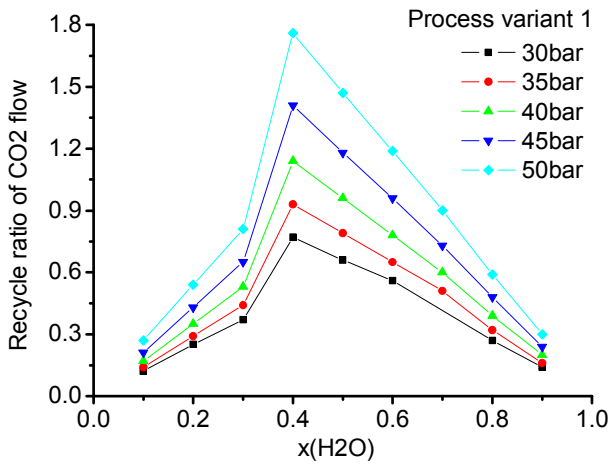


Figure A5.20: Recycle ratio of CO₂ flow of process variant 1

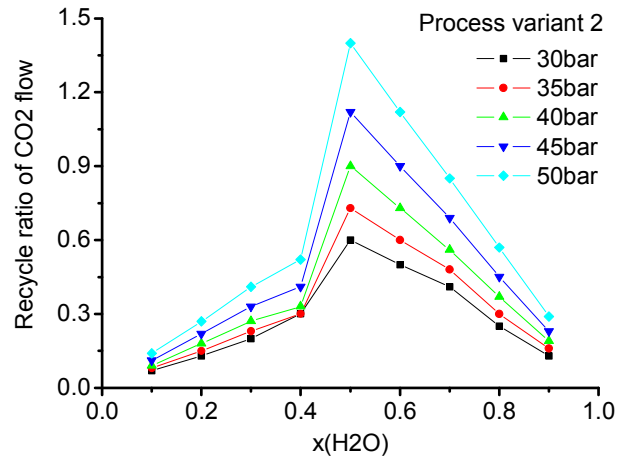


Figure A5.21: Recycle ratio of CO₂ flow of process variant 2

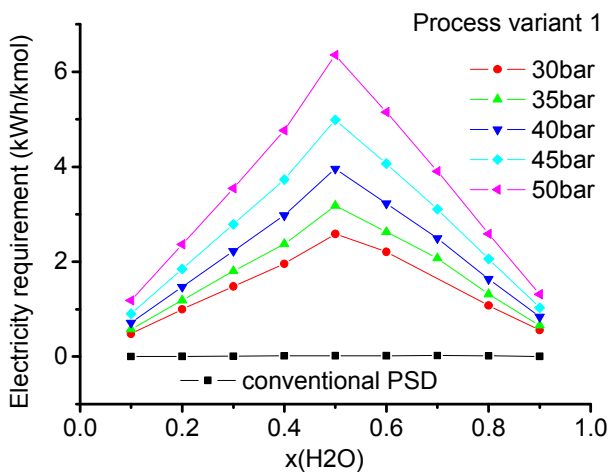


Figure A5.22: Electricity requirement of process variant 1

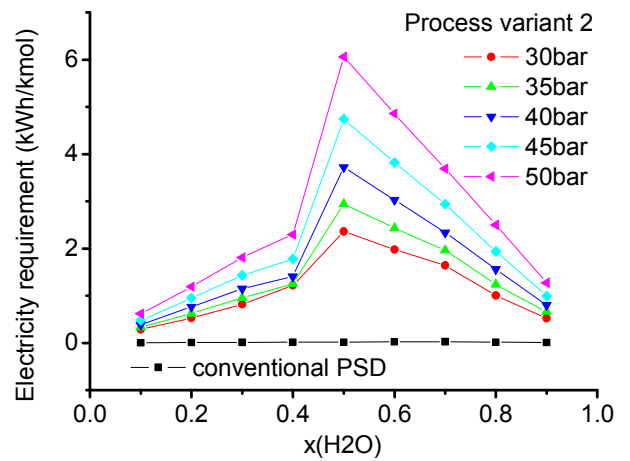


Figure A5.23: Electricity requirement of process variant 2

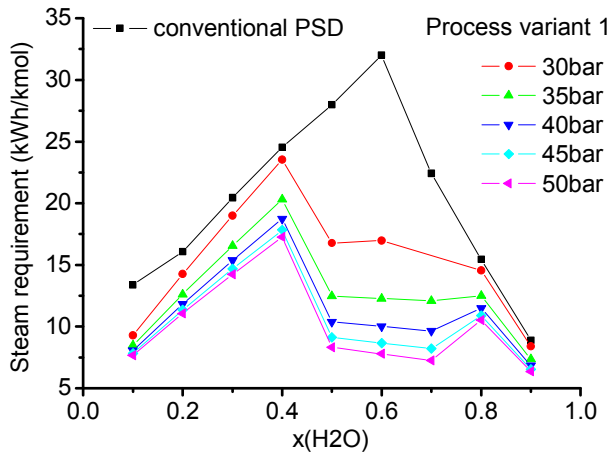


Figure A5.24: Steam requirement of process variant 1

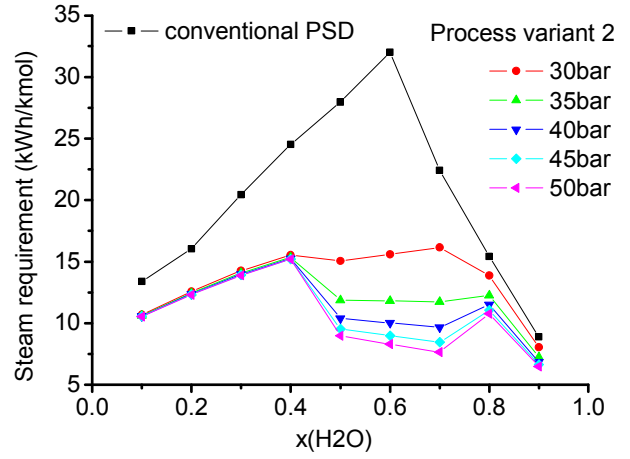


Figure A5.25: Steam requirement of process variant 2

Appendix 6: Extra Diagrams of Chapter 5

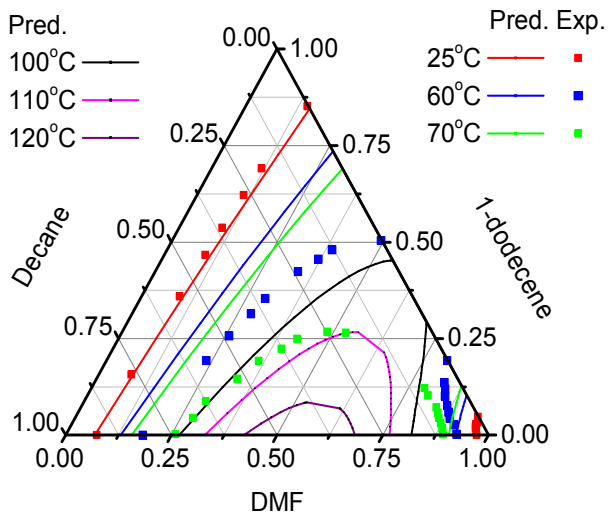


Figure A6.1: The ternary diagram of DMF/1Do/C10 system predicted by UNIFAC-Do with original interaction parameters, data reference [214]

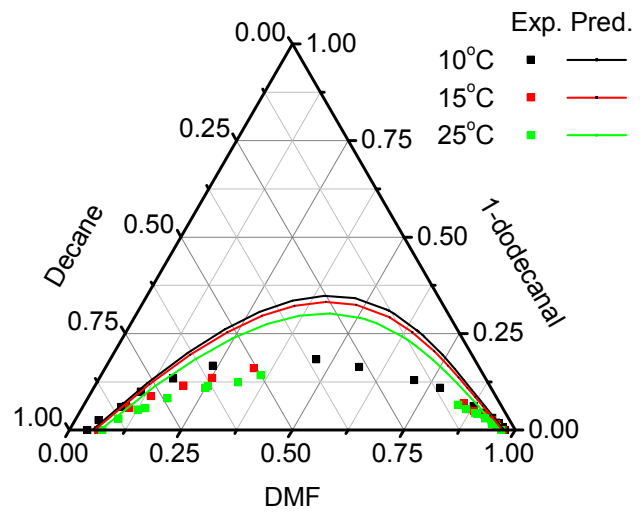


Figure A6.2: The ternary diagram of DMF/NC13/C10 system predicted by UNIFAC-Do with original interaction parameters, data reference [214]

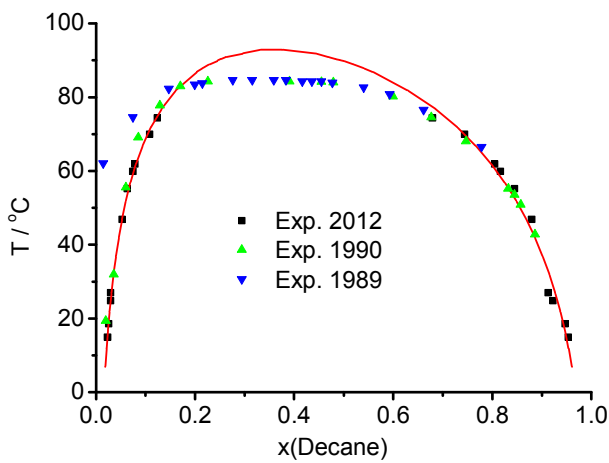


Figure A6.3: Correlation of LLE data of DMF/C12 system using UNIFAC-DO, data reference [214, 229, 230]

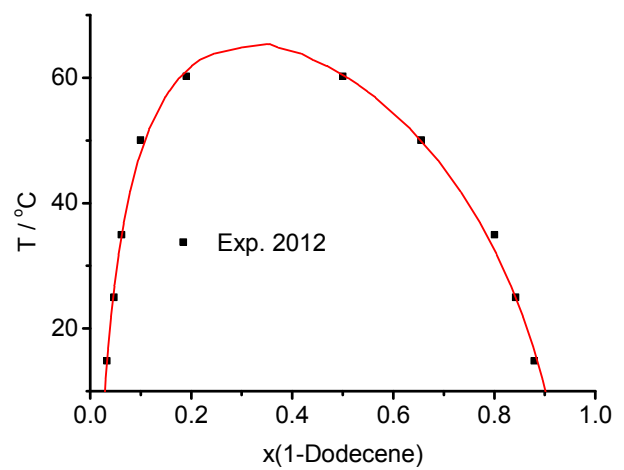


Figure A6.4: Correlation of LLE data of DMF/1Do system using UNIFAC-DO, data reference [214]

Bibliography

1. *National Emissions Inventory (NEI) Air Pollutant Emissions Trends Data*, <http://www.epa.gov/ttn/chieftrends/index.html>. 2012.
2. Jones, A.P., *Indoor air quality and health*. Atmospheric Environment, 1999. **33**(28): 4535-4564.
3. Anastas, P.T. and J.B. Zimmerman, *Design through the 12 principles of green engineering*. Environmental Science & Technology, 2003. **37**(5): 94-101.
4. Molina, M.J. and L.T. Molina, *Megacities and atmospheric pollution*. Journal of the Air & Waste Management Association, 2004. **54**(6): 644-680.
5. Jessop, P.G. and B. Subramaniam, *Gas-expanded liquids*. Chemical Reviews, 2007. **107**(6): 2666-2694.
6. DeSimone, J.M., *Practical approaches to green solvents*. Science, 2002. **297**(5582): 799-803.
7. <http://www.epa.gov/p2/pubs/p2policy/act1990.htm>.
8. Al-Hunaiti, A., Niemi, T., Sibaouih, A., et al., *Solvent free oxidation of primary alcohols and diols using thymine iron(iii) catalyst*. Chemical Communications, 2010. **46**(48): 9250-9252.
9. Enache, D.I., Edwards, J. K., Landon, P., et al., *Solvent-free oxidation of primary alcohols to aldehydes using Au-Pd/TiO₂ catalyst*. Science, 2006. **311**(5759): 362-365.
10. Kesavan, L., Tiruvalam, R., Rahim, M. H. A., et al., *Solvent-free oxidation of primary carbon-hydrogen bonds in toluene using Au-Pd alloy nanoparticles*. Science, 2011. **331**(6014): 195-199.
11. Thorwirth, R., Stolle, A., Ondruschka, B., et al., *Fast, ligand- and solvent-free copper-catalyzed click reactions in a ball mill*. Chemical Communications, 2011. **47**(15): 4370-4372.
12. Zhu, F.X., Wang, W., and H.X. Li, *Water-medium and solvent-free organic reactions over a bifunctional catalyst with Au nanoparticles covalently bonded to HS/SO₃H functionalized periodic mesoporous organosilica*. Journal of the American Chemical Society, 2011. **133**(30): 11632-11640.
13. Eckert, C.A., B.L. Knutson, and P.G. Debenedetti, *Supercritical fluids as solvents for chemical and materials processing*. Nature, 1996. **383**(6598): 313-318.
14. Rogers, R.D. and K.R. Seddon, *Ionic liquids - Solvents of the future?* Science, 2003. **302**(5646): 792-793.
15. Leitner, W., *Supercritical carbon dioxide as a green reaction medium for catalysis*. Accounts of Chemical Research, 2002. **35**(9): 746-756.
16. Nalawade, S.P., F. Picchioni, and L.P.B.M. Janssen, *Supercritical carbon dioxide as a green solvent for processing polymer melts: Processing aspects and applications*. Progress in Polymer Science (Oxford), 2006. **31**(1): 19-43.
17. Licence, P., Ke, J., Sokolova, M., et al., *Chemical reactions in supercritical carbon dioxide: From laboratory to commercial plant*. Green Chemistry, 2003. **5**(2): 99-104.

18. Garcia-Verdugo, E., et al., *Is it possible to achieve highly selective oxidations in supercritical water? Aerobic oxidation of methylaromatic compounds*. *Advanced Synthesis and Catalysis*, 2004. **346**(2-3): 307-316.
19. Blanchard, L.A., Hancu, D., Beckman, E. J., et al., *Green processing using ionic liquids and CO₂*. *Nature*, 1999. **398**(6731): 28-29.
20. Han, X. and D.W. Armstrong, *Ionic liquids in separations*. *Accounts of Chemical Research*, 2007. **40**(11): 1079-1086.
21. Sheldon, R., *Catalytic reactions in ionic liquids*. *Chemical Communications*, 2001(23): 2399-2407.
22. Zhao, D., Wu, M., Kou, Y., et al., *Ionic liquids: Applications in catalysis*. *Catalysis Today*, 2002. **74**(1-2): 157-189.
23. Moody, C.A. and J.A. Field, *Perfluorinated surfactants and the environmental implications of their use in fire-fighting foams*. *Environmental Science & Technology*, 2000. **34**(18): 3864-3870.
24. Cornils, B., *Fluorous biphasic systems - The new phase-separation and immobilization technique*. *Angewandte Chemie (International Edition in English)*, 1997. **36**(19): 2057-2059.
25. Luo, Z., Zhang, Q., Oderaotoshi, Y., et al., *Fluorous mixture synthesis: A fluorous-tagging strategy for the synthesis and separation of mixtures of organic compounds*. *Science*, 2001. **291**(5509): 1766-1769.
26. Studer, A., Hadida, S., Ferritto, R., et al., *Fluorous synthesis: A fluorous-phase strategy for improving separation efficiency in organic synthesis*. *Science*, 1997. **275**(5301): 823-826.
27. Horváth, I.T. and J. Rábai, *Facile catalyst separation without water: Fluorous biphasic hydroformylation of olefins*. *Science*, 1994. **266**(5182): 72-75.
28. Jin, H., Subramaniam, B., Ghosh, A., et al., *Intensification of catalytic olefin hydroformylation in CO₂-expanded media*. *AIChE Journal*, 2006. **52**(7): 2575-2581.
29. Chen, Y.C. and C.S. Tan, *Hydrogenation of p-chloronitrobenzene by Ni-B nanocatalyst in CO₂-expanded methanol*. *Journal of Supercritical Fluids*, 2007. **41**(2): 272-278.
30. Lee, H.J., Ghanta, M., Busch, D. H., et al., *Toward a CO₂-free ethylene oxide process: Homogeneous ethylene oxide in gas-expanded liquids*. *Chemical Engineering Science*, 2010. **65**(1): 128-134.
31. Beckman, E.J., *Supercritical and near-critical CO₂ in green chemical synthesis and processing*. *Journal of Supercritical Fluids*, 2004. **28**(2-3): 121-191.
32. Dzyuba, S.V. and R.A. Bartsch, *Recent advances in applications of room-temperature ionic liquid/supercritical CO₂ systems*. *Angewandte Chemie - International Edition*, 2003. **42**(2): 148-150.
33. Keskin, S., Kayrak-Talay, D., Akman, U., et al., *A review of ionic liquids towards supercritical fluid applications*. *Journal of Supercritical Fluids*, 2007. **43**(1): 150-180.
34. Freund, H. and K. Sundmacher, *Process Intensification*. *Ullmann's Encyclopedia of Industrial Chemistry*. 2008.
35. Adrian, T., Wendland, M., Hasse, H., et al., *High-pressure multiphase behaviour of ternary systems carbon dioxide water polar solvent: Review and modeling with the Peng-Robinson equation of state*. *Journal of Supercritical Fluids*, 1998. **12**(3): 185-221.
36. Sandler, S.I., *Chemical and Engineering Thermodynamics*. 3rd ed. 1999: Wiley-VCH.
37. Johnston, K.P., D.G. Peck, and S. Kim, *Modeling Supercritical Mixtures - How predictive is it*. *Industrial & Engineering Chemistry Research*, 1989. **28**(8): 1115-1125.
38. Muhlbauer, A.L. and J.D. Raal, *Computation and thermodynamic interpretation of high-pressure vapour-liquid equilibrium - A review*. *Chemical Engineering Journal and the Biochemical Engineering Journal*, 1995. **60**(1-3): 1-29.
39. Ghosh, P., *Prediction of vapor-liquid equilibria using Peng-Robinson and Soave-Redlich-Kwong equations of state*. *Chemical Engineering & Technology*, 1999. **22**(5): 379-399.

40. Panagiotopoulos, A.Z., *Direct Determination of Fluid-Phase Equilibria by Simulation in the Gibbs Ensemble - a review*. *Molecular Simulation*, 1992. **9**(1): 1-23.
41. Houndonougbo, Y., Kuczera, K., Subramaniam, B., et al., *Prediction of phase equilibria and transport properties in carbon-dioxide expanded solvents by molecular simulation*. *Molecular Simulation*, 2007. **33**(9-10): 861-869.
42. Houndonougbo, Y., Jin, H., Rajagopalan, B., et al., *Phase equilibria in carbon dioxide expanded solvents: Experiments and molecular simulations*. *Journal of Physical Chemistry B*, 2006. **110**(26): 13195-13202.
43. Soave, G., *Equilibrium constants from a modified Redlich-Kwong equation of state*. *Chemical Engineering Science*, 1972. **27**(6): 1197-1203
44. Peng, D.Y. and D.B. Robinson, *A new two-constant equation of state*. *Industrial and Engineering Chemistry Fundamentals*, 1976. **15**(1): 59-64.
45. Han, F., Xue, Y., Tian, Y. L., et al., *Vapor-liquid equilibria of the carbon dioxide plus acetone system at pressures from (2.36 to 11.77) MPa and temperatures from (333.15 to 393.15) K*. *Journal of Chemical and Engineering Data*, 2005. **50**(1): 36-39.
46. Lazzaroni, M.J., Bush, D., Brown, J. S., et al., *High-pressure vapor-liquid equilibria of some carbon dioxide plus organic binary systems*. *Journal of Chemical and Engineering Data*, 2005. **50**(1): 60-65.
47. Lopez-Castillo, Z.K., Aki, S. N. V. K., Stadtherr, M. A., et al., *Enhanced solubility of oxygen and carbon monoxide in CO₂-expanded liquids*. *Industrial & Engineering Chemistry Research*, 2006. **45**(15): 5351-5360.
48. Chin, H.Y., M.J. Lee, and H.M. Lin, *Vapor-liquid phase boundaries of binary mixtures of carbon dioxide with ethanol and acetone*. *Journal of Chemical and Engineering Data*, 2008. **53**(10): 2393-2402.
49. Lopez-Castillo, Z.K., Aki, S. N. V. K., Stadtherr, M. A., et al., *Enhanced solubility of hydrogen in CO₂-expanded liquids*. *Industrial & Engineering Chemistry Research*, 2008. **47**(3): 570-576.
50. Xie, Z.Z., Snavely, W. K., Scurto, A. M., et al., *Solubilities of CO and H₂ in neat and CO₂-expanded hydroformylation reaction mixtures containing 1-Octene and Nonanal up to 353.15 K and 9 MPa*. *Journal of Chemical and Engineering Data*, 2009. **54**(5): 1633-1642.
51. Ren, W., B. Rutz, and A.M. Scurto, *High-pressure phase equilibrium for the hydroformylation of 1-octene to nonanal in compressed CO₂*. *Journal of Supercritical Fluids*, 2009. **51**(2): 142-147.
52. Ye, K.M., Freund, H., Xie, Z. Z., et al., *Prediction of multicomponent phase behavior of CO₂-expanded liquids using CEoS/GE models and comparison with experimental data*. *Journal of Supercritical Fluids*, 2012. **67**: 41-52.
53. Huron, M.J. and J. Vidal, *New mixing rules in simple equations of state for representing vapour-liquid equilibria of strongly non-ideal mixtures*. *Fluid Phase Equilibria*, 1979. **3**(4): 255-271.
54. Vidal, J., *Mixing rules and excess properties in cubic equations of state*. *Chemical Engineering Science*, 1978. **33**(6): 787-791.
55. Kurihara, K., K. Tochigi, and K. Kojima, *Mixing rule containing regular-solution and residual excess free-energy*. *Journal of Chemical Engineering of Japan*, 1987. **20**(3): 227-231.
56. Wong, D.S.H. and S.I. Sandler, *A theoretically correct mixing rule for cubic equations of state*. *AIChE Journal*, 1992. **38**(5): 671-680.
57. Orbey, H. and S.I. Sandler, *On the combination of equation of state and excess free-energy models*. *Fluid Phase Equilibria*, 1995. **111**(1): 53-70.
58. Twu, C.H. and J.E. Coon, *CEoS/A^E mixing rules constrained by vdW mixing rule and second virial coefficient*. *AIChE Journal*, 1996. **42**(11): 3212-3222.
59. Orbey, H. and S.I. Sandler, *A comparison of Huron-Vidal type mixing rules of mixtures of compounds with large size differences, and a new mixing rule*. *Fluid Phase Equilibria*, 1997. **132**(1-2): 1-14.
60. Twu, C.H., Coon, J. E., Bluck, D., et al., *Connection between zero-pressure mixing rules and infinite-pressure mixing rules*. *Fluid Phase Equilibria*, 1998. **153**(1): 29-44.

61. Esmailzadeh, F., H. As'adi, and M. Lashkarbolooki, *Calculation of the solid solubilities in supercritical carbon dioxide using a new G^{ex} mixing rule*. Journal of Supercritical Fluids, 2009. **51**(2): 148-158.
62. Mollerup, J., *A note on the derivation of mixing rules from excess Gibbs energy models*. Fluid Phase Equilibria, 1986. **25**(3): 323-327.
63. Michelsen, M.L., *A method for incorporating excess Gibbs energy models in equations of state*. Fluid Phase Equilibria, 1990. **60**(1-2): 47-58.
64. Michelsen, M.L., *A modified Huron-Vidal mixing rule for cubic equations of state*. Fluid Phase Equilibria, 1990. **60**(1-2): 213-219.
65. Dahl, S. and M.L. Michelsen, *High-pressure vapor-liquid equilibrium with a UNIFAC-based equation of state*. AIChE Journal, 1990. **36**(12): 1829-1836.
66. Dahl, S., A. Fredenslund, and Rasmussen, *The MHV2 model – a UNIFAC-based equation of state model for prediction of gas solubility and vapor-liquid-equilibria at low and high-pressures*. Industrial & Engineering Chemistry Research, 1991. **30**(8): 1936-1945.
67. Heidemann, R.A. and S.L. Kokal, *Combined excess free energy models and equations of state*. Fluid Phase Equilibria, 1990. **56**(C): 17-37.
68. Holderbaum, T. and J. Gmehling, *PSRK – a group contribution equation of state based on UNIFAC*. Fluid Phase Equilibria, 1991. **70**(2-3): 251-265.
69. Horstmann, S., Jabloniec, A., aKrafczyk, J., et al., *PSRK group contribution equation of state: comprehensive revision and extension IV, including critical constants and alpha-function parameters for 1000 components*. Fluid Phase Equilibria, 2005. **227**(2): 157-164.
70. Soave, G., *A new expression of $Q(\alpha)$ for the modified Huron-Vidal method*. Fluid Phase Equilibria, 1992. **72**: 325-327.
71. Tochigi, K., Kolar, P., Iizumi, T., et al., *A note on a modified Huron-Vidal mixing rule consistent with the 2nd virial-coefficient condition*. Fluid Phase Equilibria, 1994. **96**: 215-221.
72. Kurihara, K. and K. Kojima, *An implicit type Eos- $G^{E(Vp)}$ model employing vapor-pressure standard state .1. prediction of high-pressure vapor-liquid-equilibria based on low-temperature data*. Fluid Phase Equilibria, 1995. **113**(1-2): 27-43.
73. Kalospiros, N.S., Tzouvaras, N., Coutzikos, P., et al., *Analysis of zero-reference-pressure Eos/ G^E models*. AIChE Journal, 1995. **41**(4): 928-937.
74. Twu, C.H., J.E. Coon, and D. Bluck, *Equations of state using an extended Twu-Coon mixing rule incorporating UNIFAC for high temperature and high pressure phase equilibrium predictions*. Fluid Phase Equilibria, 1997. **139**(1-2): 1-13.
75. Chen, Z.H., Yao, Z., Li, Y., et al., *Prediction of vapor-liquid equilibrium at high pressure using a new excess free energy mixing rule coupled with the original UNIFAC method and the SRK equation of state*. Industrial & Engineering Chemistry Research, 2009. **48**(14): 6836-6845.
76. Gupte, P.A., P. Rasmussen, and A. Fredenslund, *A new group-contribution equation of state for vapor-liquid-equilibria*. Industrial & Engineering Chemistry Fundamentals, 1986. **25**(4): 636-645.
77. Boukouvalas, C., Spiliotis, N., Coutzikos, P., et al., *Prediction of vapor-liquid-equilibrium with the LCVM model - a coupled combination of the Vidal and Michelsen mixing rules coupled with the original UNIFAC and the T-MPR equation of state*. Fluid Phase Equilibria, 1994. **92**: 75-106.
78. Boukouvalas, C.J., Magoulas, K. G., Stamatakis, S. K., et al., *Prediction of vapor-liquid equilibria with the LCVM model: Systems containing light gases with medium and high molecular weight compounds*. Industrial & Engineering Chemistry Research, 1997. **36**(12): 5454-5460.
79. Han, X. and G. Chen, *New Wong-Sandler-type mixing rule*. Huagong Xuebao/Journal of Chemical Industry and Engineering (China), 2004. **55**(8): 1365-1368.
80. Orbey, S.I.S.H., *Modeling vapor-liquid equilibria: Cubic Equations of State and Their Mixing Rules*. 1998.

81. Constantinescu, D., A. Klamt, and D. Geana, *Vapor-liquid equilibrium prediction at high pressures using activity coefficients at infinite dilution from COSMO-type methods*. Fluid Phase Equilibria, 2005. **231**(2): 231-238.
82. Lee, M.T. and S.T. Lin, *Prediction of mixture vapor-liquid equilibrium from the combined use of Peng-Robinson equation of state and COSMO-SAC activity coefficient model through the Wong-Sandler mixing rule*. Fluid Phase Equilibria, 2007. **254**(1-2): 28-34.
83. Ye, K., H. Freund, and K. Sundmacher, *Modelling (vapour + liquid) and (vapour + liquid + liquid) equilibria of {water (H₂O) + methanol (MeOH) + dimethyl ether (DME) + carbon dioxide (CO₂)} quaternary system using the Peng-Robinson EoS with Wong-Sandler mixing rule*. Journal of Chemical Thermodynamics, 2011(43): 2002-2014.
84. Lazzaroni, M.J., Bush, D., Jones, R., et al., *High-pressure phase equilibria of some carbon dioxide-organic-water systems*. Fluid Phase Equilibria, 2004. **224**(1): 143-154.
85. Poling, B.E., J.M. Prausnitz, and J.P. O'Connell, *The Properties of Gases and Liquids*. 5th ed. 2000.
86. Kondepudi, D. and I. Prigogine, *Modern Thermodynamics, from heat engines to dissipative structures*. 1998: John Wiley and Sons.
87. Wang, J., *Modern Thermodynamics Based on the Extended Carnot Theorem*. 1st ed. Vol. 1. 2010, Shanghai: Fudan University Press. 301.
88. O'Connell, J.P. and J.M. Haile, *Thermodynamics: fundamentals for applications*. 1st ed. 2005: Cambridge University Press.
89. Sandler, S.I., *Chemical, biochemical, and engineering thermodynamics*. 4th ed. 2006: John Wiley & Sons, Inc.
90. Gmehling, J., Kolbe, B., Kleiber, M., et al., *Chemical Thermodynamics for Process Simulation*. 2012: Wiley-VCH.
91. Rachford, H.H. and J.D. Rice, *Procedure for use of electronic digital computers in calculating flash vaporization hydrocarbon equilibrium*. Transactions of the American Institute of Mining and Metallurgical Engineers, 1952. **195**: 327-328.
92. Teh, Y.S. and G.P. Rangaiah, *A study of equation-solving and Gibbs free energy minimization methods for phase equilibrium calculations*. Chemical Engineering Research & Design, 2002. **80**(A7): 745-759.
93. Tang, Y.P. and S. Saha, *An efficient method to calculate three-phase free-water flash for water-hydrocarbon systems*. Industrial & Engineering Chemistry Research, 2003. **42**(1): 189-197.
94. Eubank, P.T., *Equations and procedures for VLLE calculations*. Fluid Phase Equilibria, 2006. **241**(1-2): 81-85.
95. Juanes, R., *A robust negative flash based on a parameterization of the tie-line field*. Fluid Phase Equilibria, 2008. **267**(1): 6-17.
96. Lapene, A., Nichita, D. V., Debenest, G., et al., *Three-phase free-water flash calculations using a new modified Rachford-Rice equation*. Fluid Phase Equilibria, 2010. **297**(1): 121-128.
97. Haugen, K.B., A. Firoozabadi, and L.X. Sun, *Efficient and robust three-phase split computations*. AIChE Journal, 2011. **57**(9): 2555-2565.
98. Li, Y.H., R.T. Johns, and K. Ahmadi, *A rapid and robust alternative to Rachford - Rice in the flash calculations*. Fluid Phase Equilibria, 2012. **316**: 85-97.
99. Gibbs, J.W., *Graphical methods in the thermodynamics of fluids*. Transactions of the Connecticut Academy, 1873. **2**: 311-342.
100. Gibbs, J.W., *A method of geometrical representation of thermodynamic properties of substances by means of surfaces*. Transactions of the Connecticut Academy, 1873. **2**: 382-404.
101. Lucia, A., L. Padmanabhan, and S. Venkataraman, *Multiphase equilibrium flash calculations*. Computers & Chemical Engineering, 2000. **24**(12): 2557-2569.
102. Nichita, D.V., S. Gomez, and E. Luna, *Multiphase equilibria calculation by direct minimization of Gibbs free energy with a global optimization method*. Computers & Chemical Engineering, 2002. **26**(12): 1703-1724.

103. Nichita, D.V., S. Gomez, and E. Luna-Ortiz, *Multiphase equilibria calculation by direct minimization of Gibbs free energy using the tunnelling global optimization method*. Journal of Canadian Petroleum Technology, 2004. **43**(5): 13-16.
104. Lucia, A., Bonk, B. M., Waterman, R. R., et al., *A multi-scale framework for multi-phase equilibrium flash*. Computers & Chemical Engineering, 2012. **36**: 79-98.
105. McDonald, C.M. and C.A. Floudas, *GLOPEQ: A new computational tool for the phase and chemical equilibrium problem*. Computers & Chemical Engineering, 1997. **21**(1): 1-23.
106. Baker, L.E., A.C. Pierce, and K.D. Luks, *Gibbs energy analysis of phase-equilibria*. Society of Petroleum Engineers Journal, 1982. **22**(5): 731-742.
107. Michelsen, M.L., *The isothermal flash problem 1. stability*. Fluid Phase Equilibria, 1982. **9**(1): 1-19.
108. Michelsen, M.L., *The isothermal flash problem 2. phase-split calculation*. Fluid Phase Equilibria, 1982. **9**(1): 21-40.
109. Tessier, S.R., J.F. Brennecke, and M.A. Stadtherr, *Reliable phase stability analysis for excess Gibbs energy models*. Chemical Engineering Science, 2000. **55**(10): 1785-1796.
110. Zhu, Y.S. and K. Inoue, *Calculation of chemical and phase equilibrium based on stability analysis by QBB algorithm: application to NRTL equation*. Chemical Engineering Science, 2001. **56**(24): 6915-6931.
111. Nichita, D.V., S. Gomez, and E. Luna, *Phase stability analysis with cubic equations of state by using a global optimization method*. Fluid Phase Equilibria, 2002. **194**: 411-437.
112. Bonilla-Petriciolet, A., Vazquez-Roman, R., Iglesias-Silva, G. A., et al., *Performance of stochastic global optimization methods in the calculation of phase stability analyses for nonreactive and reactive mixtures*. Industrial & Engineering Chemistry Research, 2006. **45**(13): 4764-4772.
113. Srinivas, M. and G.P. Rangaiah, *A study of differential evolution and tabu search for benchmark, phase equilibrium and phase stability problems*. Computers & Chemical Engineering, 2007. **31**(7): 760-772.
114. Saber, N. and J.M. Shaw, *Rapid and robust phase behaviour stability analysis using global optimization*. Fluid Phase Equilibria, 2008. **264**(1-2): 137-146.
115. Nichita, D.V. and S. Gomez, *Efficient location of multiple global minima for the phase stability problem*. Chemical Engineering Journal, 2009. **152**(1): 251-263.
116. Bonilla-Petriciolet, A. and J.G. Segovia-Hernandez, *A comparative study of particle swarm optimization and its variants for phase stability and equilibrium calculations in multicomponent reactive and non-reactive systems*. Fluid Phase Equilibria, 2010. **289**(2): 110-121.
117. Kangas, J., I. Malinen, and J. Tanskanen, *Modified bounded homotopies in the solving of phase stability problems for liquid-liquid phase-splitting calculations*. Industrial & Engineering Chemistry Research, 2011. **50**(11): 7003-7018.
118. Michelsen, M.L., *Calculation of multiphase equilibrium*. Computers & Chemical Engineering, 1994. **18**(7): 545-550.
119. Makkuni, A., A.V. Phoenix, and S. Rohani, *An aqueous phase equilibrium calculation algorithm*. Canadian Journal of Chemical Engineering, 2002. **80**(4): 741-752.
120. Canas-Marin, W.A., Ortiz-Arango, J. N. D., Guerrero-Aconcha, U. E., et al., *Improved two-sided tangent plane initialization and two-phase-split calculations*. Industrial & Engineering Chemistry Research, 2007. **46**(16): 5429-5436.
121. Henderson, N., N.E. Barufatti, and W.F. Sacco, *The Least Dot Products method: A new numerical paradigm for phase stability analysis of thermodynamic mixtures*. Chemical Engineering Science, 2011. **66**(22): 5684-5702.
122. Gaganis, V. and N. Varotsis, *Non-iterative phase stability calculations for process simulation using discriminating functions*. Fluid Phase Equilibria, 2012. **314**: 69-77.
123. Eubank, P.T., Elhassan, A. E., Barrufet, M. A., et al., *Area method for prediction of fluid-phase equilibria*. Industrial & Engineering Chemistry Research, 1992. **31**(3): 942-949.

124. Eubank, P.T. and K.R. Hall, *Equal-area rule and algorithm for determining phase compositions*. AIChE Journal, 1995. **41**(4): 924-927.
125. Shyu, G.S., Hanif, N. S. M., Alvarado, J. F. J., et al., *Equal-area rule methods for ternary-systems*. Industrial & Engineering Chemistry Research, 1995. **34**(12): 4562-4570.
126. Hanif, N.S.M., Shyu, G. S., Hall, K. R., et al., *Calculation of multi-phase equilibria using the equal area rule with application to hydrocarbon/water mixtures*. Fluid Phase Equilibria, 1996. **126**(1): 53-70.
127. Shyu, G.S., Hanif, N. S. M., Hall, K. R., et al., *Maximum partial area rule for phase equilibrium calculations*. Industrial & Engineering Chemistry Research, 1996. **35**(11): 4348-4353.
128. Han, G.J. and G.P. Rangaiah, *A method for multiphase equilibrium calculations*. Computers & Chemical Engineering, 1998. **22**(7-8): 897-911.
129. Avami, A. and Y. Saboohi, *A simultaneous method for phase identification and equilibrium calculations in reactive mixtures*. Chemical Engineering Research & Design, 2011. **89**(10A): 1901-1908.
130. Shyamsundar, V. and G.P. Rangaiah, *A method for simulation and optimization of multiphase distillation*. Computers & Chemical Engineering, 2000. **24**(1): 23-37.
131. They, R., Llovel, F., Meyer, X., et al., *Modelling of a dynamic multiphase flash: the positive flash Application to the calculation of ternary diagrams*. Computers & Chemical Engineering, 2004. **28**(12): 2469-2480.
132. Wei, Q.-S., Hu, Y.-D., An, W.-Z., et al., *Equilibrium calculation of multiphase and multicomponent system by using modified τ method*. Chemical Engineering (China), 2007. **35**(12): 38-41.
133. Hoteit, H. and A. Firoozabadi, *Simple phase stability-testing algorithm in the reduction method*. AIChE Journal, 2006. **52**(8): 2909-2920.
134. Jalali, F. and J.D. Seader, *Homotopy continuation method in multi-phase multi-reaction equilibrium systems*. Computers & Chemical Engineering, 1999. **23**(9): 1319-1331.
135. Bausa, J. and W. Marquardt, *Quick and reliable phase stability test in VLE flash calculations by homotopy continuation*. Computers & Chemical Engineering, 2000. **24**(11): 2447-2456.
136. Khaleghi, S. and F. Jalali, *Multiple solutions in stability analysis using homotopy continuation in complex space*. Chemical Engineering Communications, 2007. **194**(9): 1241-1258.
137. Jalali, F., J.D. Seader, and S. Khaleghi, *Global solution approaches in equilibrium and stability analysis using homotopy continuation in the complex domain*. Computers & Chemical Engineering, 2008. **32**(10): 2333-2345.
138. Patel, K.S. and A.K. Sunol, *Automatic generation of global phase equilibrium diagrams for binary systems from equations of state*. Computers & Chemical Engineering, 2009. **33**(11): 1793-1804.
139. Rahimian, S.K., Jalali, F., Seader, J. D., et al., *A new homotopy for seeking all real roots of a nonlinear equation*. Computers & Chemical Engineering, 2011. **35**(3): 403-411.
140. Rahimian, S.K., Jalali, F., Seader, J. D., et al., *A robust homotopy continuation method for seeking all real roots of unconstrained systems of nonlinear algebraic and transcendental equations*. Industrial & Engineering Chemistry Research, 2011. **50**(15): 8892-8900.
141. Steyer, F., D. Flockerzi, and K. Sundmacher, *Equilibrium and rate-based approaches to liquid-liquid phase splitting calculations*. Computers & Chemical Engineering, 2005. **30**(2): 277-284.
142. Smith, J.V., R.W. Missen, and W.R. Smith, *General optimality criteria for multiphase multireaction chemical-equilibrium*. AIChE Journal, 1993. **39**(4): 707-710.
143. Leitner, W., *Designed to dissolve*. Nature, 2000. **405**(6783): 129-130.

144. Baker, L.C.W. and T.F. Anderson, *Some phase relationships in the 3-component liquid system CO₂-H₂O-C₂H₅OH at high pressures*. Journal of the American Chemical Society, 1957. **79**(9): 2071-2074.
145. Elgin, J.C. and J.J. Weinstock, *Phase equilibrium at elevated pressures in ternary systems of ethylene and water with organic liquids. Salting out with a supercritical gas*. Journal of Chemical and Engineering Data, 1959. **4**(1): 3-12.
146. Panagiotopoulos, A.Z. and R.C. Reid, *High-pressure phase-equilibria in ternary fluid mixtures with a supercritical component*. Abstracts of Papers of the American Chemical Society, 1985. **190**(Sep): 45-FUL.
147. Wendland, M., H. Hasse, and G. Maurer, *Multiphase high-pressure equilibria of carbon-dioxide-water-isopropanol*. Journal of Supercritical Fluids, 1993. **6**(4): 211-222.
148. Yoon, J.H., Chun, M. K., Hong, W. H., et al., *High-pressure phase equilibria for carbon dioxide-methanol-water system: Experimental data and critical evaluation of mixing rules*. Industrial and Engineering Chemistry Research, 1993. **32**(11): 2881-2887.
149. Ulanova, T., D. Tuma, and G. Maurer, *Phase equilibria and partitioning of L-histidine and three pharmaceuticals to pH-adjusted high-pressure liquid phases of the ternary system (Ethene + Water+2-Propanol)*. Journal of Chemical and Engineering Data, 2011. **56**(12): 4376-4391.
150. Blasucci, V.M., Husain, Z. A., Fadhel, A. Z., et al., *Combining homogeneous catalysis with heterogeneous separation using tunable solvent systems*. Journal of Physical Chemistry A, 2010. **114**(11): 3932-3938.
151. Lu, J., Lazzaroni, J., Hallett, J. P., et al., *Tunable solvents for homogeneous catalyst recycle*. Industrial & Engineering Chemistry Research, 2004. **43**(7): 1586-1590.
152. <http://en.wikipedia.org/wiki/Chlorofluorocarbon>.
153. http://en.wikipedia.org/wiki/Nitrous_oxide.
154. Knapp, J.P. and M.F. Doherty, *A new pressure-swing-distillation process for separating homogeneous azeotropic mixtures*. Industrial & Engineering Chemistry Research, 1992. **31**(1): 346-357.
155. Repke, J.U., F. Forner, and A. Klein, *Separation of homogeneous azeotropic mixtures by pressure swing distillation - Analysis of the operation performance*. Chemical Engineering & Technology, 2005. **28**(10): 1151-1157.
156. Modla, G. and P. Lang, *Feasibility of new pressure swing batch distillation methods*. Chemical Engineering Science, 2008. **63**(11): 2856-2874.
157. Repke, J.U. and A. Klein, *Homogeneous azeotropic pressure swing distillation: Continuous and batch process*. Computer Aided Chemical Engineering, 2005. **20**: 721-726.
158. Repke, J.U., Klein, A., Bogle, D., et al., *Pressure swing batch distillation for homogeneous azeotropic separation*. Chemical Engineering Research and Design, 2007. **85**(4 A): 492-501.
159. Huang, K.J., Shan, L., Zhu, Q. X., et al., *Adding rectifying/stripping section type heat integration to a pressure-swing distillation (PSD) process*. Applied Thermal Engineering, 2008. **28**(8-9): 923-932.
160. Matsuda, K., Huang, K. J., Iwakabe, K., et al., *Separation of binary azeotrope mixture via pressure-swing distillation with heat integration*. Journal of Chemical Engineering of Japan, 2011. **44**(12): 969-975.
161. Ye, K., H. Freund, and K. Sundmacher, *A new process for azeotropic mixture separation by phase behavior tuning using pressurized carbon dioxide*. Industrial & Engineering Chemistry Research, 2013. **52**(43): 15154-15164..
162. Kerler, B., Robinson, R. E., Borovik, A. S., et al., *Application of CO₂-expanded solvents in heterogeneous catalysis: A case study*. Applied Catalysis B: Environmental, 2004. **49**(2): 91-98.
163. Caravati, M., J.D. Grunwaldt, and A. Baiker, *Solvent-modified supercritical CO₂: A beneficial medium for heterogeneously catalyzed oxidation reactions*. Applied Catalysis A: General, 2006. **298**(1-2): 50-56.
164. Subramaniam, B., *Gas-expanded liquids for sustainable catalysis and novel materials: Recent advances*. Coordination Chemistry Reviews, 2010. **254**(15-16): 1843-1853.

165. Floris, T., Kluson, P., Muldoon, M. J., et al., *Notes on the asymmetric hydrogenation of methyl acetoacetate in neoteric solvents*. Catalysis Letters, 2010. **134**(3-4): 279-287.
166. Dong, L.B., McVicker, G. B., Kiserow, D. J., et al., *Hydrogenation of polystyrene in CO₂-expanded liquids: The effect of catalyst composition on deactivation*. Applied Catalysis A: General, 2010. **384**(1-2): 45-50.
167. Bogel-Lukasik, E., Wind, J., Bogel-Lukasik, R., et al., *The influence of hydrogen pressure on the heterogeneous hydrogenation of β -myrcene in a CO₂-expanded liquid*. Journal of Supercritical Fluids, 2010. **54**(1): 46-52.
168. Phiong, H.S., Cooper, C. G., Adesina, A. A., et al., *Kinetic modelling of the catalytic hydrogenation of CO₂-expanded α -methylstyrene*. Journal of Supercritical Fluids, 2008. **46**(1): 40-46.
169. Bogel-Lukasik, E., Bogel-Lukasik, R., Kriaa, K., et al., *Limonene hydrogenation in high-pressure CO₂: Effect of hydrogen pressure*. Journal of Supercritical Fluids, 2008. **45**(2): 225-230.
170. Xie, X., C.L. Liotta, and C.A. Eckert, *CO₂-protected amine formation from nitrile and imine hydrogenation in gas-expanded liquids*. Industrial and Engineering Chemistry Research, 2004. **43**(24): 7907-7911.
171. Jessop, P.G., Stanley, R. R., Brown, R. A., et al., *Neoteric solvents for asymmetric hydrogenation: Supercritical fluids, ionic liquids, and expanded ionic liquids*. Green Chemistry, 2003. **5**(2): 123-128.
172. Thomas, C.A., Bonilla, R. J., Huang, Y., et al., *Hydrogenation of carbon dioxide catalyzed by ruthenium trimethylphosphine complexes - Effect of gas pressure and additives on rate in the liquid phase*. Canadian Journal of Chemistry, 2001. **79**(5-6): 719-724.
173. Fang, J., Guha, D., Tunge, J., et al., *Homogeneous olefin hydroformylation by transition metal complexes in CO₂-expanded media: Solvent effects and kinetics*. 2007.
174. Jin, H., Ghosh, A., Fang, J., et al., *Catalytic hydroformylation of higher olefins in CO₂-expanded media: Kinetic, mechanistic and economic aspects*. 2005.
175. Jin, H. and B. Subramaniam, *Homogeneous catalytic hydroformylation of 1-octene in CO₂-expanded solvent media*. Chemical Engineering Science, 2004. **59**(22-23): 4887-4893.
176. Hemminger, O., Marteel, A., Mason, M. R., et al., *Hydroformylation of 1-hexene in supercritical carbon dioxide using a heterogeneous rhodium catalyst. 3. Evaluation of solvent effects*. Green Chemistry, 2002. **4**(5): 507-512.
177. Bohnen, H.W. and B. Cornils, *Hydroformylation of alkenes: An industrial view of the status and importance*. Advances in Catalysis, Vol 47, 2002. **47**: 1-64.
178. <http://www.inprompt.tu-berlin.de/>.
179. Peschel, A., Hentschel, B., Freund, H., et al., *Design of optimal multiphase reactors exemplified on the hydroformylation of long chain alkenes*. Chemical Engineering Journal, 2012. **188**: 126-141.
180. Wasserscheid, P., Waffenschmidt, H., Machnitzki, P., et al., *Cationic phosphine ligands with phenylguanidinium modified xanthene moieties - A successful concept for highly regioselective, biphasic hydroformylation of oct-1-ene in hexafluorophosphate ionic liquids*. Chemical Communications, 2001(5): 451-452.
181. Wasserscheid, P. and H. Waffenschmidt, *Ionic liquids in regioselective platinum-catalysed hydroformylation*. Journal of Molecular Catalysis A: Chemical, 2000. **164**(1-2): 61-67.
182. Haumann, M. and A. Riisager, *Hydroformylation in room temperature ionic liquids (RTILs): Catalyst and process developments*. Chemical Reviews, 2008. **108**(4): 1474-1497.
183. Dupont, J., S.M. Silva, and R.F. De Souza, *Mobile phase effects in Rh/sulfonated phosphine/molten salts catalysed the biphasic hydroformylation of heavy olefins*. Catalysis Letters, 2001. **77**(1-3): 131-133.
184. Brasse, C.C., Englert, U., Salzer, A., et al., *Ionic phosphine ligands with cobaltocenium backbone: Novel ligands for the highly selective, biphasic,*

- rhodium-catalyzed hydroformylation of 1-octene in ionic liquids*. *Organometallics*, 2000. **19**(19): 3818-3823.
185. Riisager, A., Fehrmann, R., Haumann, M., et al., *Supported Ionic Liquid Phase (SILP) catalysis: An innovative concept for homogeneous catalysis in continuous fixed-bed reactors*. *European Journal of Inorganic Chemistry*, 2006(4): 695-706.
186. Riisager, A., Fehrmann, R., Haumann, M., et al., *Stability and kinetic studies of supported ionic liquid phase catalysts for hydroformylation of propene*. *Industrial and Engineering Chemistry Research*, 2005. **44**(26): 9853-9859.
187. Monnereau, L., Sémeril, D., Matt, D., et al., *Micellar effects in olefin hydroformylation catalysed by neutral, calix[4]arene-diphosphite rhodium complexes*. *Advanced Synthesis and Catalysis*, 2009. **351**(10): 1629-1636.
188. Giménez-Pedros, M., Aghmiz, A., Claver, C., et al., *Micellar effect in hydroformylation of high olefin catalysed by water-soluble rhodium complexes associated with sulfonated diphosphines*. *Journal of Molecular Catalysis A: Chemical*, 2003. **200**(1-2): 157-163.
189. Chen, H., Li, Y., Chen, J., et al., *Micellar effect in high olefin hydroformylation catalyzed by water-soluble rhodium complex*. *Journal of Molecular Catalysis A: Chemical*, 1999. **149**(1-2): 1-6.
190. Mathivet, T., Monflier, E., Castanet, Y., et al., *Hydroformylation of higher olefins by rhodium/tris-((1H,1H,2H,2H-perfluorodecyl)phenyl)phosphites complexes in a fluorocarbon/hydrocarbon biphasic medium: Effects of fluorinated groups on the activity and stability of the catalytic system*. *Tetrahedron*, 2002. **58**(20): 3877-3888.
191. Foster, D.F., Gudmunsen, D., Adams, D. J., et al., *Hydroformylation in perfluorinated solvents; improved selectivity, catalyst retention and product separation*. *Tetrahedron*, 2002. **58**(20): 3901-3910.
192. Fish, R.H., *Fluorous biphasic catalysis: A new paradigm for the separation of homogeneous catalysts from their reaction substrates and products*. *Chemistry - A European Journal*, 1999. **5**(6): 1677-1680.
193. Aghmiz, A., Claver, C., Masdeu-Bultó, A. M., et al., *Hydroformylation of 1-octene with rhodium catalysts in fluorous systems*. *Journal of Molecular Catalysis A: Chemical*, 2004. **208**(1-2): 97-101.
194. Shaharun, M.S., H. Mukhtar, and B.K. Dutta, *Solubility of carbon monoxide and hydrogen in propylene carbonate and thermomorphic multicomponent hydroformylation solvent*. *Chemical Engineering Science*, 2008. **63**(11): 3024-3035.
195. Shaharun, M.S., Dutta, B. K., Mukhtar, H., et al., *Hydroformylation of 1-octene using rhodium-phosphite catalyst in a thermomorphic solvent system*. *Chemical Engineering Science*, 2010. **65**(1): 273-281.
196. Behr, A., Turkowski, B., Roll, R., et al., *Multiphase catalysis in temperature-dependent multi-component solvent (TMS) systems*, 2008. 19-52.
197. Behr, A., D. Obst, and B. Turkowski, *Isomerizing hydroformylation of trans-4-octene to n-nonanal in multiphase systems: Acceleration effect of propylene carbonate*. *Journal of Molecular Catalysis A: Chemical*, 2005. **226**(2): 215-219.
198. Subramaniam, B., Fang, J., Jin, H., et al., *Economic and environmental impact analyses of catalytic olefin hydroformylation in CO₂-expanded liquid (CXL) media*. *Industrial & Engineering Chemistry Research*, 2007. **46**(25): 8687-8692.
199. Jin, H. and B. Subramaniam, *Homogeneous catalytic hydroformylation of 1-octene in CO₂-expanded solvent media*. *Chemical Engineering Science*, 2004. **59**(22-23): 4887-4893.
200. Kainz, S. and W. Leitner, *Catalytic asymmetric hydroformylation in the presence of compressed carbon dioxide*. *Catalysis Letters*, 1998. **55**(3-4): 223-225.
201. Koch, D. and W. Leitner, *Rhodium-catalyzed hydroformylation in supercritical carbon dioxide*. *Journal of the American Chemical Society*, 1998. **120**(51): 13398-13404.
202. Rathke, J.W., R.J. Klingler, and T.R. Krause, *Propylene hydroformylation in supercritical carbon dioxide*. *Organometallics*, 1991. **10**(5): 1350-1355.

203. Sellin, M.F., P.B. Webb, and D.J. Cole-Hamilton, *Continuous flow homogeneous catalysis: Hydroformylation of alkenes in supercritical fluid-ionic liquid biphasic mixtures*. Chemical Communications, 2001(8): 781-782.
204. Webb, P.B., Sellin, M. F., Kunene, T. E., et al., *Continuous flow hydroformylation of alkenes in supercritical fluid-ionic liquid biphasic systems*. Journal of the American Chemical Society, 2003. **125**(50): 15577-15588.
205. Sharma, A., Lebigue, C. J., Deshpande, R. M., et al., *Hydroformylation of 1-octene using [Bmim][PF(6)]-decane biphasic media and rhodium complex catalyst: Thermodynamic properties and kinetic study*. Industrial & Engineering Chemistry Research, 2010. **49**(21): 10698-10706.
206. Koeken, A.C.J., van den Broeke, L. J. P., Deelman, B. J., et al., *Full kinetic description of 1-octene hydroformylation in a supercritical medium*. Journal of Molecular Catalysis a-Chemical, 2011. **346**(1-2): 1-11.
207. Bernas, A., Maki-Arvela, P., Lehtonen, J., et al., *Kinetic modeling of propene hydroformylation with Rh/TPP and Rh/CHDPP catalysts*. Industrial & Engineering Chemistry Research, 2008. **47**(13): 4317-4324.
208. Chansarkar, R., A.A. Kelkar, and R.V. Chaudhari, *Hydroformylation of 1,4-diacetoxy-2-butene using HRh(CO)(PPh(3))(3) tethered on alumina as a catalyst: kinetic study*. Industrial & Engineering Chemistry Research, 2009. **48**(21): 9479-9489.
209. Feng, J. and M. Garland, *Unmodified homogeneous rhodium-catalyzed hydroformylation of styrene. The detailed kinetics of the regioselective synthesis*. Organometallics, 1999. **18**(3): 417-427.
210. Murzin, D.Y., A. Bernas, and T. Salmi, *Kinetic modelling of regioselectivity in alkenes hydroformylation over rhodium*. Journal of Molecular Catalysis a-Chemical, 2010. **315**(2): 148-154.
211. Freund, H. and K. Sundmacher, *Towards a methodology for the systematic analysis and design of efficient chemical processes. Part 1. From unit operations to elementary process functions*. Chemical Engineering and Processing: Process Intensification, 2008. **47**(12): 2051-2060.
212. Peschel, A., H. Freund, and K. Sundmacher, *Methodology for the design of optimal chemical reactors based on the concept of elementary process functions*. Industrial and Engineering Chemistry Research, 2010. **49**(21): 10535-10548.
213. Behr, A., Henze, G., Obst, D., et al., *Selection process of new solvents in temperature-dependent multi-component solvent systems and its application in isomerising hydroformylation*. Green Chemistry, 2005. **7**(9): 645-649.
214. Schafer, E., Brunsch, Y., Sadowski, G., et al., *Hydroformylation of 1-dodecene in the thermomorphic solvent system dimethylformamide/decane. Phase behavior-reaction performance-catalyst recycling*. Industrial & Engineering Chemistry Research, 2012. **51**(31): 10296-10306.
215. Nagarajan, N. and R.L. Robinson, *Equilibrium phase compositions, phase densities, and interfacial-tensions for CO₂ + hydrocarbon systems 2. CO₂ + normal-decane*. Journal of Chemical and Engineering Data, 1986. **31**(2): 168-171.
216. Kordikowski, A., Schenk, A. P., VanNielen, R. M., et al., *Volume expansions and vapor-liquid equilibria of binary mixtures of a variety of polar solvents and certain near-critical solvents*. Journal of Supercritical Fluids, 1995. **8**(3): 205-216.
217. *Aspen Plus Internal Database (V7.1)*.
218. Larsen, B.L., P. Rasmussen, and A. Fredenslund, *A Modified UNIFAC group-contribution model for prediction of phase-equilibria and heats of mixing*. Industrial & Engineering Chemistry Research, 1987. **26**(11): 2274-2286.
219. Zhu, R.J., Zhou, J. G., Liu, S. C., et al., *Vapor-liquid equilibrium data for the binary systems in the process of synthesizing diethyl carbonate*. Fluid Phase Equilibria, 2010. **291**(1): 1-7.
220. Gmehling, J., J.D. Li, and M. Schiller, *A modified UNIFAC model .2. Present parameter matrix and results for different thermodynamic properties*. Industrial & Engineering Chemistry Research, 1993. **32**(1): 178-193.

221. Suzuki, K., Sue, H., Arai, K., et al., *Vapor-liquid-equilibria for synthetic alcohols process*. Fluid Phase Equilibria, 1990. **59**(2): 115-134.
222. Patel, N.C., V. Abovsky, and S. Watanasiri, *Calculation of vapor-liquid equilibria for a 10-component system: comparison of EOS, EOS- G^E and G^E -Henry's law models*. Fluid Phase Equilibria, 2001. **185**(1-2): 397-405.
223. Marcilla, A., Olaya, M. M., Serrano, M. D., et al., *Gibbs energy based procedure for the correlation of type 3 ternary systems including a three-liquid phase region*. Fluid Phase Equilibria, 2009. **281**(1): 87-95.
224. Maslan, F.D. and E.A. Stoddard, *Acetonitrile-water liquid-vapor equilibrium*. Journal of Physical Chemistry, 1956. **60**(7): 1146-1147.
225. Blackfor.Ds and R. York, *Vapor-liquid equilibria of system acrylonitrile - acetonitrile - water*. Journal of Chemical and Engineering Data, 1965. **10**(4): 313-&.
226. Gmehling, J., Onken, U., Arlt, W., et al., *Vapor-Liquid Equilibrium Data Collection, Chemistry Data Series, DECHEMA. Part 1: Aqueous-Organic Systems*. 1991.
227. Acosta, J., Arce, A., Rodil, E., et al., *A thermodynamic study on binary and ternary mixtures of acetonitrile, water and butyl acetate*. Fluid Phase Equilibria, 2002. **203**(1-2): 83-98.
228. Nayak, J.N., Aralaguppi, M.I., Naidu, B.V.K., et al., *Thermodynamic properties of water plus tetrahydrofuran and water plus 1,4-dioxane mixtures at (303.15, 313.15, and 323.15) K*. Journal of Chemical and Engineering Data, 2004. **49**(3): 468-474.
229. Hradetzky, G., Hammerl, J., Kisan, W., et al., *Data of Selective Solvents DMFA-NMC-NMP*. 1989: Deutscher Verlag der Wissenschaften, Berlin.
230. Antosik, M., A. Stafiej, and R. Stryjek, *Mutual solubility of binary trans-decalin + and normal-decane + polar component mixtures*. Fluid Phase Equilibria, 1990. **58**(3): 325-333.

List of Figures

Chapter 1

Figure 1.1: VOC annual emissions.

Figure 1.2: Motivation of research on benign alternatives.

Figure 1.3: The publication review involved CO₂ based solvents.

Figure 1.4: A schematic diagram of CO₂ application in chemical engineering.

Figure 1.5: Pyramid of production processes in chemical engineering.

Figure 1.6: Work structure of this thesis.

Chapter 2

Figure 2.1: Structure of the CEoS/GE model.

Figure 2.2: Isothermal VLE diagram of H₂O/MeOH system.

Figure 2.3: Isothermal VLE diagram of MeOH/DME system.

Figure 2.4: VLE diagram of CO₂/CO/OCT at 80bar, 40°C-80°C.

Figure 2.5: VLE diagram of CO₂/CO/NAL at 80bar, 40°C-80°C.

Figure 2.6: VLE parity plot of H₂/CO/CO₂/OCT system between the experimental results and the calculation at 40°C-60°C, 23.0bar-65.6bar.

Figure 2.7: VLE parity plot of H₂/CO/CO₂/NAL system between the experimental results and the calculation at 40°C-60°C, 26.9bar-67.1bar.

Figure 2.8: Isothermal VLE diagram of H₂O/DME system.

Figure 2.9: Isothermal VLLE diagram of H₂O/DME system.

Figure 2.10: Isothermal VLLE diagram of H₂O/CO₂/MeCN system at 39.85°C, 24bar-52bar.

Figure 2.11: Isothermal VLLE diagram of H₂O/CO₂/DIOX system at 39.85°C, 28bar-57bar.

Chapter 3

Figure 3.1: A schematic review of phase equilibrium calculation.

Figure 3.2: Schematic diagram of mass transfer and reaction in a closed system.

Figure 3.3: Calculation of the ten component VLLE case with random initialization (SID=13).

Figure 3.4: Calculation of the three component LLE case with random initialization (SID=14).

Figure 3.5: Entropy productions of four systems.

Figure 3.6: First derivation of entropy production of four systems.

Figure 3.7: The VLE (SID=6, NC=10) calculated by a VLLLE (30 unknowns) with random initialization cases.

Figure 3.8: The LLE (SID=14, NC=3) calculated by a LLLLE (12 unknowns) with random initialization cases.

Figure 3.9: A view of link between non-equilibrium and equilibrium state for different approaches of phase equilibrium.

Chapter 4

Figure 4.1: The phase changes observed upon expanding a mixture of two miscible liquids past a LCSP and a UCSP.

Figure 4.2: Separation principle of the PSD process.

Figure 4.3: Separation principle of process variant 1.

Figure 4.4: Separation principle of process variant 2.

Figure 4.5: Schematic of a conventional PSD process.

Figure 4.6: Schematic flowsheet of process variant 1.

Figure 4.7: Schematic flowsheet of process variant 2.

Figure 4.8: Separation costs contrasting the conventional PSD process and the two process variants.

Figure 4.9: Separation costs reduction of the two process variants based on the conventional PSD process.

Figure 4.10: Separation costs contrast among the conventional PSD process and new process.

Figure 4.11: Operating pressure influence on the separation costs of process variant 2.

Figure 4.12: Recycle ratio of CO₂ flow in process variant 2.

Figure 4.13: Electricity requirement of process variant 2.

Figure 4.14: Recycle ratio of condensate flow in process variant 2.

Figure 4.15: Steam requirement of process variant 2.

Figure 4.16: Separation costs contrast among the conventional PSD process and the new process variants.

Figure 4.17: Separation costs reduction of the two process variants based on the conventional PSD process.

Figure 4.18: Recycle ratio of condensate flow in process variant 1.

Figure 4.19: Recycle ratio of condensate flow in process variant 2.

Figure 4.20: Asymmetry and symmetry of a binary azeotropic system.

Figure 4.21: Two system classes of a binary azeotropic system considering the position of the azeotropic system under low pressure.

Chapter 5

Figure 5.1: Publication review of hydroformylation.

Figure 5.2: H₂ concentration in liquid dependent on solvent quantity and type.

Figure 5.3: CO concentration in liquid dependent on solvent quantity and type.

Figure 5.4: H₂/CO ratio in liquid dependent on solvent quantity and type.

Figure 5.5: CO₂ concentration in liquid dependent on solvent quantity and type.

Figure 5.6: H₂ concentration in liquid dependent on temperature.

Figure 5.7: CO concentration in liquid dependent on temperature.

Figure 5.8: H₂/CO ratio in liquid dependent on temperature.

Figure 5.9: CO₂ concentration in liquid dependent on temperature.

Figure 5.10: H₂ concentration in liquid dependent on pressure.

Figure 5.11: CO concentration in liquid dependent on pressure.

Figure 5.12: H₂/CO ratio in liquid dependent on pressure.

Figure 5.13: CO₂ concentration in liquid dependent on pressure.

Figure 5.14: The H₂/CO ratio varies along the reaction, solvent is ACE.

Figure 5.15: The H₂/CO ratio varies along the reaction, solvent is THF.

Figure 5.16: Publication review of TMS and hydroformylation in TMS.

Figure 5.17: The ternary diagram of DMF/1Do/C10 system predicted by UNIFAC-Do.

Figure 5.18: The ternary diagram of DMF/NC13/C10 system predicted by UNIFAC-Do.

Appendix 3

Figure A3.1: Isothermal VLE diagram of H₂O/CO₂ system.

Figure A3.2: Isothermal VLE diagram of DME/CO₂ system.

Figure A3.3: Isothermal VLE diagram of MeOH/CO₂ system.

Figure A3.4: Y-X diagram of H₂O/DME system.

Figure A3.5: VLE diagram of H₂O/MeOH/DME system for 60°C-120°C.

Figure A3.6: VLE diagram of MeOH/DME/CO₂ system for 40°C-60°C.

Figure A3.7: VLE diagram of CO₂/H₂/OCT 80bar, 40°C-60°C.

Figure A3.8: VLE diagram of CO₂/H₂/OCT 80bar, 40°C-60°C.

Figure A3.9: VLE diagram of H₂/CO₂/ACE system under 25.1bar -90.1bar, 40°C.

Figure A3.10: VLE parity plot of H₂/CO/CO₂/OCT/NAL system between the experimental results and the calculation at 40°C-50°C, 22.7bar-39.8bar.

Figure A3.11: VLE parity plot of H₂O/MeOH/DME/CO₂ system between the experimental results and the calculation at 80°C.

Figure A3.12: VLLE parity plot of H₂O/MeOH/DME/CO₂ system between the experimental results and the calculation at 25°C- 45°C.

Appendix 4

Figure A4.1: Calculation of the VLE case with random initialization (SID=6, NC=10).

Figure A4.2: Calculation of the LLE case with random initialization (SID=9, NC=7).

Figure A4.3: Calculation of the LLE case with random initialization (SID=10, NC=10).

Figure A4.4: The VLE (SID=6, NC=10) calculated by a VLLE (20 unknowns) with random initialization cases.

Figure A4.5: The LLE (SID=10, NC=10) calculated by a LLLE (20 unknowns) with random initialization case.

Figure A4.6: The VLLE (SID=14, NC=10) calculated by a VLLLE (30 unknowns) with random initialization case.

Figure A4.7: The LLLE (SID=15, NC=3) calculated by a LLLLE (9 unknowns) with random initialization cases.

Appendix 5

Figure A5.1: Isobaric VLE diagram of H₂O/MeCN system with atmospheric pressure.

Figure A5.2: Isobaric VLE diagram of H₂O/MeCN system with elevated pressures.

Figure A5.3: Isothermal Y-X diagram of H₂O/MeCN system at 30.35°C.

Figure A5.4: Isobaric VLE diagram of H₂O/DIOX system with elevated pressures.

Figure A5.5: Operation of the conventional PSD process in a Y-X diagram of MeCN/H₂O system.

Figure A5.6: Operation of the conventional PSD process in a Y-X diagram of DIOX/H₂O system.

Figure A5.7: Operation of process variant 1 in a Y-X diagram of MeCN/H₂O system.

Figure A5.8: Operation of process variant 2 in a Y-X diagram of MeCN/H₂O system.

Figure A5.9: Operation of process variant 1 in a Y-X diagram of DIOX/H₂O system.

Figure A5.10: Operation of process variant 2 in a Y-X diagram of DIOX/H₂O system.

Figure A5.11: Operating pressure influence on the separation costs of process variant 1.

Figure A5.12: Recycle ratio of CO₂ flow in process variant 1.

Figure A5.13: Electricity requirement of process variant 1 dependent on pressure and feed.

Figure A5.14: Recycle ratio of condensate flow in process variant 1.

Figure A5.15: Steam requirement of process variant 1.

Figure A5.16: Separation costs contrast between the conventional PSD process and process variant 1.

Figure A5.17: Separation costs contrast between the conventional PSD process and process variant 2.

Figure A5.18: Operating pressure influence on the separation costs of process variant 1.

Figure A5.19: Operating pressure influence on the separation costs of process variant 2.

Figure A5.20: Recycle ratio of CO₂ flow of process variant 1.

Figure A5.21: Recycle ratio of CO₂ flow of process variant 2.

Figure A5.22: Electricity requirement of process variant 1.

Figure A5.23: Electricity requirement of process variant 2.

Figure A5.24: Steam requirement of process variant 1.

Figure A5.25: Steam requirement of process variant 2.

Appendix 6

Figure A6.1: The ternary diagram of DMF/1Do/C10 system predicted by UNIFAC-Do with original interaction parameters.

Figure A6.2: The ternary diagram of DMF/NC13/C10 system predicted by UNIFAC-Do with original interaction parameters.

Figure A6.3: Correlation of LLE data of DMF/C12 system using UNIFAC-DO.

Figure A6.4: Correlation of LLE data of DMF/1Do system using UNIFAC-DO.

List of Tables

Chapter 2

Table 2.1: A review of mixing rules incorporating GE

Table 2.2: Investigated VLE systems

Table 2.3: Investigated VLLE systems predicted by the CEoS/GE in this thesis

Chapter 3

Table 3.1: A brief review of phase equilibrium criteria

Table 3.2: A brief review of objective function for current two approaches

Table 3.3: Dynamic equations for calculating the phase equilibria

Table 3.4: A review of investigated systems and phase types in this work

Chapter 4

Table 4.1: Review of investigated water- hydrophilic solvent systems involved the concept

Table 4.2: Simulation specifications of the conventional PSD process for the two systems

Table 4.3: Specification of simulation of new process

Table 4.4: The price of used utilities

Table 4.5: General results of case studies

Chapter 5

Table 5.1: A review of reactions in CXLs

Table 5.2: Specification of cases

Table 5.3: A table for qualitative illustrating the impacts of CXLs and the appropriate actions
for hydroformylation

Table 5.4: Features of CXTMS and possible benefits for hydroformylation process

Appendix

Table A1.1: Formula list of EoS/GE mixing rules

Table A2.1: Property parameters for various substances

Table A2.2: k_j of PRWS model

Table A2.3: Group parameters of the UNIFAC-PSRK and UNIFAC-Lby

Table A2.4: UNIFAC-PSRK interaction Parameters $a_{j,1}$, $a_{j,2}$, $a_{j,3}$

Table A2.5: UNIFAC-Lby interaction Parameters $a_{j,1}$, $a_{j,2}$, $a_{j,3}$

Table A2.6: NRTL parameters

Table A2.7: UNIFAC-Do parameters, part 1: R, Q

Table A2.8: UNIFAC-Do Interaction parameters, part 2: $a_{j,1}$, $a_{j,2}$, $a_{j,3}$

Table A4.1: Detailed information of investigated systems

Table A4.2: Results of selected systems in equilibrium state in comparison with reference

Table A4.3: Results of selected systems in equilibrium state calculated without prior
determination of phase number

Declarations

This dissertation contains material that has previously been published elsewhere. Other parts have been submitted for publication. The following list gives the details.

Articles:

- [1] K. Ye, H. Freund, K. Sundmacher, Modelling (vapour + liquid) and (vapour + liquid + liquid) equilibria of water (H₂O)+methanol (MeOH)+dimethyl ether (DME)+carbon dioxide (CO₂) quaternary system using the Peng–Robinson EoS with Wong–Sandler mixing rule. *Journal of Chemical Thermodynamics* 43 (2011): 2002-2014.
The author collected the experimental data, modeled the system, and prepared the manuscript.
- [2] K. Ye, H. Freund, Z. Xie, B. Subramaniam, K. Sundmacher, Prediction of multicomponent phase behavior of CO₂-expanded liquids using CEoS/GE models and comparison with experimental data. *Journal of Supercritical Fluids* 67 (2012): 41-52;
The author programmed the modeling work and validated it with experimental data. He has also prepared the manuscript.
- [3] K. Ye, H. Freund, K. Sundmacher, A New Separation Process for Azeotropic Mixture Separation by Phase Behavior Tuning using Pressurized Carbon Dioxide. *Industrial & Engineering Chemistry Research*, 2013. 52(43): 15154-15164.
The author developed the new separation process, selected case and modeled the system, and simulated and evaluated the processes. The manuscript was also prepared by him.

Conferences:

1. K. Ye, H. Freund, K. Sundmacher, New Separation Process for Azeotropic Mixture Separation by Phase Behavior Tuning using Pressurized Carbon Dioxide. *9th European Congress of Chemical Engineering* (oral presentation), 2013.

Invited Talks:

1. K. Ye, H. Freund, K. Sundmacher, A New Separation Process for Azeotropic Mixture Separation by Phase Behavior Tuning using Pressurized Carbon Dioxide. Group of Users of Technology for Separation in the Netherlands (NL GUTS) (oral presentation), 2013.

Curriculum Vitae

Personal Details

Name Ye, Kongmeng (叶孔萌)
Birth 16 April 1982
Zhejiang Province, China

Education

10.2002 - 07.2006 Zhejiang University, China
Chemical Engineering and Technology, Bachelor of Science
09.2006 - 07.2008 Zhejiang University, China
Chemical Engineering, Master of Science
Supervisor: Prof. Jia Wu (吴嘉 教授)
09.2008 - 06.2013 Max-Planck Institute, Magdeburg, Germany
Promotion for Dr. -Ing.
Supervisor: Prof. Dr.-Ing. Kai Sundmacher

Scholarships and Awards

2003/04/05 Scholarship Award of Zhejiang University
2003/04/05/06 Excellent student of Zhejiang University
06.2005 Award of Chemical Process Design, Bayer-East China Contest
06.2006 Excellent graduate of Zhejiang University
06.2006 Excellent graduate of Zhejiang Province
09.2007 Award of Air Products, Award of Haizheng
